

UNDERSTANDING AND TARGETING LIPID METABOLISM OF

MYCOBACTERIUM TUBERCULOSIS

A Dissertation

by

ZHEN LIU

Submitted to the Office of Graduate and Professional Studies of
Texas A&M University

in partial fulfillment of the requirements for the degree of

DOCTOR OF PHILOSOPHY

Chair of Committee,	James C. Sacchetti
Committee Members,	David P. Barondeau
	Kevin Burgess
	Tatyana Igumenova
Head of Department,	David H. Russell

December 2013

Major Subject: Chemistry

Copyright 2013 Zhen Liu

ABSTRACT

Mycobacterium tuberculosis (*M. tuberculosis*) contains a wide array of genes responsible for the synthesis and secretion of a variety of bioactive lipids. The genes represent attractive drug-targets due to their involvement in essential cell cycles, the implication in pathogenesis, and the interference with therapeutics. In this thesis, I report our efforts to understand the biological functions of, and to develop inhibitors against, multiple genes related to *M. tuberculosis* lipid metabolism. Firstly, dioctylamine, a substrate mimic of the mycolic acid cyclopropane synthases, is shown to inhibit CmaA2 *in vitro*. Its inhibition action is explained by the structural characterization. Together with our collaborators, we have found dioctylamine able to intervene multiple mycolic acid cyclopropane synthases *in vivo*, and hence established the first model study for the single-drug-multiple-target strategy to inhibit the mycolic acid biosynthesis of *M. tuberculosis*. In addition, dioctylamine can serve as the platform for the design of more potent and selective drugs in the future. Secondly, the action mechanism of isoniazid and ethionamide, both of which are pro-drugs targeting the mycolic acid biosynthesis, is explored via biochemical, X-ray crystallographic or modeling studies. We have determined that the intracellular target of isoniazid is the enoyl reductase InhA; and we have discovered the correlation between mycothiol and ethionamide susceptibility. Thirdly, I have investigated the function and mechanism of FadD10, an enzyme involved in the synthesis of a virulence-related lipopeptide. The results reveal that FadD10 was mis-annotated as a fatty acyl-CoA ligase, but it indeed transfers fatty acids to an acyl carrier protein (Rv0100). Further crystallographic characterization provides

the molecular basis for the mechanism of FadD10, leading to the discovery of a new type of adenylate-forming enzyme.

TABLE OF CONTENTS

	Page
ABSTRACT	ii
TABLE OF CONTENTS	iv
LIST OF FIGURES	vii
LIST OF TABLES	ix
 CHAPTER	
I INTRODUCTION AND LITERATURE REVIEW	1
<i>Mycobacterium Tuberculosis</i> Lipid Metabolism Harbor Virulence Factors And Drug Targets	1
Mycolic Acids	3
The biosynthesis and functions of <i>M. tuberculosis</i> mycolic acids	3
Direct inhibitors and pro-drugs targeting mycobacterial mycolate biosynthesis	7
Prospects of the <i>M. tuberculosis</i> CMASs as drug targets	11
Complex Surface Lipids	13
FASs, PKSs, and NRPSs are responsible for the synthesis of complex lipids	13
Complex lipids in <i>M. tuberculosis</i>	16
Other virulence factors related to complex lipids biosynthesis in <i>M.</i> <i>tuberculosis</i>	20
II MYCOLIC ACID CYCLOPROPANATION IS ESSENTIAL FOR VIABILITY, DRUG RESISTANCE AND CELL WALL INTEGRITY OF MYCOBACTERIUM TUBERCULOSIS	25
Summary	25
Introduction	26
Results	29
Deletion of <i>cmaA2</i> from BCG pasteur is only possible after complementation with a functional <i>mmaA3</i>	29
Dioctylamine inhibits multiple pathways of mycolic acid modification	33
Mycolic acid methyltransferases are direct targets of dioctylamine	36
Dioctylamine inhibits the methyltransferase activity of <i>CmaA2 in</i> <i>vitro</i>	38
The structure of <i>CmaA2</i> with bound dioctylamine reveals the	

molecular basis for activity.....	40
Dioctylamine is a growth inhibitor of BCG and <i>M. tuberculosis</i>	43
Mycolic acid modification is required for acid fastness and intrinsic resistance to antibiotics.....	46
Discussion.....	48
Experimental Procedures.....	51
Bacterial strains and growth conditions.....	51
Construction of mutant strains.....	51
Mycolic acid preparation and analysis.....	52
Radiolabeled ciprofloxacin permeability.....	52
Production of <i>M. tuberculosis</i> CmaA2.....	53
Crystallization and data collection.....	53
Structure determination and model refinement.....	54
Enzymatic assay for CmaA2.....	54
Additional Unpublished Results.....	55
Dioctylamine binds to CmaA2 <i>in vitro</i>	55
Fragment-based screening of ligands for CmaA2.....	57
Additional Unpublished Experimental Procedures.....	62
Determination of dissociation constant by fluorescence titration.....	62
Differential scanning fluorimetry (DSF).....	63
Saturation transfer difference (STD)-NMR.....	63

III CRYSTALLOGRAPHIC AND MODELING STUDIES AID THE UNDERSTANDING OF PRODRUG MECHANISM.....	64
Introduction.....	64
Results and Discussion.....	68
INH-NADP adduct formation was not observed in an <i>E. coli</i> -based activation system coexpressing <i>katG</i> and <i>dhfR</i>	68
INH-NAD adduct was detected in the <i>E. coli</i> based activation system co-expressing <i>katG</i> and <i>inhA</i>	69
Spontaneous mutants of <i>M. tuberculosis</i> , co-resistant to INH and ETH, map to <i>mshA</i>	72
Comparison of the MshA structures of <i>M. tuberculosis</i> and <i>Corynebacterium glutamicum</i> establishes a rationale for the inactivation of MshA in the mutants.....	74
Mycothiol promotes ETH activation by the <i>ethA</i> -encoded mono-oxygenase.....	77
Experimental Procedure.....	79
Cloning, expression, and purification.....	79
Enzymatic assays.....	80
Mass spectroscopy analysis.....	80
Crystallization of InhA in complex with INH-NAD adduct and data collection.....	81
Structure determination and model refinement.....	81

CHAPTER

Isolation of INH- and ETH-resistant spontaneous mutants	82
MIC determination	82
EthA enzymatic activity assay	82
IV STRUCTURES OF MYCOBACTERIUM TUBERCULOSIS FAD D10 PROTEIN REVEAL A NEW TYPE OF ADENYLATE-FORMING ENZYME	84
Summary	84
Introduction	85
Results and Discussion	90
Crystal structures of <i>M. tuberculosis</i> FadD10 subunit	90
A novel ligand-bound conformation of <i>M. tuberculosis</i> FadD10	95
The conformation of <i>M. tuberculosis</i> FadD10 prevents Coenzyme A binding	98
Modeling studies of the interactions between <i>M. tuberculosis</i> FadD10 and Rv0100	101
Substrate binding site of <i>M. tuberculosis</i> FadD10	103
Conclusion	108
Experimental Procedure	109
Cloning, protein expression, and purification	109
Crystallization	110
Data collection and processing	111
Structure determination and model refinement	113
Enzymatic assays to detect acylation of Rv0100	114
HPLC-MS analysis of dodecanoyl-amino acids	114
Additional Unpublished Results	115
Kinetics of the adenylation activity of FadD10	115
Gel filtration analysis of the interaction between FadD10 and Rv0100	116
Additional Unpublished Experimental Procedures	117
Enzymatic assays for adenylation activity	117
V CONCLUSION	119
REFERENCES	121
APPENDIX AUTHOR CONTRIBUTIONS FOR THE REPRINTED ARTICLES	141

LIST OF FIGURES

FIGURE	Page
1-1. Schematic diagram of the architecture and chemical composition of the <i>Mycobacterium tuberculosis</i> cell envelope.	4
1-2. Schematic representation of the biosynthetic pathway of <i>Mycobacterium tuberculosis</i> mycolic acids.....	6
1-3. Structures of several direct inhibitors and pro-drugs that target the <i>Mycobacterium tuberculosis</i> mycolate biosynthesis.....	8
1-4. Schematic representation of the catalytic mechanisms of PKSs and NRPSs, with minimal configuration of domains shown with cognate key active site residues.	14
1-5. Acyl loading mechanisms discovered in the biosynthesis of complex lipids.	16
1-6. Schematic diagram of the architecture and chemical composition of the <i>Mycobacterium tuberculosis</i> cell envelope.....	17
1-7. Structural and biochemical characterization of <i>M. tuberculosis</i> PKS11 led to the discovery of a new type of mycobacterial complex lipids.....	22
2-1. Chemical structures of the major mycolic acids of <i>M. tuberculosis</i> and BCG-R..	27
2-2. Genetic analysis of mycolic acid methyltransferase synthetic phenotypes.	31
2-3. Dioctylamine inhibits multiple pathways of mycolic acid modification.....	34
2-4. Mycolic acid methyltransferases are direct targets of dioctylamine.....	37
2-5. Dioctylamine inhibits CmaA2 <i>in vitro</i>	39
2-6. Structures of <i>M. tuberculosis</i> CmaA2 in complex with dioctylamine and DDDMAB/SAH.....	43
2-7. Dioctylamine inhibits growth of <i>M. tuberculosis</i>	45
2-8. Mycolic acid methyltransferases are required for drug resistance and acid fastness of <i>Mycobacteria</i>	47

FIGURE	Page
2-9. Dioctylamine binds to CmaA2 <i>in vitro</i>	56
2-10. Fragment-based screening for ligands that bind to CmaA2.....	58
3-1. The <i>Fo – Fc</i> map that is used to model the INH-NAD adduct into the active site of InhA.	70
3-2. Comparison of the MshA structures of <i>M. tuberculosis</i> and <i>Corynebacterium glutamicum</i>	76
3-3. Mycothiol promotes ETH activation by the ethA-encoded mono-oxygenase.....	78
4-1. Mutisequence-alignment of <i>M. tuberculosis</i> FadDs reveals a signature insertion for FAALs cluster..	90
4-2. The structures of apo- and complexed FadD10 with dodecanoyl-AMP.....	93
4-3. The unique inter-domain interaction of FadD10 contributes to the conformational maintenance.....	96
4-4. Modeling studies of the interactions between <i>M. tuberculosis</i> FadD10 and Rv0100.....	103
4-5. Biochemical and structural analyses suggest the biological substrate of FadD10.....	107
4-6. Kinetics of the adenylation activity of FadD10.....	117
4-7. Gel filtration analysis of the interaction between FadD10 and Rv0100.....	118

LIST OF TABLES

TABLE	Page
2-1. Data collection and refinement statistics for CmaA2 in complex with dioctylamine.	42
2-2. Lead fragments identified by DSF followed by STD-NMR.....	59
3-1. Data collection and refinement statistics for InhA in complex with INH-NAD..	71
3-2. Point mutations in and deletion of <i>mshA</i> cause different levels of resistance to INH and ETH in <i>M. tuberculosis</i>	72
3-3. The effect of mycothiol on EthA activity.....	79
4-1. Data collection and refinement statistics for FadD10 structures.....	113

CHAPTER I

INTRODUCTION AND LITERATURE REVIEW

***Mycobacterium Tuberculosis* Lipid Metabolism Harbor Virulence Factors And**

Drug Targets

Tuberculosis (TB), caused by the human pathogen *Mycobacterium tuberculosis* (*M. tuberculosis*), is a notoriously contagious disease infecting billions of people world-wide. The World Health Organization (WHO) has estimated that ten percent of this population would develop active TB in their lifetimes. Previously, the mortality caused by the disease was usually accompanied by immune system deficiency of the patients, e. g. the young, the old, and especially the HIV virus carriers. But in recent years the cases of Multi-Drug Resistant (MDR) and Extensively-Drug Resistant (XDR) tuberculosis spurt world-wide, which has made TB an alarming threat to the global health. The typical treatment of TB is the combined use of several first-line drugs including ethambutol, isoniazid, pyrazinamide, and rifampicin. Yet almost 40 years after the first use of such therapy, the category is not expanded, and the application of most second-line drugs is limited by availability, low efficacy, side-effect, or short half-life. The narrow choices of the chemotherapeutic reagents and lengthy treatment have led to the emergence of MDR and XDR-TB. Indeed, in 2010, the TB community had to exclude streptomycin, a veteran antibiotic that has been used to fight against TB for decades, from the first-line treatment due to high rates of bacterial resistance to the drug (Roger Clark, 2010). All these alarming facts have made the development of new anti-TB strategies

more urgent than ever. In this respect, extensive efforts have been made to understand the basis of *M. tuberculosis* infection, validate drug-targets, and design new drugs, facilitated by advanced informatic, genetic and proteomic tools.

M. tuberculosis, as one of the most persistent pathogen in the human society, has a very effective strategy to invade and sustain in human body. This is accompanied by a network of virulence factors that allow the bacteria to evade the human immune response, to adapt a living in host, and to withstand many antibiotics (Marina Forrellad et al., 2013). Along with the development of modern technologies, such as comparative genetics (Michelle Lopes Ribeiro-Guimarães and Maria Cristina Vidal Pessolani, 2007), transposon mutant library (Jyothi Rengarajan et al., 2005), high-throughput, proteomics (Sang Hyun Choa et al., 2006), numerous virulence factors of *M. tuberculosis* have been identified. The involvement of these factors span from essential metabolism, secretion systems, signal transduction, to interaction with host cells and defense against aggressive intracellular environment. Hence, many of them are considered promising targets for the development of new chemotherapies against TB. Multiple criteria, such as the non-homology to host (Baharak Khoshkholgh-Sima et al., 2011), the functional or structural acquisition (Solomon Nwaka and Alan Hudson, 2006), the feasibility to monitor inhibition *in vivo* (Tanjore Balganes and B. J. Furr, 2007), have been taken into account to evaluate the druggability of these virulence factors. It is noteworthy that the enzymes involved in the mycobacterial lipid metabolism have always turned out as favorite picks in different approaches for prioritizing drug targets.

The deciphering of the *M. tuberculosis* genome reveals a large number of genes,

accounting for almost 20% of the open reading frames on the genome(Stewart Cole, 1999), which are involved in the lipid metabolism. They are responsible for the biosynthesis of a wide variety of lipophilic products ranging from simple fatty acids to very-long-chain or branched species and to complexed lipids associated with multiple functional groups(S. T. Cole et al., 1998). A lot of them are unique to mycobacteria while absent in human being, and have been shown to play pivotal roles in the *M. tuberculosis* pathogenesis. Taken together with the potentially hydrophobic binding pockets implicated by their lipophilic substrates or products, the enzymes involved in the mycobacterial lipid metabolic pathways offer highly prioritized targets for the drug development against TB. Thus, understanding and eventually targeting these enzymes has become an essential and urgent subject in the field of *M. tuberculosis* studies.

Mycolic Acids

The biosynthesis and functions of M. tuberculosis mycolic acids

Cell wall is the key component in the *M. tuberculosis* cell envelope that enables the bacterium to thrive under the harsh environment inside human macrophage and intrinsically resist antimycobacterial agents(Mamadou Daffe and Philip Draper, 1998). This highly impermeable layer has a distinctive structure composed of three covalently linked macromolecules: peptidoglycan, arabinogalactan, and mycolic acids, as well as minor amount of embedded lipids. Mycolic acids are extremely long-chain (70-90 carbons totally) α -alkyl β -hydroxyl fatty acids unique to mycobacteria. The α -branch of mycolic acids is a saturated chain of 22-26 carbons. The C₄₀-C₆₀ meromycolyl chain

bears two *cis*-double bonds with different modifications which define the three sub-types (α -, keto-, and methoxy-) (Figure 1-1) of mycolates found in *M. tuberculosis*.

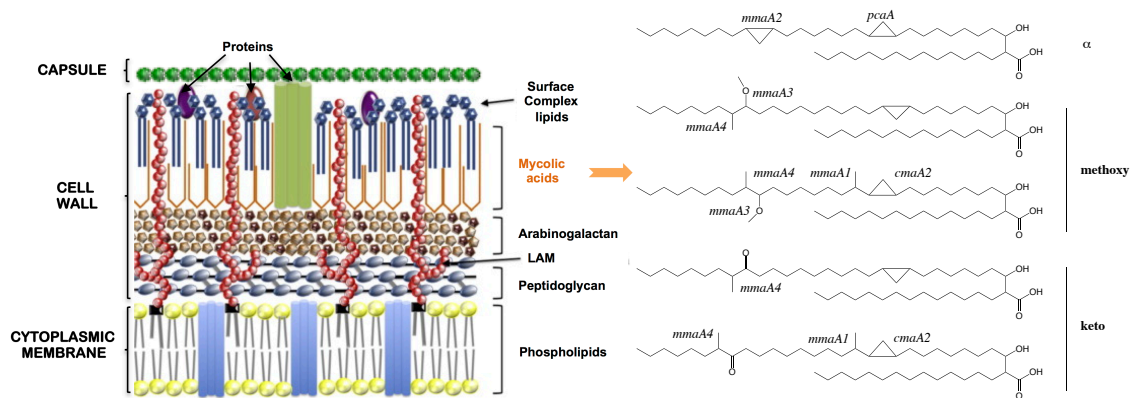


Figure 1-1. Schematic diagram(Hugues Ouellet et al., 2010) of the architecture and chemical composition of the *Mycobacterium tuberculosis* cell envelope. The chemical structures of three sub-types of mycolates (α -, keto-, and methoxy-), as well as the genes responsible for the concomitant modifications are shown in the right panel(Daniel Barkan et al., 2009).

The biosynthetic pathways of mycolic acids have been largely, but not completely, understood over years of extensive studies(Evelyn Schroeder et al., 2002; Kuni Takayama et al., 2005) (Figure 1-2). Firstly, the type I fatty acid synthetase (FAS-I), a modular enzyme elongating fatty acyl chain by repetitive catalytic cycles, produces saturated fatty acids up to C₂₆. Secondly, the very long-chain meroacids are generated based on further elongation of the FAS-I products. This is performed by the type II fatty acid synthetase (FAS-II) system composed of discrete proteins that adopt the same catalytic mechanism as FAS-I but with different substrate preferences. How the two

double bonds are placed into the meroacids is unclear, however, it is likely to involve desaturase and isomerase activities (Evelyn Schroeder et al., 2002; Kuni Takayama et al., 2005; S. T. Cole et al., 1998). Thirdly, different functional modifications are introduced to the distal and proximal double bonds on the meromycolyl chain by 8 paralogous S-adenosyl-methionine (SAM) dependent methyltransferases, also called cyclopropane mycolic acid synthases (CMASs). The last step is the condensation between the fatty acyl and meromycolyl precursors, which is mediated by the gene products of *fadD32-pks13-accD4* cluster (Damien Portevin et al., 2005) and *cmrA* (David Lea-Smith et al., 2007). The synthesized mycolyl molecules are then transported to the cell wall to esterify with arabinogalactan, glycerol or trehalose (John Belisle et al., 1997).

In addition to a constructive role as one of the cell envelope components, *M. tuberculosis* mycolic acids have also been demonstrated an explicit involvement in pathogenesis and interference with clinical practice. First, they weigh in the sustainability and persistence of *M. tuberculosis* within the hostile environment of human macrophage. This is via forming biofilms (Anil Ojha et al., 2008), maintaining the viscosity of the cell wall (Clifton Barry III et al., 1998), controlling the permeation of nutrients (Clifton Barry III et al., 1998; Joaquim Trias et al., 1992), and *et al.*. Second, mycolic acids are heavily implicated in the mycobacterial virulence. The cell wall bound mycoloyl-arabinan induces secretion of tumor necrosis factor- α (Akihiro Ishiwata et al., 2006). The mycolated glycolipids non-covalently associated to the cell wall demonstrate strong adjuvant activities, including to inhibit the migration of blood leukocytes (Samuel Martin et al., 1950), to produce granulomatous inflammation (Yuriko

Ozeki et al., 1997), to induce strong antibody response(Bekierkunst et al., 1971), and *et al.*(Clifton Barry III et al., 1998; Michael Glickman and William Jacobs Jr., 2001).

Third, the impermeable mycolate layer leads to several important features with respect to the diagnosis and treatment of TB, including acid-fast staining(Hajime Fukunaga et al., 2002) and antibiotic resistance(Clifton Barry III et al., 1998).

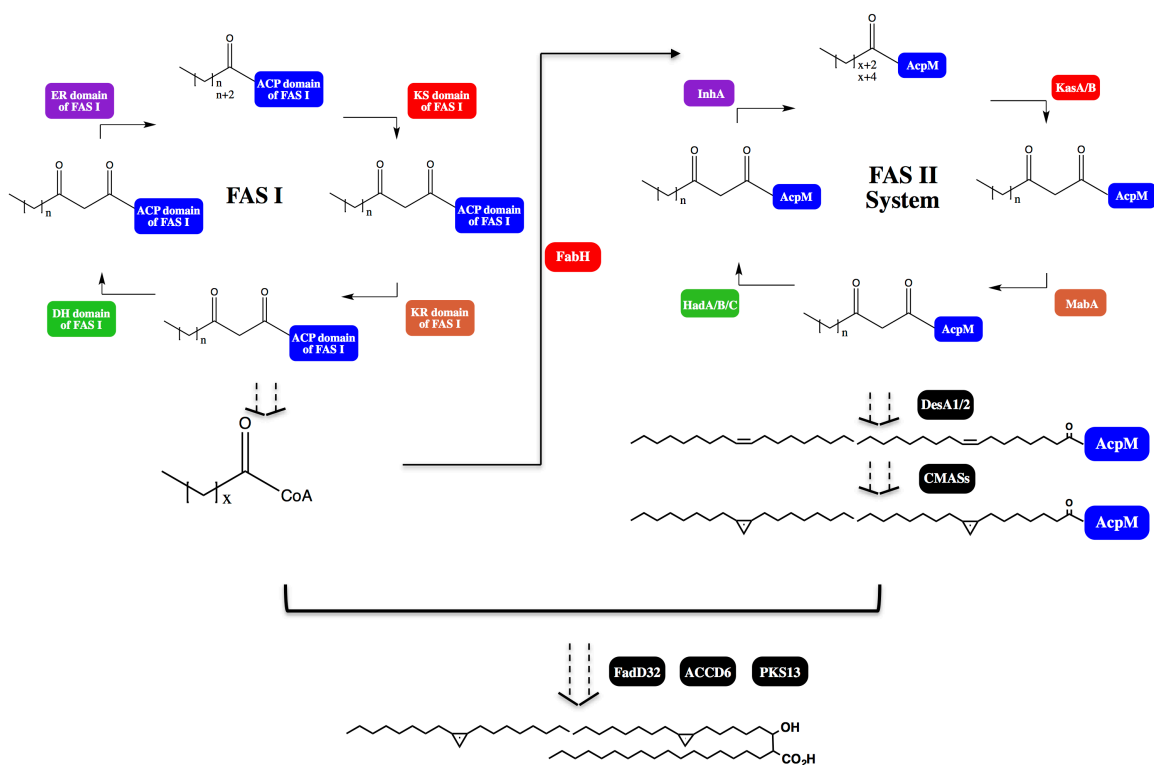


Figure 1-2. Schematic representation of the biosynthetic pathway of *Mycobacterium tuberculosis* mycolic acids. The acyl carrier protein (ACP) or ACP domain are colored blue. The enzymes or catalytic domains with β -keto acyl synthase (KS) activity, β -keto acyl reductase (KR) activity, dehydrase (DH) activity, and enoyl acyl reductase (ER) activity are colored red, brown, green, and purple, respectively.

Direct inhibitors and pro-drugs targeting mycobacterial mycolate biosynthesis

Because of their crucial biological functions, the enzymes involved in the biosynthesis of mycolic acids represent promising drug targets for combating TB. Indeed, a number of effective inhibitors interfering mycolate synthesis have been discovered and some used in practice (Evelyn Schroeder et al., 2002), which has further convinced the efficacy and prospects to target this pathway. The mode of the inhibition by these drugs or candidates can be distinguished as either directly binding at the active site of a target enzyme or being structurally modified intracellular to become a direct binder to a target enzyme.

Multiple direct inhibitors (Figure 1-3), designed or adapted from known antiseptics, of the enzymes engaged in the mycolate biosynthesis have potent anti-mycobacterial activity. For example, thiolactomycin, a natural product inhibitor of the keto-acyl-ACP synthase KasA, demonstrates excellent activity in mice (Satohide Miyakawa et al., 1982), and its analogues with improved stability and affordability are under development (James Douglas et al., 2002; Kanishk Kapilashrami et al., 2013). N-Octanesulfonylacetamide, designed to mimic the transition state intermediate of keto-acyl-ACP synthases, has promising antimicrobial activity *in vitro* (Nikki Parrish et al., 2001). Several analogues of triclosan, a widely-used antiseptics that binds to enoyl-acyl-ACP reductases, showed decent improvement in bactericidal effect after structure-guided modifications (Joel Freundlich et al., 2009).

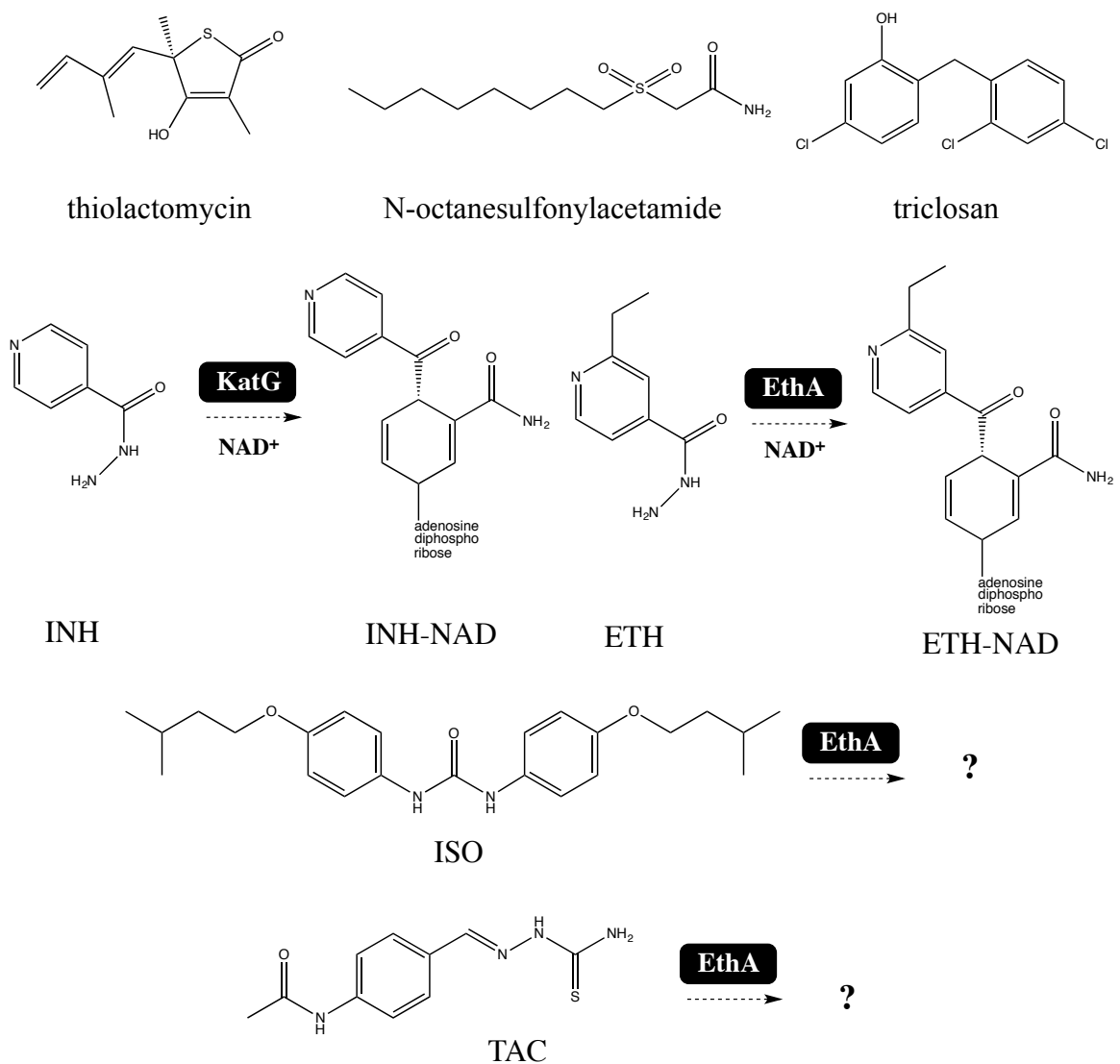


Figure 1-3. Structures of several direct inhibitors and pro-drugs that target the *Mycobacterium tuberculosis* mycolate biosynthesis.

Aside from the direct inhibitors, pro-drugs (Figure 1-3), which are converted to bioactive forms intracellular, have gained more pharmacological success in the treatment of TB. One outstanding example is isoniazid (INH), a first-line and the most prescribed anti-tubercular drug. The molecule INH itself is not toxic to the bacteria. However, once

activated by the *M. tuberculosis* catalase-peroxidase KatG, it is transformed into isonicotinoyl radical, followed by Minisci addition with NAD^+ to form the adduct INH-NAD (Martin Wilming and Kai Johnsson, 1999) which binds to the active site of the enoyl-acyl-ACP reductase InhA and strongly inhibits the enzyme ($K_i = 0.75 \text{ nM}$) (Richa Rawat et al., 2003). (*S*)-INH-NAD, the bioactive form of INH, can be readily purified from the incubation of KatG with INH and NAD^+ *in vitro* (Denise Rozwarski et al., 1998). The structure of InhA co-crystallized with (*S*)-INH-NAD has identified the chemical structure of the active adduct, interpreted explicitly the molecular basis of the binding (Denise Rozwarski et al., 1998), and explained the resistance mechanism of a highly frequent clinical isolate *M. tuberculosis S94A* (Catherine Vilchèze et al., 2006). Though the chemically synthesized isomer (*R*)-INH-NAD showed ability to bind to several other enzymes *in vitro* (Argyrides Argyrou et al., 2006a; Argyrides Argyrou et al., 2006b), there is no evidence, up to now, for the presence of such isomer in cell. In other word, InhA is the only confirmed molecular target of the prominent anti-tubercular activity of INH (Feng Wang et al., 2010), which is elaborated in CHAPTER III.

Another clinically effective pro-drug via inhibiting mycolate biosynthesis is ethionamide (ETH). It was discovered by screening a series of INH analogues for anti-tubercular activity (D. Gupta, 1977), and it indeed inhibits the same target (InhA) as INH. However, its activation is performed by a different enzyme that is the Baeyer-Villiger monooxygenase EthA (Marco Fraaije et al., 2004). Though having been used as a second-line chemotherapeutics since 1956 in the TB treatment, the active form of ETH was not identified until recently. Using a whole-cell based activation system, where *M.*

tuberculosis EthA and InhA were co-expressed by *E. coli* in presence of ETH, Sacchettini and associates (Feng Wang et al., 2007b) were able to isolate InhA bound to the bioactive adduct formed by ETH. Biochemical and structural characterizations have elucidated the compound to be ethyl isonicotinoyl-NAD (ETH-NAD). It is very similar to INH-NAD in both the structure and the binding mode in the InhA active site (Feng Wang et al., 2007b). EthA is clearly not as efficient as KatG to activate the cognate pro-drug *in vitro*. The function of EthA can only be realized *in vivo*, while its *in vitro* activity ($K_{cat} = 0.0063 \text{ s}^{-1}$) is unusually low compared with the other homologous monooxygenases. This indicates that other cellular components are involved to complete the EthA function. We have found out that one of these factors is the reducing agent mycothiol by genetic, biochemical, and modeling studies (Catherine Vilchèze et al., 2008), which are discussed in CHAPTER III.

Isoxyl (ISO) and thiacetazone (TAC), two pro-drugs for treating MDR-TB strains, are also implicated to interfere with the synthetic pathway of mycolic acids. Both drugs share a thioamide motif and a common activator EthA with ETH (Lynn Dover et al., 2007). Spontaneous ISO- and TAC-resistant mutations have been located at multiple genes responsible for the mycolate synthesis. They include CMASs (*mmaA2*, *mmaA4*) and hydroxyacyl-ACP dehydratases (*had ABC*) (Anna Grzegorzewicz et al., 2012). It is also shown that over-expression of CMASs (*CmaA2*, *PcaA*) (Anuradha Alahari et al., 2007) or the desaturase (*DesA3*) (Benjawan Phetsuksiri et al., 2003) confers certain level of resistance to TAC or ISO. Though the bioactive metabolites and the precise

mechanism of TAC and ISO are still elusive, it is likely that their cellular targets are among the identified relevant enzymes.

Prospects of the M. tuberculosis CMASs as drug targets

Certainly pro-drugs have exhibited chemotherapeutic values, but their disadvantages in drug development and clinical administration are obvious. First, the complication of a pro-drug's mechanism makes the drug development more challenging. As discussed above, we still lack a lot of knowledge regarding their intracellular metabolism and functional mode. This has prevented the pursuit of a better inhibition and less side effects based on a known pro-drug's structure. Second, the involvement of activating enzymes poses a higher chance for the development of drug-resistant mutants, which have been observed in numerous clinical isolates when patients are treated with pro-drugs (Andrea DeBarber et al., 2000; Angelo Scorpio et al., 1997; Stephen Gillespie, 2002; Ying Zhang et al., 1992). Therefore, it is still our hope to pursue antimicrobials that can directly inhibit the enzymes in the mycolic acid synthetic pathway.

The improper usage of antibiotics and lengthy treatment have led to a steady increase of drug-resistant *M. tuberculosis* strains. The need for new anti-tubercular agents is more urgent than ever, especially to enable shorter-course therapy and to delay the occurrence of drug resistance. For this purpose, a very promising strategy is to use a single inhibitor against multiple targets (Richard Morphy and Zoran Rankovic, 2005). This prefers the targeted proteins to have similar binding affinity but non-redundant functions, exemplified by acyl-AMP analogues to inhibit several *M. tuberculosis* FadD

proteins which are involved in separate lipid synthetic pathways(Pooja Arora et al., 2009). The CMASs also satisfy such criteria.

Eight SAM dependent CMASs are identified in *M. tuberculosis*, sharing a high sequence homology (~ 50% identity to each other). Cell-based analyses and *in vitro* experiment using radioactive precursors have determined their biochemical activities (Figure 1-1), except for CmaA1(Eugenie Dubnau et al., 1997; Laxman Meena et al., 2013; Michael Glickman et al., 2000; Michael Glickman et al., 2001; Ying Yuan and Clifton Barry III, 1996; Ying Yuan et al., 1997). Separate knock-out strains of each CMAS have been generated and evaluated the physiological properties(Dee Dao et al., 2008; Eugenie Dubnau et al., 2000; Michael Glickman et al., 2000; Pascale Peyron et al., 2008; Vivek Rao et al., 2006; Vivek Rao et al., 2005). The studies reveal that each CMAS performs a distinct chemical modification on the meroacyl chain of *M. tuberculosis* mycolate and is implicated at a different stage of infection. In addition, five CMASs have been structurally characterized, which exhibit an apparent similarity in their active site composition(Chih-chin Huang et al., 2002; Fanny Boissier et al., 2006). This, coupled with the distinct biological functions of CMASs, suggests that CMASs are applicable as targets of a single drug. Indeed, we(Daniel Barkan et al., 2009) and Lionel Mourey *et al.*(Julien Vaubourgei et al., 2009) have independently showed dioctylamine (elaborated in CHAPTER II) and S-adenosyl-N-decyl-aminoethyl, respectively, able to inhibit multiple CMASs and consequently the mycobacterial growth. These studies together have unequivocally indicated CMASs as promising targets for the drug

development and have proven the feasibility to inhibit multiple CMASs simultaneously by a single compound.

Complex Surface Lipids

FASs, PKSs, and NRPSs are responsible for the synthesis of complex lipids

Complex lipids are based on simple fatty acids which are incorporated with a variety of functional groups including phosphate, glycosidic, peptidyl moieties, and *et al.* They widely occur in nature, especially in plants and bacteria, as secondary metabolites, and demonstrate broad bioactivities such as antibiotics, surfactants, and virulence factors(Mohamed Marahiel et al., 1997). The major chemical scaffolds of the complex lipids are typically synthesized by three multifunctional enzymes that are fatty acyl synthase (FASs), polyketide synthases (PKSs) and non-ribosomal peptide synthases (NRPSs). They are similar in the architecture in terms of that all of them can occur as either modular multi-enzymes or enzyme clusters with discrete members. They are also mechanistically analogous in the way to catalyze repetitive reaction cycles (Figure 1-1, Figure 1-4). Together with these “megasyntases”(Timm Maier et al., 2008), other enzymes or functional domains are associated in the biosynthetic pathways of complex lipids. They are responsible for either the crosswalk between the multi-enzymes(Darren Hansen et al., 2007; Debasisa Mohanty et al., 2011) or the introduction of specific chemical modifications on the core structures(Deborah Miller et al., 2001; Thomas Keating et al., 2002).

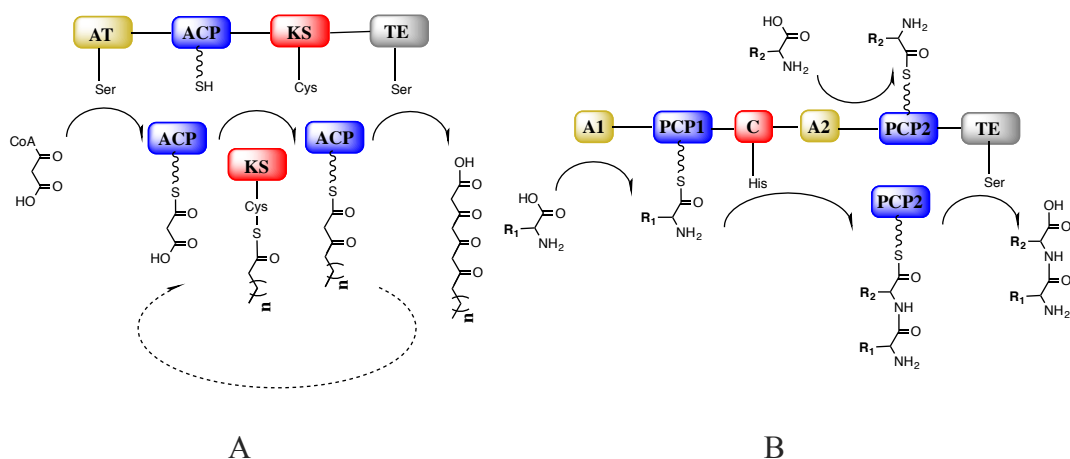


Figure 1-4. Schematic representation of the catalytic mechanisms of PKSs (A) and NRPSs (B), with minimal configuration of domains shown with cognate key active site residues. Both ACPs (acyl carrier protein domains) of PKSs and PCPs (peptidyl carrier protein domains) of NRPSs are phosphopantetheinated so that to bear free thiol termini. The reactions catalyzed by both types of the enzymes undergo a process including: substrate loading, repetitive cycles of elongation, and product release.

(A) For PKSs, in each reaction cycle, a malonyl group is loaded by AT (acyltransferase domain) onto ACP; each elongation step involves decarboxylation of malonyl followed by claisen condensation with the template acyl chain, mediated by KS (β -keto acyl synthase domain); the thioesterified product is eventually hydrolyzed and released by TE (thioesterase domain).

(B) NRPSs require three domains to assemble peptides – adenylation (A), PCP, and condensation (C) domains. Each A domain selectively activates an amino acid substrate and loads in onto the cognate PCP. C domain catalyzes the nucleophilic attack from the downstream PCP-carried amino group to the upstream PCP-carried aminoacyl or peptidylacyl moieties, forming a new peptide bond. The final products are typically released by TE domain, similar to PKSs.

Because of the chemotherapeutic values and physiological significance of complex lipids, tremendous efforts have been made to decipher their biosynthesis. Yet the territory seems borderless while novel mechanisms are discovered time after time. One example is the discovery of an acyl loading mechanism alternative to the predominant O-fatty acyl transferases (AT). The latter are found either as a catalytic domain of a multi-enzyme (mostly a FAS or PKS) or an individual enzyme. They use

selective fatty acyl-CoAs as substrates and are able to uptake the fatty acyl moieties by esterification with the conserved active site serine residue. The acyl chains are then transferred to ACPs for transport to other catalytic centers in a biosynthesis (Figure 1-5 A). This acyl-CoA and acyltransferase dependent mode was the only recognized acyl loading mechanism for the biosynthesis of naturally occurred complex lipids, until recently an alternative scheme is discovered. In the new mechanism, an adenylate-forming enzyme directly uses fatty acids to generate fatty acyl-AMPs as intermediates and transfer fatty acyl moieties to cognate ACPs for further process (Figure 1-5 B). The first biochemical presentation of such a mechanism was reported when the *M. tuberculosis* adenylate-forming enzymes FadD26, FadD30, FadD32 were shown to transfer the cognate fatty acid substrates to their cooperative PKSs, which are PpsA, PKS6, and PKS13, respectively(Omita Trivedi et al., 2004). The function of this subclass of adenylate-forming enzymes is further established with the demonstration of fatty acyl transfer by *Bacillus subtilis* ATP dependent acyl ligase AL onto the acyl carrier protein ACP1. Both proteins were isolated from the lipopeptide mycosubtilin synthetic pathway, and the acyl transfer occurred in absence of CoenzymeA or derivatives(Darren Hansen et al., 2007). This newly discovered activity of adenylate-forming enzymes has been classified as fatty acyl-AMP ligases (FAALs) which are discussed more detailed later in this CHAPTER and CHAPTER IV.

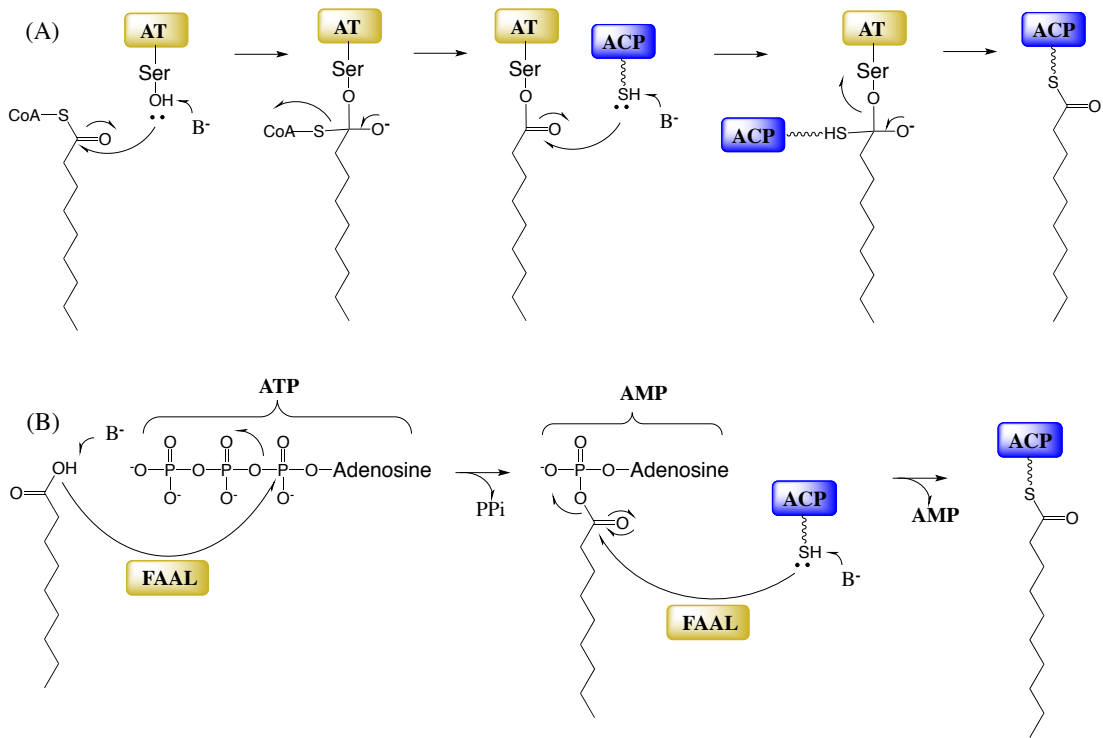


Figure 1-5. Acyl loading mechanisms discovered in the biosynthesis of complex lipids. They can be catalyzed by, respectively, (A) a fatty acyl transferase (AT), and (B) a fatty acyl-AMP ligase (FAAL).

Complex lipids in M. tuberculosis

Analyses of the *M. tuberculosis* genome reveal the presence of a *fas I* gene, a *fas II* gene cluster, 2 *nrps* containing gene clusters, and 25 *pks* genes (S. T. Cole et al., 1998). Consistent with the variety of these genes related to lipid metabolism, an unusually large amount and diversity of complex lipids have been discovered in *M. tuberculosis*, which outweigh any other pathogenic bacteria. All of these complex lipids are found in the extract of *M. tuberculosis* cell envelope, and hence are likely to function in determining the physical properties of the cell envelope or mediating specific host-pathogen interactions. The lipid components anchoring at *M. tuberculosis* capsule are at minor

amount and their identities remain elusive. Other than that, multiple complex lipids associated to the plasma membrane and the cell wall are present at reasonable amount to be isolated and chemically characterized (Figure 1-6).

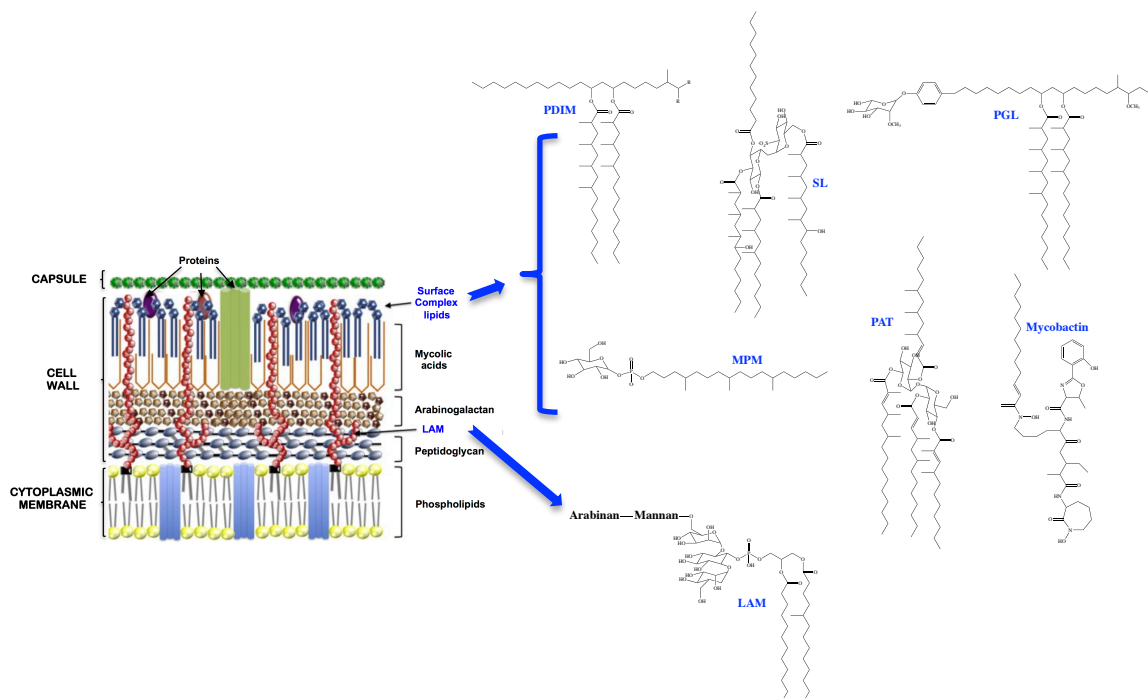


Figure 1-6. Schematic diagram(Hugues Ouellet et al., 2010) of the architecture and chemical composition of the *Mycobacterium tuberculosis* cell envelope. The chemical structures of complex lipids, identified up to date, are shown in the right panel.

Lipomannan (LM) and lipoarabinomannan (LAM) (Anna Grzegorzewicz et al.), two major mycobacterial glycolipids, are found to be non-covalently associated to the plasma membrane and extend their lipidic tails beyond the cell wall. Defects in LM/LAM synthesis result in an increased susceptibility of *M. tuberculosis* to β -lactam antibiotics which implies a higher permeability of the cell envelope(Takeshi Fukudaa et

al., 2013). The mannosyl cap of LAM is suggested to interact with the mannose receptor of human macrophage so that to induce cell entry at the early stage of infection(Jordi Torrelles and Larry Schlesinger, 2010). Complex lipids intercalated in the cell wall, as identified up to date, include phthiocerol dimycocerosates (PDIMs), sulfolipids (SLs), polyacyl trehaloses (PATs), mannosyl phosphomycoketides (MPMs), and phenolic glycolipids (PGLs). PDIMs are heavily implicated in the *M. tuberculosis* virulence especially at the early stage of infection(Cécile Rousseau et al., 2004). They can insert into the membrane of human macrophage and alter the lipid organization on the surface of the macrophage, which eventually facilitates the invasion of *M. tuberculosis* bacilli into the host(Catherine Astarie-Dequeker et al., 2009). SLs are also abundant complex lipids, second to PDIMs, found in the *M. tuberculosis* cell wall. Apart from a role in maintaining the cell wall integrity, their precise function in virulence is not yet established as the compounds induce a wide-profile of transcriptional effects in human immature dendritic cells(Sarah Gilmore et al., 2012). PATs are located on the exterior surface of the cell wall. They have a wax nature to prevent the mycobacterial cells to clump with each other(Vinod Dubey et al., 2002). Yet there is no evidence for their contribution to virulence, the production of PATs responds to different stress environments *in vivo*(Kyle Rohde et al., 2007). MPMs are produced at a low amount in the slow-growing pathogenic mycobacteria. They display antigenicity via interacting with the human CD1 proteins that are produced by antigen expressing cells(Isamu Matsunaga and Masahiko Sugita, 2012). This has been delineated by the crystal structure of human CD1 protein in complex with the *M. tuberculosis* MPM(Louise Scharf et al.,

2010). Mycobacterial PGLs are not observed in *M. tuberculosis* except for the hypervirulent Beijing strains. The lipids directly suppress the release of three different pro-inflammatory mediators of human macrophage, and consequently lead to the hyperlethality of certain *M. tuberculosis* strains (Michael Reed et al., 2004). *M. tuberculosis* Mycobactins are present either as associates to the cell wall or secreted molecules. The secreted mycobactins are responsible to extract extracellular iron, while the cell wall associated mycobactins store the iron for following acquisition into the cell (Minkui Luo et al., 2005).

The biosynthesis of complex lipids is as complicated as their structures, but genome sequencing, knock-out studies, and biochemical demonstrations have provided chances to decipher the synthetic pathways of the *M. tuberculosis* complex lipids. Except for LM and LAM, they all engage at least one PKS or NRPS multi-enzyme. Multiple PKSs annotated as PpsA-E are responsible to elongate and incorporate diol groups onto the phthiocerol chain of PDIMs; the mycocerosic chains are synthesized by another PKS annotated as Mas; and the phthiocerol dimycocerosyl transferase PapA5 catalyzes the condensation between the mycocerosic and phthiocerol chains. The synthesis of PGLs shares the same core steps as PDIMs, except that a gene cluster of *Rv2949-pks15-pks1* generates the phenolic precursor prior to the action of PpsA-E. PKS2 produces the long acyl moieties of SLs, and the acyltransferases PapA1, PapA2 and Chp1 link different acyl chains to the trehalose hydroxyl groups (Jessica Seeliger et al., 2012). PATs have similar chemical scaffolds, as well as synthetic scheme as SLs, just involving a different set of PKS (PKS3/4) and acyltransferase (PapA3).

Mycobacterial PKS12 is responsible to synthesize the long mycoketide chain of MPMs. Consistent with the discovery of MPMs, PKS12 is only found in the pathogenic mycobacteria. It catalyzes alternative and repetitive cycles of reactions to incorporate ethylene and isopropyl moieties into the growing chain (Tarun Chopra et al., 2008). However, no enzymes have been identified for the reduction, phosphorylation, or mannosylation step to generate the final products MPMs. The biosynthesis of mycobactins is carried out by a hybrid system of PKSs (annotated as MbtC/D) and NRPSs (MbtB/E/F) cooperated with the ligase MbtA, the salicylate synthases MbtI, the hydroxylase MbtG, and four lipid binding proteins (MbtK, MbtL, FadD33, and FadE14) (Matthew McMahon et al., 2012).

Other virulence factors related to complex lipids biosynthesis in M. tuberculosis

The composition of surface lipids is an important feature that distinguishes pathogenic and non-pathogenic mycobacteria. For example, MPMs and PGLs are only found in pathogenic species while glycopeptidyl lipids are only produced by some opportunistic pathogenic species (Jeffrey Schorey and Lindsay Sweet, 2008). It is tempting to believe that surface lipids are one of the predominant factors among all the virulence effectors of the pathogenic mycobacteria, such as *M. tuberculosis*. Therefore, to better understand the survival mechanism of this notorious bacteria against the human immune system, it is critical for us to identify these surface lipids and elucidate their biosynthesis. However, our knowledge in both aspects remains at large. As discussed above, most PKSs found in the *M. tuberculosis* genome have not been attributed to the

synthesis of known metabolites. In addition, there are wide array of probable lipid binding proteins that have been shown to contribute the *M. tuberculosis* pathogenesis. They together indicate the presence of many other virulence related lipids to be identified, and also highlight the need to functionally characterize the proteins likely involved in the biosynthesis of surface lipids. At least three categories of targets should be deliberately investigated in this respect.

First, 15 among the 25 PKSs discovered in the *M. tuberculosis* genome have been confirmed with functions in the biosynthesis of mycolate, cell wall complex lipids, and mycobactins, respectively, while the functions of the other 10 PKSs remain ambiguous. The prevailing strategy to explore the roles of PKSs is to generate the knock-out strains followed by analyses of the change in lipid composition. This method has provided valuable insights as well as some biased outputs. The challenge of the method lies in the complicated cellular activities associated with many unknown regulation mechanisms. For example, *pks12* was once linked to the synthesis of PDIMs as the gene deletion caused deficient PDIMs in the cell wall (Tatiana Sirakova et al., 2003). However, explicit biochemical demonstration later on amended the true function of PKS12 as a mycoketide synthase (Tarun Chopra et al., 2008), though its regulatory role in PDIM production is still mysterious. In addition to the *in vivo* approach, structural and biochemical characterization has shown potential to imply the function of a PKS. It is exemplified by the studies on *M. tuberculosis* PKS11 (Kuppan Gokulan et al., 2013). When expressed by *M. smegmatis*, a soil organism closely related to *M. tuberculosis*, PKS11 is naturally bound to palmitic acid which is likely to be the

biological substrate. A more revealing observation is that the addition of malonyl-CoA and methylmalonyl-CoA leads to the formation of methylbranched alkylpyrone (Figure 1-7) which is bound at the active site of PKS11, clearly evidenced by both X-ray structure and mass spectra. Though there is no reported isolation of methylbranched alkylpyrones from *M. tuberculosis*, the studies of PKS11 has strongly indicated the presence of such lipids. Moreover, it proves the hypothesis that versatile lipids still remain to be identified and functional characterization of the enzymes related to lipid metabolism is highly applicable to address the issue.

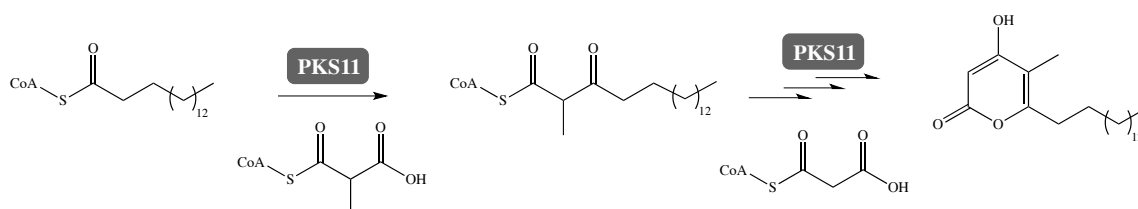


Figure 1-7. Structural and biochemical characterization of *M. tuberculosis* PKS11 led to the discovery of a new type of mycobacterial complex lipids- methylbranched alkylpyrones(Kuppan Gokulan et al., 2013).

Second, there are two NRPS containing gene clusters identified in *M. tuberculosis*(S. T. Cole et al., 1998). While one of them has been attributed to synthesize the peptidyl moiety of mycobactins, the function of other one, *Rv0096-Rv0101* operon, is yet understood. *Rv0096* belongs to the PE/PPE family which is a immunogenetic protein. *Rv0097* is a putative oxidoreductase. *Rv0098* is a fatty acyl-CoA thioesterase(Feng Wang et al., 2007a). *Rv0099* (*fadD10*) is a lipid binding enzyme.

Rv0100 encodes an acyl carrier protein. *Rv0101*, annotated as *nrp*, is an NRPS which is highly conserved in the human pathogen *M. bovis* and *M. leprae*. While the operon is not required for the survival of *M. tuberculosis in vitro* (Christopher Sassetti et al., 2003), each of the genes correlates to the mycobacterial virulence (Christopher Sassetti and Eric Rubin, 2003; Swati Joshi et al., 2003). The precise product of the operon and its exact biological function are yet elucidated. In a transposon mutagenesis study, mutation of *Mb0100* in the *M. bovis* BCG strain (equivalent to *M. tuberculosis Rv0097*) was shown to disrupt the biosynthesis of PDIMs and glycosylphenol-PDIMs (Grant Hotter et al., 2005), but whether the components of the operon have a direct role in PDIM synthesis is uncertain. Others have argued that the product of the *PPE-nrp* operon would function via de-repressing the sigma factor SigM which further regulates synthesis of a series of surface lipids including PDIMs (Nisheeth Agarwal et al., 2007). Nrp shares significant similarity with an *M. smegmatis* NRPS-encoding gene *mps* which is involved in the production of glycopeptidyl lipids. However, no glycopeptidyl lipids or close analogues have been reported in the pathogenic mycobacteria, and hence a role of *M. tuberculosis* Nrp similar to *M. smegmatis* Mps has been ruled out. Yet the roles of Rv0098 and FadD10 in lipid metabolism suggest that the products of the operon are likely to be lipopeptides. We have determined the structure and function of FadD10, which shines light on the identification of the virulence-associated lipopeptides and the understanding of the biological role. These studies are discussed in CHAPTER IV.

Third, associated with mycobacterial lipid metabolism, are a notable variety of lipid binding proteins, which can be exemplified by 14 transmembrane lipid transport

proteins (MmpLs), 36 possible fatty acyl-CoA dehydrogenases (FadEs), and 34 possible fatty acyl-CoA synthetases (FadDs). Surely the versatility of complex lipids necessitates the diversity of the supportive proteins, but such a wide array of redundancy still induces doubt on a rough functional classification. Indeed, the annotation of FadD enzymes has been amended after further investigations into individual members. *M. tuberculosis* FadDs were initially thought to be engaged in the fatty acid degradation, analogous to *E. coli* FadD (David Clark and John Cronan, 1996). Yet soon several FadDs were found important for the synthesis of cell wall lipids, such as FadD32 for mycolates, FadD26 for PDIMs, FadD23 for SLs (Tarun Chopra and Rajesh Gokhale, 2009). A series of genetic, biochemical, and structural analyses have then been conducted to elucidate the distinctive functions of *M. tuberculosis* FadDs, which has led to the recent discovery of fatty acyl-acyl carrier protein synthetase activity in some of the them (Omita Trivedi et al., 2004; Pooja Arora et al., 2009). These FadDs which are likely to be responsible in anabolism instead of metabolism have been re-annotated as fatty acyl-AMP ligases (FAALs). However, the new annotation is solely based on sequence similarity which has been proven to be a rough criteria. As elaborated in CHAPTER IV, we have found that FadD10, mis-annotated as fatty acyl-CoA synthetase, is indeed an FAAL to transfer fatty acyl chains to an acyl carrier protein (Rv0100) (Zhen Liu et al., 2013). This contradicts the current sequence-based paradigm for the classification of FadDs, and necessitates further investigations into the enzymes of the newly identified FAAL subclass.

CHAPTER II

MYCOLIC ACID CYCLOPROPANATION IS ESSENTIAL FOR VIABILITY, DRUG
RESISTANCE AND CELL WALL INTEGRITY OF MYCOBACTERIUM
TUBERCULOSIS*

Summary

Mycobacterium tuberculosis infection remains a major global health problem complicated by escalating rates of antibiotic resistance. Despite the established role of mycolic acid cyclopropane modification in pathogenesis, the feasibility of targeting this enzyme family for antibiotic development is unknown. We show through genetics and chemical biology that mycolic acid methyltransferases are essential for *M. tuberculosis* viability, cell wall structure, and intrinsic resistance to antibiotics. The tool compound dioctylamine, which we show acts as a substrate mimic, directly inhibits the function of multiple mycolic acid methyltransferases, resulting in loss of cyclopropanation, cell death, loss of acid fastness, and synergistic killing with isoniazid and ciprofloxacin. These results demonstrate that mycolic acid methyltransferases are a promising antibiotic target and that a family of virulence factors can be chemically inhibited with effects not anticipated from studies of each individual enzyme.

* This work has been published in and is reprinted with permission from: Daniel Barkan[#], Zhen Liu[#], James Sacchettini, and Michael Glickman (# equal contribution). “Mycolic acid cyclopropanation is essential for viability, drug resistance and cell wall integrity of *Mycobacterium tuberculosis*” *Chemistry & Biology* 2009, 16(5), 499-509 Copyright 2009 (Elsevier Inc.)

Introduction

Human infection with *Mycobacterium tuberculosis* continues to cause unrelenting suffering. Although infection with *M. tuberculosis* is curable with prolonged multidrug antibiotic therapy, the drug regimens are often toxic or difficult to complete. In the developing world, curative therapy for *M. tuberculosis* is difficult to execute, leading to two million deaths per year worldwide (Christopher Dye, 2006). Infection with antibiotic-resistant *M. tuberculosis* is an increasing problem and requires more prolonged antibiotic therapy for cure (World Health Organization, 2008). In the case of extensively drug-resistant tuberculosis, therapy is often impossible (Neel Gandhi et al., 2006). This dire reality has prompted a significant worldwide effort to discover new drugs to treat *M. tuberculosis* infection. Although any new agent active against *M. tuberculosis* would be welcome, of particular interest are new drugs that would allow shortening of tuberculosis chemotherapy through rational targeting of gene products important for persistent infection. An increasing number of potential drug targets in *M. tuberculosis* are cell wall biosynthetic enzymes, including enzymes involved in mycolic acid biosynthesis and modification.

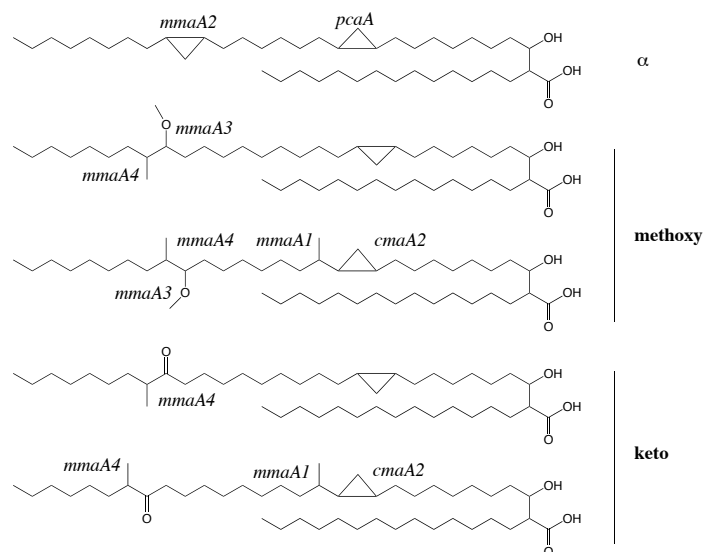


Figure 2-1. Chemical structures of the major mycolic acids of *M. tuberculosis* and BCG-R. Cyclopropane rings and methyl branches are shown and annotated with the methyltransferase responsible for their synthesis. BCG-P lacks methoxymycolates due to a mutation in *MmaA3*.

Mycolic acids are α -alkyl, β -hydroxy fatty acids that are produced by all mycobacteria and are the signature lipid of the hydrophobic mycobacterial cell wall. Mycolic acid biosynthesis has been intensely studied due to the unique structure of these lipids and their importance for tuberculosis antibiotic therapy and *M. tuberculosis* pathogenesis (Clifton Barry III et al., 1998). *M. tuberculosis* and *Mycobacterium bovis* produce three major mycolic acid types: alpha mycolate, methoxymycolate, and ketomycolate. The chemical structures of these lipids shown in Figure 2-1 were determined over years of exhaustive study (Clifton Barry III et al., 1998; Motoko Watanabe et al., 2002; Motoko Watanabe et al., 2001). Although the core mycolate structure is conserved among mycobacteria, only pathogenic slow growing mycobacteria produce significant amounts of cyclopropanated mycolic acids. Alpha mycolic acids

contain two *cis* cyclopropane rings on the meromycolate chain. Oxygenated mycolates contain either a distal methoxy or ketone group and a proximal *cis* or *trans* cyclopropane ring. The cyclopropane rings and methyl branches of these lipids are synthesized by a family of S-adenosyl methionine-dependent methyltransferases. The enzymes of this family are highly homologous both in primary sequence and tertiary structure (Chih-chin Huang et al., 2002). Despite this structural similarity, genetic deletion of each methyltransferase in *M. tuberculosis* has revealed highly specific biosynthetic roles of each enzyme. PcaA and MmaA2 are required for alpha mycolate cyclopropanation (Michael Glickman, 2003; Michael Glickman et al., 2000), CmaA2 for *trans* cyclopropanation of the oxygenated mycolates (Michael Glickman et al., 2001), MmaA4 and MmaA3 for distal functionality of the oxygenated mycolates (Eugenie Dubnau et al., 2000; Marcel Behr et al., 2000), and MmaA1 for methyl branch formation preceding the cyclopropanation step by CmaA2 (M.S.G., unpublished data).

M. tuberculosis strains deficient for cyclopropanation have revealed an important role for this lipid modification in pathogenesis. Loss of *pcaA* in *M. tuberculosis* causes an early growth defect in the lungs, defective persistence during late infection, and failure to activate macrophage innate immune responses (Michael Glickman et al., 2000; Vivek Rao et al., 2005). In contrast, loss of *cmaA2* results in hypervirulence and hyperinflammatory innate immune activation in macrophages (Vivek Rao et al., 2006) and loss of *mmaA4* causes excessive IL-12 production (Dee Dao et al., 2008). These phenotypes are due to altered inflammatory activity of cyclopropane-deficient trehalose dimycolate, implicating cyclopropanation as an immunomodulatory lipid

modification(Dee Dao et al., 2008; Vivek Rao et al., 2006; Vivek Rao et al., 2005). However, these results do not clearly define mycolic acid methyltransferases as an attractive drug target in *M. tuberculosis* because the consequences of complete cyclopropane loss are unknown and targeting of CmaA2 alone in preference to other methyltransferases might be deleterious to the host.

In this study we address the suitability of mycolic acid methyltransferases as *M. tuberculosis* drug targets. We show that the mycolic acid methyltransferase enzyme family can be targeted by a single tool compound and that this inhibition has pleiotropic effects on *M. tuberculosis* cells, including loss of cell wall integrity and eventual cell death.

Results

Deletion of cmaA2 from BCG pasteur is only possible after complementation with a functional mmaA3

Previous work from our laboratory and others has shown that mycolic acid methyltransferases are individually nonessential for growth in vitro(Dubnau et al., 1998; Eugenie Dubnau et al., 2000; Marcel Behr et al., 2000; Michael Glickman, 2003; Michael Glickman et al., 2000; Michael Glickman et al., 2001), including the *trans* cyclopropane synthase of the oxygenated mycolates CmaA2. As we have shown that deletion of *cmaA2* from *M. tuberculosis* produces a hypervirulent strain(Vivek Rao et al., 2006), we attempted to delete this gene from BCG Pasteur (BCG-P) to study its effect on BCG immunogenicity. To delete *cmaA2*, we infected BCG-P with a

temperature-sensitive specialized transducing phage designed to replace the entire *cmaA2* coding sequence with a hygromycin resistance gene. To our surprise, despite our prior deletion of *cmaA2* from *M. tuberculosis* using the same technique, we were unable to obtain hygromycin-resistant transductants on multiple attempts (data not shown). We have successfully deleted multiple genes from BCG-P using specialized transduction (data not shown; (Hideki Makinoshima and Michael Glickman, 2005; Michael Glickman et al., 2000), indicating that our failure to obtain a *cmaA2* knockout was not due to a general failure of this technique in this strain. BCG-P, along with many other BCG substrains, lacks methoxymycolates due to a point mutation in *mmaA3*, the gene encoding the methyltransferase that adds the methoxy group to methoxymycolates (Marcel Behr et al., 2000). BCG Russia (BCG-R) has a functional *MmaA3* and therefore synthesizes methoxymycolates. We were able to delete *cmaA2* from BCG-R using the same specialized transducing phage that failed in BCG-P (Figure 2-2 A), indicating that lack of methoxymycolates may be the factor preventing *cmaA2* deletion in BCG-P. To test this idea, we complemented BCG-P at the chromosomal *attB* site with the *mmaA3* gene (BCG-P *attB::mmaA3*). As previously reported (Adam Belley et al., 2004; Dubnau et al., 1998; Marcel Behr et al., 2000), BCG-P *attB::mmaA3* synthesized methoxymycolates (Figure 2-2 B). Transduction of BCG-P *attB::mmaA3* with the *cmaA2* knockout phage resulted in successful deletion of *cmaA2* (Figure 2-2 C). To confirm that the function of *cmaA2* in BCG is to synthesize *trans* cyclopropane rings, as previously shown in *M. tuberculosis* (Michael Glickman et al., 2001), we isolated total mycolic acids from the BCG *attB::mmaA3 cmaA2::hyg* strain and analyzed them by

nuclear magnetic resonance (NMR). *Trans* cyclopropane rings were not detected in the $\Delta cmaA2$ strain, confirming that the function of CmaA2 is identical in BCG and *M. tuberculosis*. This data suggested that null mutations in *mmaA3* and *cmaA2* may be synthetically lethal for slow growing mycobacteria.

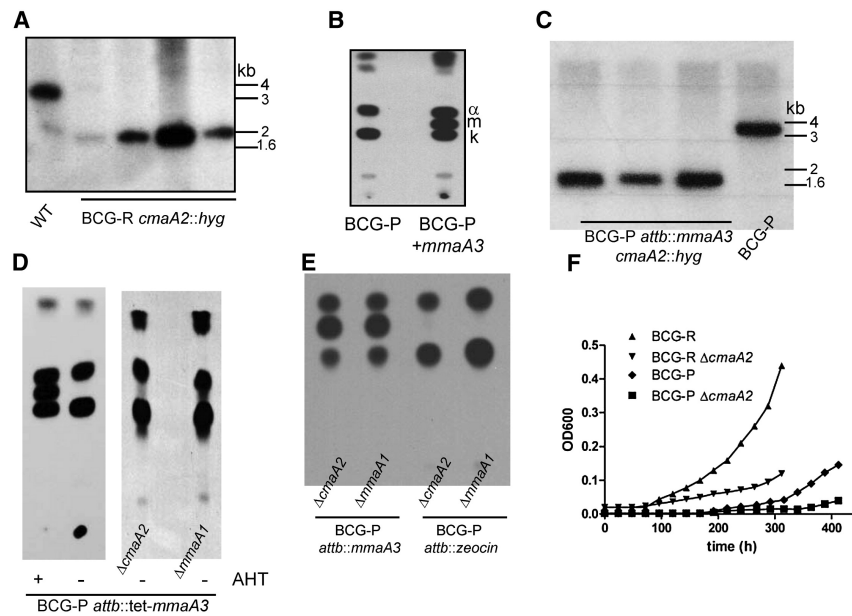


Figure 2-2. Genetic analysis of mycolic acid methyltransferase synthetic phenotypes. (A) Southern blot showing the deletion of *cmaA2* from BCG-R. Genomic DNA was cut with EcoRI and probed with a DNA fragment flanking *cmaA2*. The predicted size for wild-type is 3.8 kb and for $\Delta cmaA2$ is 1.8 kb. (B) Radio TLC from BCG-P and BCG-P *attB:: mmaA3*, showing the appearance of methoxymycolates in the complemented strain. α , alpha mycolates; m, methoxymycolates; k, ketomycolates. (C) Southern blot showing deletion of *cmaA2* from BCG-P *attB::mmaA3*. Fragment sizes are as in (A). (D) BCG-P was complemented at the *attB* site with *mmaA3* gene under an AHT-sensitive promoter and mycolic acids were analyzed from strains grown with (+AHT) and without (-AHT) inducer. After the deletion of *cmaA2* or *mmaA1* from this strain (while supplementing with AHT), AHT was withdrawn and mycolic acids were prepared. (E) Radio TLC showing the removal of *mmaA3* by zeocin marker exchange. Mycolates from parent strains and zeocin-resistant transformants were analyzed by TLC. (F) Growth curve (represented as OD600 measurements) at 32.5°C of BCG-P (◆), BCG-P $\Delta cmaA2$ (MGM1919; ■), BCG-R (▲), and BCG-R $\Delta cmaA2$ (MGM295; ▼).

To further confirm synthetic lethality, we created an *mmaA3* depletion strain that expressed *mmaA3* from a tetracycline- inducible promoter. This strain displayed anhydrotetracycline (AHT)-dependent synthesis of methoxymycolates (Figure 2-2 D, left). Using specialized transduction, *cmaA2* and *mmaA1* were deleted from this strain in the presence of AHT. Southern blotting confirmed successful deletion of *cmaA2* and *mmaA1* (data not shown) and NMR of total mycolic acids from these strains confirmed lack of *trans* cyclopropane rings. To our surprise, depletion of *mmaA3* by AHT withdrawal did not result in cell death (data not shown). Examination of these strains revealed minimal methoxymycolate production without AHT (Figure 2-2 D, right), ruling out constitutive expression of *mmaA3* due to a mutation in the tetracycline repressor. This result could indicate that *mmaA3/mmaA1* and *mmaA3/cmaA2* are not synthetically lethal. However, the tetracycline regulation is somewhat leaky, which could allow survival due to the low-level methoxymycolate production that is visible in Figure 2-2 D. To completely remove the *mmaA3* cassette from the Δ *mmaA1* and Δ *cmaA2* strains, we used marker exchange (Carey Pashley and Tanya Parish, 2003). A zeocin marked vector replaced the *mmaA3* cassette after transformation and the resulting zeocin-resistant transformants lacked methoxymycolates (Figure 2-2 E), indicating that sequential deletion of *cmaA2/mmaA3* or *mmaA1/mmaA3* is possible. Taken together, one interpretation of these genetic studies is that compensatory changes in membrane fluidity in the tetracycline depletion and zeocin strains allowed isolation of the double mutants, possibly due to the order in which the genes were deleted. To test whether the *cmaA2/mmaA3* double mutants have alterations in membrane fluidity that would support

this model, we grew these strains in low temperature. We found that deletion of *cmaA2* from BCG-R moderately impaired growth at 32° (Figure 2-2 F). Strikingly, BCG-P grew poorly at 32° and inactivation of *cmaA2* in BCG-P abolished growth (Figure 2-2 F). These findings support the genetic data indicating that loss of *cmaA2/ mmaA3* impairs viability due to alteration in membrane fluidity.

Diocylamine inhibits multiple pathways of mycolic acid modification

To investigate the phenotypic consequences caused by loss of mycolic acid modification, we sought a chemical inhibitor of these enzymes. Diocylamine was recently identified as an inhibitor of *Escherichia coli* CFAS, an enzyme that cyclopropanates the membrane fatty acids of *E. coli* (Dennis Grogan and John Cronan, 1997; Dominique Guianvarc'h et al., 2006). The IC₅₀ of diocylamine for CFAS was 4 μM. Diocylamine is chemically similar to didecyldimethylammonium bromide (DDDMAB), which we have previously crystallized in the active site of CmaA2 (Chih-chin Huang et al., 2002) (see Figure 2- 3A for structures), suggesting that diocylamine might also inhibit mycolic acid methyltransferases by acting as a substrate mimic. To test whether diocylamine is an inhibitor of cyclopropanation, we grew BCG-R (which has a mycolic acid profile highly similar to that of *M. tuberculosis*) with ¹⁴C acetic acid and in escalating concentrations of diocylamine ranging from 0.125 to 10 μM or vehicle control. After 6 hr, ¹⁴C -labeled mycolic acid methyl esters were prepared and analyzed by radio thin layer chromatography (TLC). We observed that 2 μM diocylamine completely inhibited methoxymycolate production, consistent with loss of MmaA3

function (see arrowhead in Figure 2-3 B).

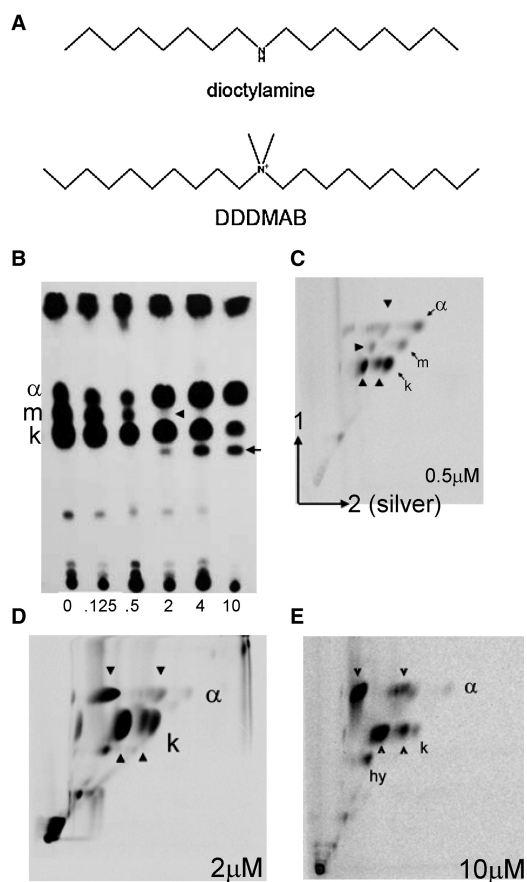


Figure 2-3. Diocetylamine inhibits multiple pathways of mycolic acid modification. (A) Chemical structures of dioctylamine and DDDMAB. DDDMAB was previously identified in the active site of crystals of CmaA2. (B) One-dimensional TLC of mycolates isolated from BCG-R treated with the concentration of dioctylamine (μM) indicated under each lane. Alpha mycolate (α), methoxymycolate (m), and ketomycolate (k) are indicated at the left edge. The arrowhead marks the position of methoxymycolate, which is absent from the 2 μM sample. The arrow marks hydroxymycolate. (C) Two-dimensional Argentation TLC of BCG-R treated with 0.5 μM dioctylamine. The sample was separated without silver (dimension 1) and then with silver (dimension 2). The silver dimension retards lipids on the basis of unsaturation. Two unsaturated derivatives of alpha mycolate are visible, as well as unsaturated ketomycolates and methoxymycolates (arrowhead). (D and E) Two-dimensional Argentation TLC of BCG-R treated with 2 μM (D) and 10 μM (E) dioctylamine. Unsaturated derivatives of the alpha mycolates and ketomycolates are marked with arrowheads, as are the positions of mature alpha mycolate (α), ketomycolate (k), and hydroxymycolate (hy).

In addition, treatment with 4 and 10 μM dioctylamine caused accumulation of a mycolic acid migrating slower than ketomycolate (see arrow in Figure 2-3 B), consistent with the previously reported hydroxymycolate that accumulates in the absence of functional MmaA3 (Annaik Quemard et al., 1997). This polar lipid migrated slower than authentic epoxy mycolate from *Mycobacterium smegmatis* (data not shown), confirming its likely identity as hydroxymycolate. At 10 μM , there is substantial but incomplete inhibition of ketomycolate biosynthesis (compare 0.125 to 10 μM in Figure 2-3 B). The observed mycolic acid profiles with dioctylamine treatment are consistent with loss of MmaA3 and MmaA4 function, suggesting that dioctylamine inhibits these enzymes.

Whereas inhibition of MmaA3 and MmaA4 leads to loss of an entire mycolate class and is therefore easily detected on one-dimensional TLC, chemical inhibition of other cyclopropane synthases produces unsaturated lipids that are identical in polarity to their parent lipids and therefore not detectable on one-dimensional TLC. This phenotype was previously demonstrated in *M. tuberculosis* strains lacking the mycolic acid cyclopropane synthases PcaA, MmaA2, and CmaA2 (Michael Glickman, 2003; Michael Glickman et al., 2000; Michael Glickman et al., 2001). To test the inhibition of these enzymes by dioctylamine, we performed two-dimensional argentation TLC on mycolic acids isolated from dioctylamine-treated BCG-R. In this technique, lipids are first separated by polarity and then by degree of any type of unsaturation in the second (silver) dimension. After treatment of BCG-R with 0.5 μM dioctylamine, we observed two unsaturated derivatives of the alpha mycolate, consistent with inhibition of alpha mycolate cyclopropanation (Figure 2-3 C, arrow- head to the left of mature alpha). We

also observed unsaturated derivatives of methoxymycolates and ketomycolates, consistent with impaired cyclopropanation of the proximal position of these lipids (Figure 2-3 C). Cells treated with 2 mM dioctylamine produced no mature alpha mycolate and two species of unsaturated alpha mycolate, the more abundant of which was more fully retarded (arrowheads in Figure 2-3 D). The ketomycolate appeared as three species, mature keto and two unsaturated species, likely *cis* and *trans* unsaturated. At 10 μ M, almost no mature ketomycolate was observed (Figure 2-3 E). These data strongly indicate that dioctylamine is a dose-dependent inhibitor of multiple mycolic acid methyltransferases. These TLC data, combined with extensive prior genetic characterization of mycolic acid modifications, indicate that dioctylamine inhibits the lipid modifications performed by MmaA4, MmaA3, PcaA, MmaA2, and CmaA2.

Mycolic acid methyltransferases are direct targets of dioctylamine

The data presented above strongly indicate that dioctylamine inhibits multiple pathways of mycolic acid cyclopropanation and methylation. However, this effect could be due to direct inhibition of mycolic acid methyltransferase enzymes or an indirect effect. To prove that the methyltransferases are direct dioctylamine targets, we overexpressed hemagglutinin-tagged versions of MmaA1, MmaA3, CmaA2, PcaA, MmaA2, and MmaA4 on a multicopy episomal plasmid and tested the effect on dioctylamine sensitivity.

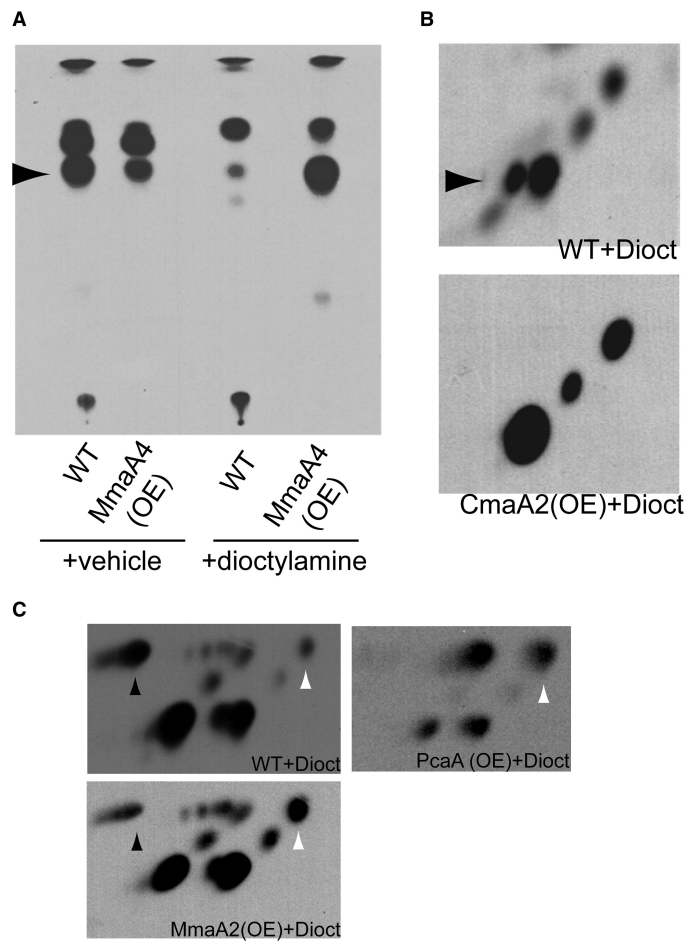


Figure 2-4. Mycolic acid methyltransferases are direct targets of dioctylamine. (A) Wild-type BCG-R (plus empty vector) or BCG-R carrying a multicopy plasmid expressing MmaA4 (MmaA4 OE) were treated with vehicle (left lanes) or dioctylamine (right lanes) and radiolabeled mycolic acids were analyzed by TLC. (B) Wild-type BCG-R (plus empty vector) (top panel) or BCG-R carrying a multicopy plasmid expressing CmaA2 (CmaA2 OE) (bottom panel) were treated with dioctylamine and radiolabeled mycolates were analyzed by two-dimensional argention TLC. (C) Wild-type BCG-R (plus empty vector) (upper left) or BCG-R carrying a multicopy plasmid expressing PcaA (PcaA OE) (upper right) or MmaA2 (MmaA2 OE) (lower left) were treated with dioctylamine and radiolabeled mycolic acids were analyzed by two-dimensional argention TLC. The black arrowhead indicates alpha mycolate with two double bonds and the white arrowhead indicates mature alpha mycolate with two cyclopropane rings.

The expression of these proteins was confirmed by western blotting in *M. smegmatis* and BCG-R. Overexpression of MmaA4 strongly reversed the inhibition of

ketomycolate synthesis observed with dioctylamine (Figure 2-4 A). Similarly, overexpression of CmaA2 reversed the accumulation of unsaturated ketomycolates seen with dioctylamine treatment (Figure 2-4 B). Overexpression of MmaA2 and PcaA also reversed the accumulation of unsaturated alpha mycolate in dioctylamine-treated cells. In MmaA2-expressing cells, the predominant alpha mycolate that accumulated was fully saturated (white arrowhead in Figure 2-4 C), whereas in PcaA-expressing cells, the alpha mycolate was mixture of monounsaturated and dicyclopropanated lipids (Figure 2-4 C). Although diunsaturated alpha mycolate is the major lipid in dioctylamine-treated cells (black arrowhead in Figure 2-4 C), none of this lipid was visible in the PcaA overexpressor. In contrast, although the lack of methoxymycolate in dioctylamine-treated cells is consistent with loss of MmaA3 function, overexpression of MmaA3 did not reverse this effect. This suggests that MmaA3 may be an indirect target of dioctylamine, possibly through other mycolic acid methyltransferases.

Dioctylamine inhibits the methyltransferase activity of CmaA2 in vitro

To examine the *in vitro* activity of *M. tuberculosis* mycolic acid methyltransferases and their inhibition of dioctylamine, we developed a new enzymatic colorimetric assay that detects conversion of S-adenosylhomocysteine (SAH) to homocysteine by SAH hydrolase (SahH) (Lozada-Ramirez et al., 2006). This assay is diagrammed in Figure 2-5 A. Using this assay, we screened unsaturated fatty acids, including oleic, nervonic, arachidonic, and cis-11,14-eicosadienoic acid as substrates of *M. tuberculosis* CmaA2. Although none of these substrates are close in structure to the

authentic substrate (i.e., a long chain acyl-ACP), we were able to demonstrate cyclopropanation of double bonds and determine kinetic parameters using a Lineweaver-Burk plot (Figure 2-5 B). Of these, Eicosadienoic acid ($K_m = 16.8 \mu\text{M}$ and $k_{\text{cat}} = 0.0027 \text{ s}^{-1}$) was the best candidate to test the inhibitory effect of dioctylamine. An accurate IC_{50} was not obtainable because we had to use a relatively large amount of protein ($4 \mu\text{M}$) in order to observe the reaction progress. However, the inhibition from dioctylamine was obvious as it reduced the activity of CmaA2 in a concentration-dependent manner (Figure 2-5 C). When $2 \mu\text{M}$ dioctylamine was added to the reaction, the rate was reduced by 50%, indicating a fairly potent inhibition against the enzyme and consistency with dioctylamine inhibition of the cyclopropane fatty acid synthase from *E. coli*. These data demonstrate that dioctylamine is a direct inhibitor of mycolic acid methyltransferases.

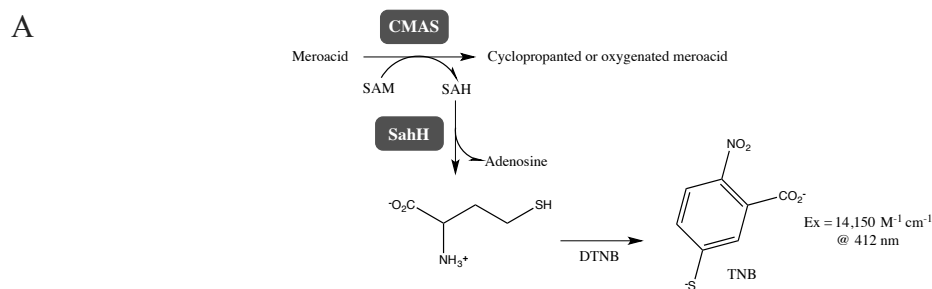
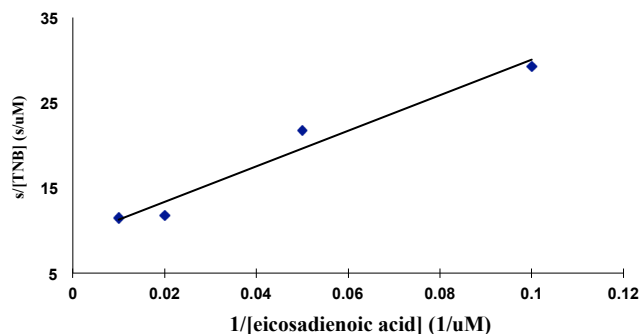


Figure 2-5. Dioctylamine inhibits CmaA2 *in vitro*. (A) Scheme of the enzymatic assays for *M. tb* CMASs. DTNB, dithiobis-(2-nitrobenzoic acid); TNB, 2-nitro-5-thiobenzoic acid. (B) Lineweaver–Burk plot using eicosadienoic acid as substrate. (C) The *in vitro* inhibitory action of dioctylamine on CmaA2 activity.

B



C

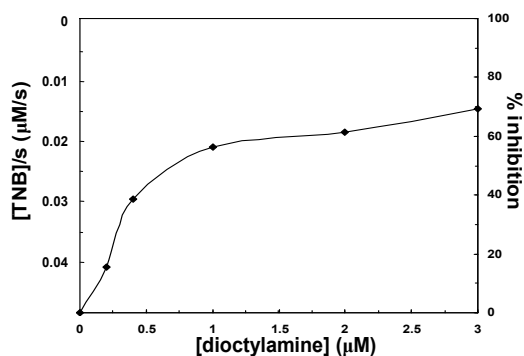


Figure 2-5 continued.

The structure of CmaA2 with bound dioctylamine reveals the molecular basis for activity

To further demonstrate that dioctylamine is a direct inhibitor of mycolic acid methyltransfer and explore the molecular basis for its activity, we solved the structure of the CmaA2 protein in complex with the compound. The structure was solved by molecular replacement at 2.67 Å resolution (Table 2-1). The overall fold is largely similar to the previously reported structure of CmaA2 complexed with DDDMAB and SAH (PDB code 1KPI)(Chih-chin Huang et al., 2002), showing an rmsd of 0.315 Å after superimposition (Figure 2-6 A). Moreover, the lipophilic ligands in the two structures are similarly oriented in the binding site of the mycolic acyl substrate. Like DDDMAB,

dioctylamine adopts a U-shape conformation with the nitrogen pointing to the previously revealed SAM binding pocket and the two aliphatic chains extending to the catalytic site entrance. Modeling SAM into the active site by superimposing the MmaA4-SAM structure (PDB code 2FK8) with CmaA2-SAH and dioctylamine complex, we see the nitrogen of dioctylamine is approximately 3.1 Å away from the active methyl group of SAM, indicating that the nitrogen is situated at the position of the substrate double bond to be modified. Whereas the hydrophobic binding pocket binds the aliphatic chains of DDDMAB and dioctylamine similarly, the ammonium or amine nitrogens differ substantially in their interaction with the protein (Figure 2-6 B). For both of the species, the residues within 5 Å distance from nitrogen include Tyr24, Tyr41, Gly145, Glu148, and Tyr247. Tyr41 stabilizes the ammonium of DDDMAB through cation- π interaction. In contrast, when dioctylamine binds to the same site, its nitrogen drifts 0.5 Å away from the face of Tyr41. Gly145 tilts toward the nitrogen at the same time, with its backbone oxygen forming a van der Waals interaction with the nitrogen atom at a 3.2 Å distance. This distance is 4.0 Å in the structure in complex with DDDMAB, which is likely the result of the steric repulsion from the two methyl groups of the ammonium. Thus, this structural analysis of the dioctylamine-CmaA2 interaction predicts that amine-based inhibitors of these will be more potent than ammonium-based inhibitors.

Table 2-1. Data collection and refinement statistics for CmaA2 in complex with dioctylamine.

Data collection	
Space group	I4 ₁ 22
Unit cell dimensions (Å)	a = b = 106.86 c = 224.98
Molecules/asymmetric unit	1
Wavelength (Å)	0.9795
Resolution (Å)	50–2.68
Completeness (%) ¹	99.7 (98.1)
No. of reflections	287,172
I/σI ¹	20.1 (1.62)
R _{sym} ¹	0.0413 (0.76)
Refinement statistics	
Resolution (Å ²)	38.74–2.68
No. of reflection work	18,719
No. of protein atoms	2,380
No. of water molecules	41
No. of heteroatoms	21
R _{cryst} (%)	22.29
R _{free} (%)	24.30
Rmsd bond lengths (Å)	0.012
Rmsd angles (Å)	1.157
Mean temperature factor (Å ²)	61.33

¹. Numbers in parenthesis indicate data for highest-resolution shell.

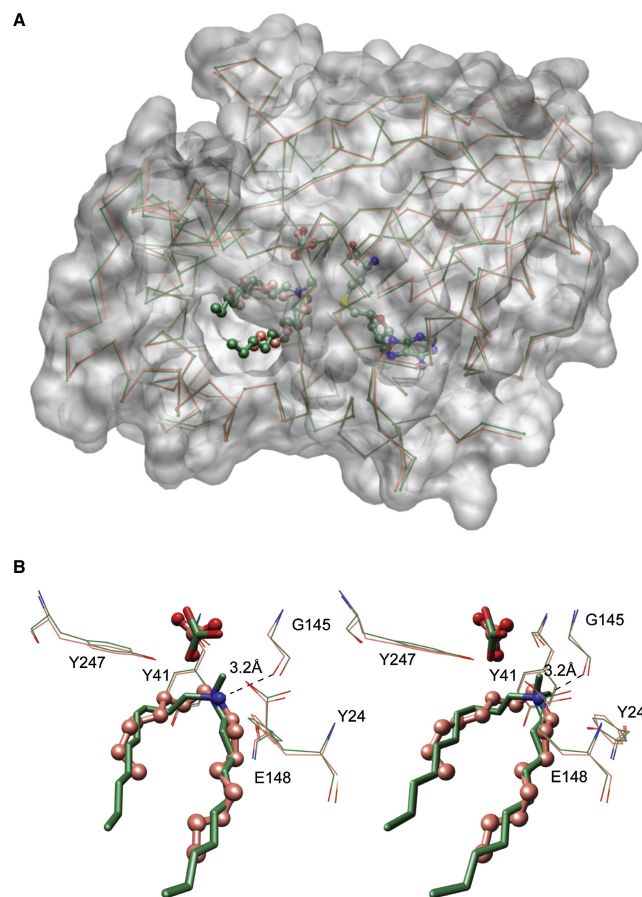


Figure 2-6. Structures of *M. tuberculosis* CmaA2 in complex with diocetylamine and DDDMAB/SAH.

(A) The α -Carbon traces and ligands of the two structures are shown with diocetylamine colored pink and DDMAB/SAH colored green. The two structures show similar overall folding. All the ligands including bicarbonate are represented as ball and stick. The surface of the protein is shown with transparency.

(B) Stereo diagram of the active site residues in proximity to diocetylamine or DDDMAB nitrogens. Diocetylamine and the cognate bicarbonate are represented as ball and stick, while DDDMAB and the cognate bicarbonate are represented as stick. The specific van der Waals interaction between the backbone oxygen of Gly145 and the nitrogen of diocetylamine is shown as dotted line.

Diocetylamine is a growth inhibitor of BCG and M. tuberculosis

To test the hypothesis that simultaneous inhibition of multiple mycolic acid methyltransferases is lethal to mycobacteria, we grew BCG-R and *M. tuberculosis*

Erdman in 7H9 media or 7H10 plates supplemented with different concentrations of dioctylamine. We found that *M. tuberculosis* growth was partially inhibited by 4 μM and completely inhibited by a 6 μM (Figure 2-7 A). Similar results were obtained with *M. tuberculosis* grown on solid media containing dioctylamine (Figure 2-7 B) and with BCG-R in liquid and solid media (data not shown). We did find that there was a considerable inoculum effect, and at higher inoculums the inhibitory effect was seen at higher concentrations of dioctylamine (data not shown). As the growth inhibitory concentration of dioctylamine is similar to the concentration active against mycolic acid methyltransferases, this data, coupled with the genetic data presented above, strongly suggest that mycolic acid modification may be an essential function for slow growing mycobacteria.

To further substantiate that growth inhibition effect of dioctylamine on mycobacteria is indeed related to its effect on cyclopropanation, we used another tool compound, hexadecyltrimethylammonium bromide (CTAB). This compound, which has some detergent properties, was previously found to crystallize in the active site of CmaA1 and shares an ammonium head group similar to DDMABB, suggesting that it should be a weaker inhibitor than dioctylamine if growth inhibition is attributable to binding to mycolic acid methyltransferases. Consistent with this structure-activity prediction, we found CTAB to be 5-fold less active than dioctylamine in inhibiting mycobacterial growth (Figure 2-7 C). CTAB was also approximately 5-fold less active than dioctylamine in inhibiting methoxymycolate synthesis *in vivo* (Figure 2-7 D).

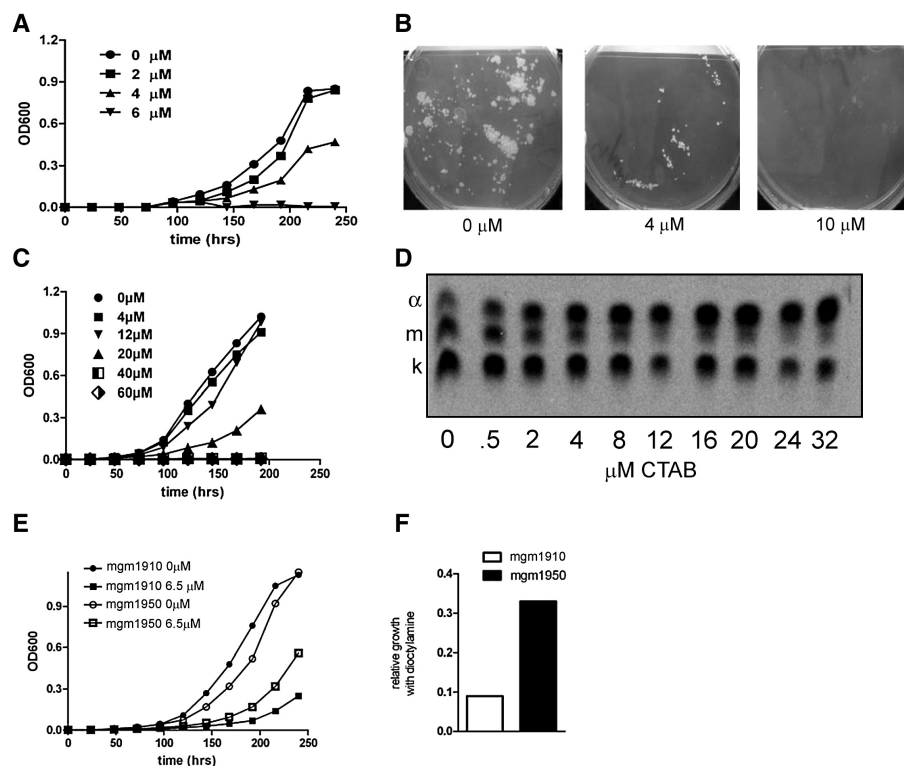


Figure 2-7. Diethylamine inhibits growth of *M. tuberculosis*

(A) *M. tuberculosis* Erdman was grown in 7H9 media, supplemented with 0 (vehicle)(●), 2 (■), 4 (▲), and 6 μM (▼) diethylamine. OD₆₀₀ measurements were taken daily. A representative experiment out of five is shown.

(B) *M. tuberculosis* Erdman was grown on 7H10 plates, impregnated with 0, 4, or 10 μM diethylamine. The plates were kept at 37°C with 5% CO₂ for 4 weeks.

(C) BCG-R was grown in the indicated concentrations of CTAB and bacterial growth was measured by OD.

(D) Radiolabeled mycolic acids from BCG-R treated with the indicated concentrations of CTAB (μM) were separated by one-dimensional TLC.

(E) BCG-R overexpressing six methyltransferases (MmaA1-4, PcaA, and CmaA2) (MGM1950) is more resistant to diethylamine than BCG-R with vector alone (MGM1910). A representative experiment out of four is shown.

(F) The ratio of growth in the presence of diethylamine to without diethylamine at the 192 hr time point from the experiment in (E).

To further demonstrate that inhibition of growth by diethylamine is the direct result of inhibition of multiple mycolic acid methyltransferases, we overexpressed these enzymes and tested for resistance to diethylamine. None of the strains overexpressing a

single enzyme (either MmaA1, MmaA2, MmaA3, MmaA4, CmaA2, or PcaA) were resistant to dioctylamine (data not shown), which is consistent with the nonessentiality of these gene products in prior genetic experiments. We then overexpressed simultaneously, from a single plasmid, six different enzymes of this family: MmaA1, MmaA2, MmaA3, MmaA4, CmaA2, and PcaA. The strain overexpressing these six enzymes (mgm1950) grew three times as fast as the control strain (mgm1910) in 6.5 μ M dioctylamine, indicating partial resistance (Figure 2-7 E and Figure 2-7 F). This data indicates that dioctylamine kills *M. tuberculosis* by inhibiting multiple methyltransferases.

Mycolic acid modification is required for acid fastness and intrinsic resistance to antibiotics

The activity of dioctylamine against mycolic acid methyltransferases allowed us to probe the physiologic function of this unique lipid modification in a way not possible using the previously isolated single gene mutants or, as in prior studies, using overexpression of individual enzymes (Ying Yuan et al., 1998). To test whether cyclopropanation contributes to antibiotic resistance, we tested sublethal concentrations of dioctylamine in combination with sublethal concentrations of isoniazid (INH), ciprofloxacin, and kanamycin. We found strong synergy between dioctylamine and both INH and ciprofloxacin (Figures 2-8 A and B), but no synergy with kanamycin (data not shown). To show that this synergy is related to increased drug penetration in dioctylamine-treated cells, we measured the uptake of radiolabeled ciprofloxacin in

bacteria treated with 4 μM dioctylamine. We found a significant increase in ciprofloxacin penetration into dioctylamine-treated cells, an effect that was most evident after 5 min, but was sustained after 40 min (Figures 2-8 C). These results suggest that the mechanism of synergy between these two antibiotics facilitated uptake of ciprofloxacin by dioctylamine's effects on the mycobacterial membrane. A similar mechanism may explain synergy between INH and dioctylamine, although it is possible that the INH synergy is also a result of their combined effect on mycolic acid synthesis.

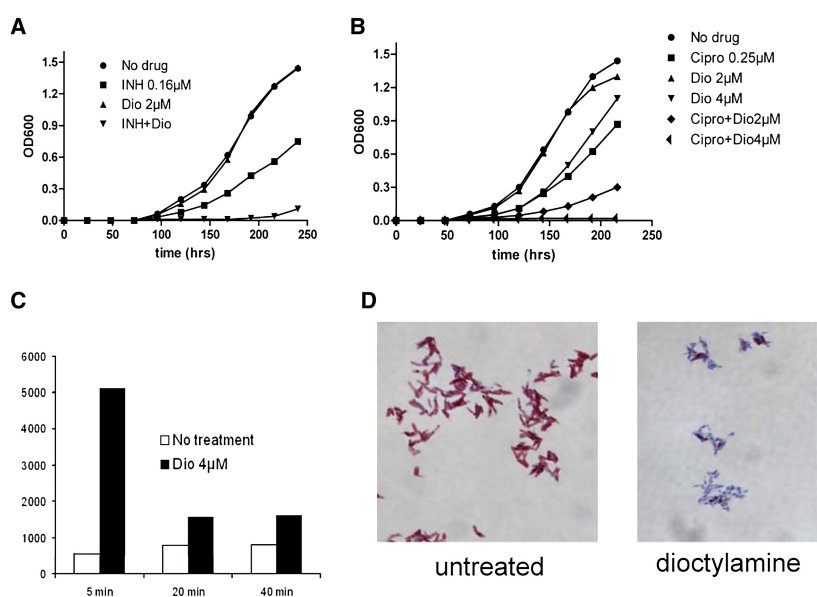


Figure 2-8. Mycolic acid methyltransferases are required for drug resistance and acid fastness of Mycobacteria.

(A) BCG-R was treated with INH, dioctylamine (Dio), or both at the indicated concentrations and growth was measured by OD at 600 nm.

(B) BCG-R was treated with ciprofloxacin (Cipro), dioctylamine (Dio), or both at the indicated concentrations and growth was measured by OD at 600 nm.

(C) Accumulation of ¹⁴C ciprofloxacin in untreated (white bar) or dioctylamine treated (4 μM ; black bar) at the indicated time points after ¹⁴C ciprofloxacin addition. The y axis is counts per minute.

(D) Untreated or dioctylamine (4 μM)-treated cells were examined by acid fast staining using the modified Kinyoun technique.

Acid fastness of mycobacteria, a hallmark of this genus, is thought to reflect the hydrophobicity and structure of mycolic acids in the cell wall. This idea is supported by prior findings that *M. tuberculosis* lacking *kasB* display both loss of acid fastness and attenuation (Apoorva Bhatt et al., 2007). We tested the effect of 4 μ M dioctylamine on the acid fastness of BCG-R and found that most of the bacteria lost their acid fastness (Figure 2-8 D), despite only partial growth inhibition.

Discussion

Cyclopropanation is a common membrane modification in bacteria and plants (Dennis Grogan and John Cronan, 1997; Xiaoming Bao et al., 2002). In most cases, the physiologic function of cyclopropanation is poorly defined, although cyclopropanation clearly has substantial effects on membrane fluidity in model systems (James McGarrity and John Armstrong, 1981; Nagamachi et al., 1991). Pathogenic mycobacteria have an extensive set of cyclopropane modifications that decorate the signature lipid of the mycobacterial cell wall, the mycolic acid. Recent studies have strongly implicated mycolic acid cyclopropanation in *M. tuberculosis* pathogenesis through its effect on the immunomodulatory properties of trehalose dimycolate (Vivek Rao et al., 2006; Vivek Rao et al., 2005). However, these studies did not clearly establish mycolic acid methyltransferases as an attractive drug target. Here we demonstrate that chemical inhibition of multiple mycolic acid methyltransferases is lethal to mycobacteria and causes pleiotropic alterations in cell envelope structure and drug susceptibility. These studies provide strong scientific basis for targeting mycolic

acid cyclopropanation as an antibiotic strategy against *M. tuberculosis*.

Our findings also reveal novel physiologic roles of cyclopropanation in mycobacteria. Although some prior studies have indicated a role for cyclopropanation in membrane fluidity and permeability (Kathleen George et al., 1995; Ying Yuan et al., 1998), the exact role of cyclopropanation in the physiology of pathogenic mycobacteria was unclear. A prior study indicated that the antitubercular thiacetazone may affect cyclopropanation, but this study concluded that the growth inhibitory effect of this drug was unrelated to its effect on cyclopropanation (Anuradha Alahari et al., 2007). This conclusion was based on the difference between the minimum inhibitory concentration of thiacetazone and the concentration required to affect cyclopropanation. In a more recent paper, the authors show that MmaA4 is required for activity of thiacetazone and that deletion of *mmaA4* confers resistance, rather than hypersensitivity, to the drug (Anuradha Alahari et al., 2009). Using dioctylamine as a tool compound, we suggest that pharmacologic inhibition of this enzyme class causes loss of viability, a novel and unanticipated finding. Our finding that mycolic acid methyltransferases are essential for viability suggests an unanticipated role for mycolic acid modification in some essential cellular process. The most likely cause of this essentiality is lethal dysregulation of membrane fluidity leading to impaired protein localization or cell division. Although an off-target effect of dioctylamine causing cell death is possible, we believe this is unlikely because: (1) cell death is observed at the same concentration required to inhibit multiple methyltransferases *in vivo*; (2) overexpression of multiple enzymes can partially reverse the growth defect; (3) the structure of CmaA2 protein with

dioctylamine both reveals that this enzyme is a direct target and that dioctylamine is acting as a substrate mimic rather than a general SAM antagonist. This makes nonspecific inhibition of other SAM-dependent methyltransferases (such as DNA methyltransferases) with nonlipid substrates unlikely. The essential physiologic role of mycolic acid methyltransferases is an area of interest that will be the subject of future investigations.

Although dioctylamine is unlikely to be a useful antimicrobial due to host toxicity (data not shown), our data provide strong support for targeting mycolic acid methyltransferases for inhibitor development and provides a structural framework for optimizing active site binding through structure guided design. The structures of CmaA2 reveal different binding determinants for ammonium or amine-based inhibitors. The ammonium ion mimics the carbocation intermediate of the cyclopropanation reaction and is stabilized by cation- π interaction. In contrast, through mimicking an electron-donating double bond, the amine nitrogen atom of dioctylamine forms a van der Waals interaction with Gly145. This interaction will not occur in a mycolate substrate and provides a structural explanation for the successful competition of dioctylamine with the natural mycolate substrates. Moreover, this interaction may contribute more than cation- π interaction to enhancing inhibitor binding, evident from our finding that acylamine compounds are more potent than ammonium compounds (CTAB) at inhibiting cyclopropanation. This indicates that amine-based inhibitors may serve as a template for further drug development.

Experimental Procedures

Bacterial strains and growth conditions

M. smegmatis mc²155 was grown in 7H9 liquid media supplemented with 0.05% Tween 80, 0.5% glycerol, and 0.5% dextrose. BCG-R (kindly provided by M. Behr), BCG-P, and *M. tuberculosis* Erdman were grown in 7H9 media supplemented with 0.05% Tween 80, 0.5% glycerol, and 10% OADC (for *M. tuberculosis*) or ADS (for BCG). Growth on plates was done on 7H10 plates supplemented with glycerol and OADC or ADS at the same concentrations.

Growth in 7H9 media was monitored by optical density (OD) at 600 nM measurement. Antibiotic concentrations were 20 µg/ml for kanamycin, 50 µg/ml for hygromycin, and 12.5 µg/ml for zeocin.

Construction of mutant strains

Deletion of *mmaA1* and *cmaA2* was done as described previously (Hideki Makinoshima and Michael Glickman, 2005; Michael Glickman et al., 2001). Briefly, a temperature-sensitive mycobacteriophage (phAE87) was used to introduce a hygromycin-resistance cassette interrupting the candidate gene at 39°C. The bacteria were plated on 7H10 plates with hygromycin. The resulting colonies were analyzed by southern blotting using a probe flanking the gene of interest. Removal of *mmaA3* previously introduced via the *attB* site on the pMV306kan plasmid (marker exchange) was done by electroporating a pMV306zeo (pMV306kan with a *zeocin-R* cassette replacing the kanamycin-R) and plating the bacteria on plates supplemented with zeocin.

Mycolic acid preparation and analysis

Mycobacteria were grown in 7H9 media to an OD₆₀₀ of 0.3–0.5 in a volume of 50–200 ml. ¹⁴C-labeled acetic acid was added to the media at a concentration of 1 μCi/ml, and the bacteria were allowed to grow for 6 hr (in the presence of dioctylamine) or 24 hr (without dioctylamine) more. The bacteria were harvested, and mycolic acids were extracted as previously described (Michael Glickman et al., 2001). Single dimension separation of mycolic acid classes was done on a normal phase silica gel HPTLC plate (Analtech) and run in a 95:5 mixture of hexanes/ethyl acetate for five to six developments. Two-dimensional separation was done by immersing 90% of the TLC plate in 10% silver nitrate, activating at 130°C for 20 min, running the sample along the line with no silver nitrate (first dimension), rotating the TLC plate 90°, and running for five to six additional developments into the silver nitrate impregnated area. After completion, autoradiograms were developed using a Kodak BioMax Transcreen LE intensifying screen at 80°C. NMR analysis was done as previously described (Michael Glickman et al., 2001). Bacteria were grown to an OD₆₀₀ of 0.8, in a volume of 400–500 ml. Bacteria were harvested and mycolic acids were prepared as before and resuspended in d-chloroform for the NMR analysis.

Radiolabeled ciprofloxacin permeability

¹⁴C-ciprofloxacin (15 mCi/mmol) was purchased from Moravek biochemicals. Permeability testing was done as described previously (Jacqueline Chevalier et al., 2000;

Jun Liu et al., 1996). Fifty milliliters total volume of BCG-R was grown with or without 4 mM dioctylamine to an OD₆₀₀ of 0.5. The cells were concentrated and resuspended in 1 ml to 1.5×10^{10} cfu/ml and left to rotate at 8 rpm at 37°C for 45 min. Carbonyl cyanide 3-chlorophenyl hydrazone (Sigma-Aldrich) was added to a final concentration of 0.1 mM for 30 min, ¹⁴C -ciprofloxacin was added to a concentration of 25 μM, and cells were left rotating at 37°C. Samples of 200 μl were removed at 5, 20, and 40 min. Each sample was washed five times with PBS, filtered through a 0.45 μm GF/C filter on a Unifilter-96 plate (Perkin-Elmer), washed again, and left to dry overnight. Radioactivity was measured by scintillation reader (Packard).

Production of M. tuberculosis CmaA2

Cloning, protein expression, and purification of CmaA2 were performed similarly as previously reported (Chih-chin Huang et al., 2002), except that a modified pET28b vector was used to incorporate TEV cleavage sequence right ahead of the N-terminus of the protein. The protease TEV was consequently used to remove the His6 tag.

Crystallization and data collection

2 mg mL⁻¹ CmaA2 in 25 mM Tris-HCl (pH 8.0) was incubated in ice with 50 mM dioctylamine for 20 min. The protein was then concentrated to 10 mg mL⁻¹ and crystallized at 18°C by hanging drop vapor diffusion. Each drop contained an equal volume of the protein solution and reservoir solution (2 M ammonium sulfate and 0.1 M

CAPS [pH 9.0]). The crystal of binary CmaA2 was flash-frozen in liquid nitrogen using cryoprotectant paratone. The diffraction data were collected at beamline 19-ID at the Advanced Photon Source, Argonne National Laboratory, and then was processed and reduced using HKL2000 (Zbyszek Otwinowski and Wlodek Minor, 1997).

Structure determination and model refinement

The structure of CmaA2 was solved by molecular replacement using Molrep (Alexei Vagin and Alexei Teplyakov, 1997) in CCP4. CmaA2-SAH-DDDMAB (PDB code 1KPI) with all nonprotein molecules removed, was used as the search model. The crystal was in a space group of I422. There was one protein molecule in each unit cell with dimensions of $a = b = 106.86 \text{ \AA}$, $c = 224.98 \text{ \AA}$, and $a = b = c = 90^\circ$. A single solution for the molecular replacement was obtained. After rigid-body and restrain refinement by Refmac5 (Murshudov et al., 1997) in CCP4, the R_{cryst} and R_{free} were 24.6% and 26.8%, respectively. These values were reduced to 23.5% and 26.0% once dioctylamine and bicarbonate ion were manually built in the model by examining the $F_o - F_c$ map in XtalView (McRee, 1999). The final model containing residues 9–302 as well as 41 water molecules was obtained after further cycles of model building and PHENIX refinement (Afonine et al., 2005) yielding R factors of 22.3% and 24.3%. The full crystallization statistics are given in Table 2-1.

Enzymatic assay for CmaA2

M. tuberculosis sahH (Rv3248c) was amplified by PCR, cloned into pET15b

vector, and then transformed into Novagen BL21(DE3) cells. The cells were cultured at 37° till OD₆₀₀ reached ~ 0.8. Then 1 mM IPTG was added to induce protein expression for 20 hours at 18°. After purified by Ni column, the protein was made apo-form by ammonium sulfate precipitation, and then dissolved in 20 mM phosphate buffer with pH = 7.5.

All assays were performed in the presence of a 100 mM (pH 7.5) phosphate buffer. Twenty-five micromoles of SahH, 250 μM NAD, and unsaturated fatty acid were preequilibrated for more than 5 min. After 400 μM DTNB was added, the solution was blanked and added to preincubated 4 μM CmaA2/100 μM SAM to start the reaction. To examine the inhibition by dioctylamine, the dioctylamine/DMSO solution was added together with DTNB to the reaction mixture containing 20 μM *cis*-11,14-eicosadienoic acid.

Additional Unpublished Results

Dioctylamine binds to CmaA2 in vitro

Analyses of known CMASs structures reveal the presence of a few tryptophans and tyrosines in the vicinity of active site, allowing us to use fluorescence quenching assay to determine the binding affinity of dioctylamine. The total fluorescence and specific tryptophan fluorescence were monitored at excitation wavelength of 279 nm (Figure 2-9 A) and 295 nm, respectively, for both CmaA2 and MmaA4 (data not shown). Titration of dioctylamine induced a more significant fluorescence change of CmaA2 than that of MmaA4 at either wavelength, indicating a higher affinity of the compound

to the former. Indeed the manner of fluorescence decrease of MmaA4 suggests it likely to be caused by nonspecific interaction. Further treatment of the data by both nonlinear regression and double reciprocal method indicate a single binding site for dioctylamine in CmaA2 with $K_d \cong 0.2 \mu\text{M}$ (Figure 2-9 B).

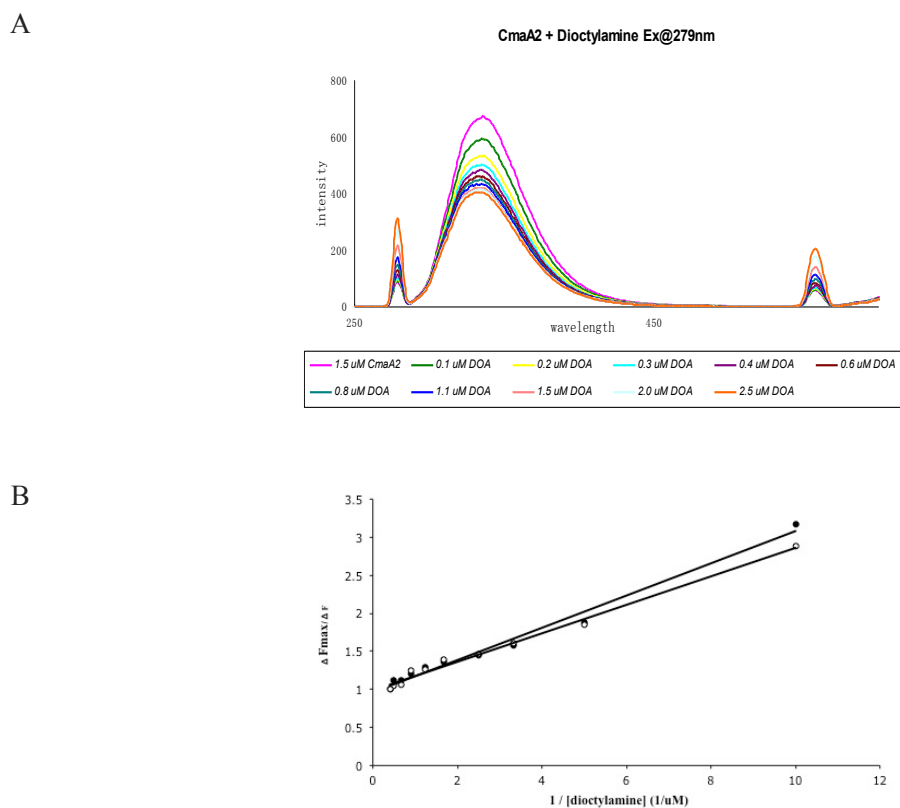
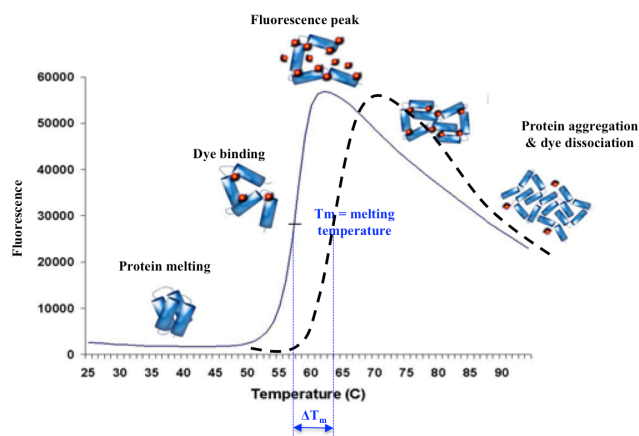


Figure 2-9. Dioctylamine binds to CmaA2 *in vitro*. (A) Fluorescence titration of CmaA2 by dioctylamine at the excitation wavelength of 279nm. (B) Double reciprocal curve fitting is applied to the normalized fluorescence change of CmaA2. Filled and unfilled spots represent data obtained at excitation 279 nm and excitation 295 nm respectively.

Fragment-based screening of ligands for CmaA2

In search for chemical scaffolds and pharmacophores that can bind to the CMASs, we have applied the fragment-based drug design approach. First, the selected compounds are screened in a high-throughput manner using differential scanning fluorimetry (DSF), a technique particularly efficient in identifying low-molecular-weight ligands that bind to a target protein (Figure 2-10 A)(Frank Niesen et al., 2007). Second, saturation transfer difference (STD)-NMR, a technique typically used in compensation to DSF in the fragment-based drug design approach (Figure 2-10 B)(Aldino Viegas et al., 2011; Lawrence Kuo, 2011), is carried out to verify the hits identified by DSF. A total of 823 compounds from Enamine Fragment Library 2012(Herman Verheij, 2006; Miles Congreve et al., 2003) were screened for binding to CmaA2 by DSF, which yielded 18 compounds that caused the melting temperature of CmaA2 to increase by more than 2.95°C (Table 2-2). We repurchased 8 out of the 18 hit compounds based on their commercial availability, and performed STD-NMR to confirm the binding for 6 of them (Figure 2-10 C and D, Table 2-2). These lead fragment compounds will serve for the design of specific and potent inhibitors against *M. tuberculosis* CMASs with rational chemical modifications guided by further structural characterizations.

A



B

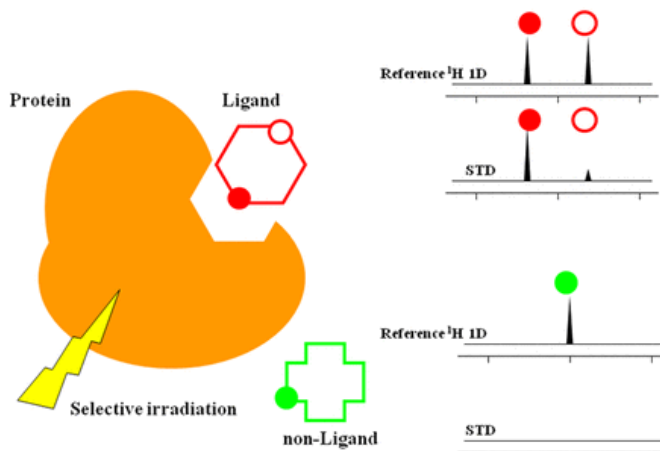


Figure 2-10. Fragment-based screening for ligands that bind to CmaA2.

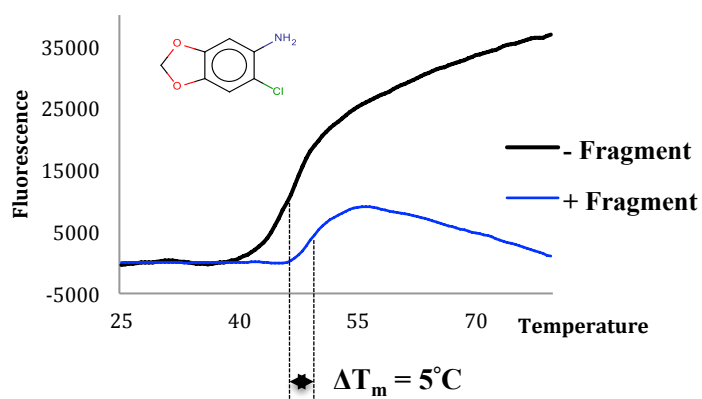
(A) Schematic diagram of DSF(Frank Niesen et al., 2007). The solid and dashed curves represent the dissociation curves of a target protein in the absence and presence, respectively, of a ligand. The molecules of SYPRO Orange dye are shown as orange particles.

(B) Schematic diagram of STD-NMR(Aldino Viegas et al., 2011).

(C) The example of typical fluorimetry obtained for a hit compound identified by DSF.

(D) The example of typical spectra obtained for a hit compound verified by STD-NMR. The assignment of the peaks is marked with the same-color arrows.

C



D

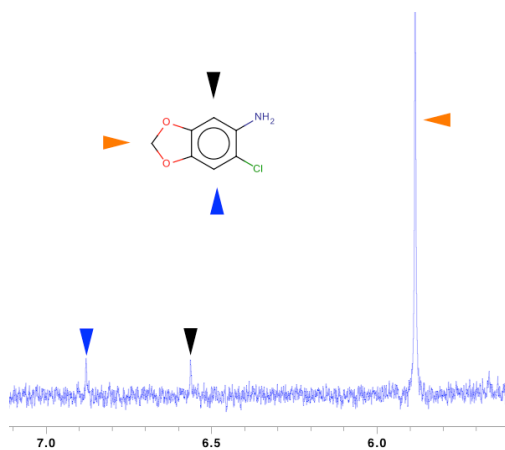


Figure 2-10 continued.

Table 2-2. Lead fragments identified by DSF followed by STD-NMR.

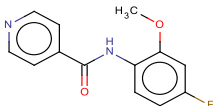
Hit compounds identified by DSF	ΔT_m ($^\circ\text{C}$)	Repurchased	Confirmed binding by STD-NMR
	5.4	YES	YES

Table 2-2 continued.

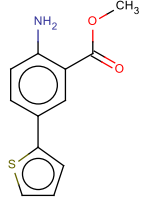
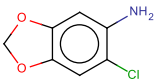
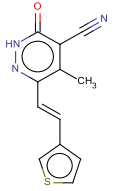
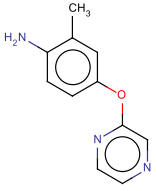
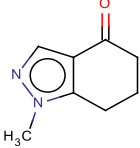
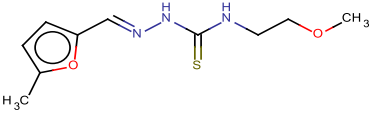
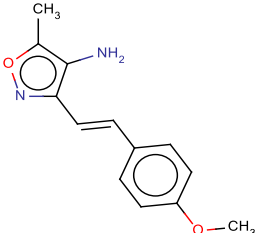
Hit compounds identified by DSF	ΔT_m (°C)	Repurchased	Confirmed binding by STD-NMR
	5.4	YES	NO
	5.0	YES	YES
	5.0		
	4.9	YES	YES
	4.9	YES	YES
	4.85		
	4.4	YES	NO

Table 2-2 continued.

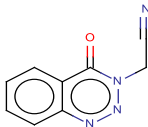
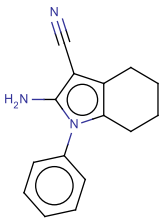
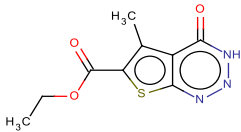
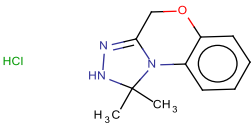
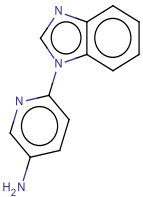
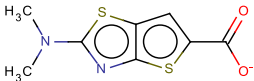
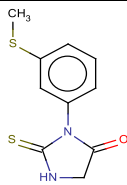
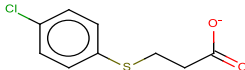
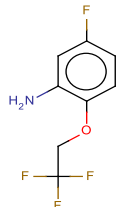
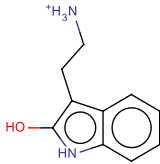
Hit compounds identified by DSF	ΔT_m ($^{\circ}\text{C}$)	Repurchased	Confirmed binding by STD-NMR
	4.35		
	4.35		
	4.05		
 HCl	3.85		
	3.85		
	3.35		

Table 2-2 continued.

Hit compounds identified by DSF	ΔT_m (°C)	Repurchased	Confirmed binding by STD-NMR
	3.40		
	3.35	YES	YES
	2.97		
	2.95	YES	YES

Additional Unpublished Experimental Procedures

Determination of dissociation constant by fluorescence titration

All measurements were performed in 100 mM HEPES buffer (pH 7.5). Emission profiles were obtained by using excitation at either 279 nm or 295 nm, and monitoring emission from 250 nm to 450 nm. Maximum emission appeared at ~ 335 nm for CmaA2 and ~ 343 nm for MmaA4. Titration experiments were carried out by adding increasing amount of dioctylamine/DMSO to 1.5 μ M protein/HEPES buffer. Fluorescence

intensities were corrected for DMSO dilution. Fluorescence intensity was normalized by $\Delta F/\Delta F_{\max}$, in which ΔF was the corrected fluorescence change of each titration and ΔF_{\max} was the maximum change through the experiment. Assuming each protein has n equivalent binding sites for dioctylamine, we determined the binding affinity (K_d) and binding sites (n) using the formula: $\Delta F_{\max}/\Delta F = n^{-1} * K_d^{-1} * [\text{dioctylamine}]^{-1} + n^{-1}$.

Differential scanning fluorimetry (DSF)

All the experiments (20 μL) were performed in 96-well RT-PCR plated by Stratagene Mx3005P QPCR system. Each reaction mixture contained 10 μM CmaA2 in presence of 100 mM MES buffer (pH 6.5), 500 μM SAM, and 2.5* SYPRO Orange protein gel stain from Life Technologies. The fragments were added in an amount of 5mM, which were later compared with the control reaction mixtures with addition of 1 μL DMSO.

Saturation transfer difference (STD)-NMR

All the experiments were performed on Bruker Avance III 400MHz NMR spectrometer. Each experiment (600 μL) contained 20 μM CmaA2 in presence of 50 mM phosphate buffer (pH 7.5), 10% D_2O , and 2 mM of the fragment compound.

CHAPTER III
CRYSTALLOGRAPHIC AND MODELING STUDIES AID THE UNDERSTANDING
OF PRODRUG MECHANISM*

Introduction

Isoniazid (INH) and ethionamide (ETH) have been used extensively in the first-line and second-line treatment of TB, respectively, since 1950s. Both reagents are pro-drugs that undergo modifications *in vivo* to become bactericidal adducts. Complicated by the involvement of intracellular activation and metabolism, the action mode of INH and ETH remained mysterious for a long period until late 1990s. The mechanism of the two pro-drugs have been gradually unraveled in the past 15 years, aided by genomic and biochemical studies, especially explicated by structural demonstrations at an atomic resolution.

INH must first be activated by KatG, an endogenous catalase/oxidase (Martin Wilming and Kai Johnsson, 1999). The mode of INH action remained unclear until an

* Portions of this work have been published in and are reprinted with permission from: Feng Wang, Paras Jain, Gulcin Gulten, Zhen Liu, Yicheng Feng, Krishna Ganesula, Alifiya Motiwala, Thomas Ioerger, David Alland, Catherine Vilchèze, William Jacobs Jr. and James Sacchettini. "Mycobacterium tuberculosis dihydrofolate reductase is not a target relevant to the antitubercular activity of isoniazid." *Antimicrobial Agents and Chemotherapy* 2010, 54 (9), 3776-3782 Copyright 2010 (American Society for Microbiology).

And

Catherine Vilchèze, Yossef Av-Gay, Rodgoun Attarian, Zhen Liu, Manzour H. Hazbón, Roberto Colangeli, Bing Chen, Weijun Liu, David Alland, James C. Sacchettini, William R. Jacobs Jr. "Mycothioliol biosynthesis is essential for ethionamide susceptibility in Mycobacterium tuberculosis." *Molecular Microbiology* 2008, 69 (5), 1316-1329 Copyright 2008 (John Wiley & Sons, Inc).

INH-NAD adduct was identified as the bound inhibitor in the active site of InhA, the enoyl-acyl ACP reductase involved in long-chain fatty acid biosynthesis, by protein crystallography (Denise Rozwarski et al., 1998). It was hypothesized that KatG cleaves the hydrazide on INH to an isonicotinoyl radical, which then reacts with NAD to form an adduct that binds to and inhibits InhA (Graham Timmins and Vojo Deretic, 2006). The crystal structure of InhA bound with the adduct indicates that an isonicotinoyl moiety was covalently attached to the 4-position of the nicotinamide ring of NAD cofactor in an S configuration. The chemical structure of the INH-NAD adduct was found to be consistent with the molecular weight obtained by the mass analysis (Denise Rozwarski et al., 1998). Later studies demonstrated that INH-NAD adduct could be generated by a KatG-catalyzed oxidation in the presence of NAD⁺ (Benfang Lei et al., 2000; Martin Wilming and Kai Johnsson, 1999), which strongly inhibits InhA ($K_i = 5$ nM) to block mycolic acid biosynthesis (Catherine Vilchèze et al., 2006; Denise Rozwarski et al., 1998; Richa Rawat et al., 2003).

ETH, a thioamide analogue of INH, also functions via inhibiting InhA and subsequently the mycolate biosynthesis (Aresh Banerjee et al., 1994). Yet its activation is not performed by KatG as the KatG mutant strains resistant to INH remain sensitive to ETH (Glenn Morlock et al., 2003). Various spontaneous mutations and clinical isolates have indicated that the Baeyer-Villiger monooxygenase EthA is essential to activate ETH (Alain Baulard et al., 2000; Andrea DeBarber et al., 2000; Marco Fraaije et al., 2004). While multiple *in vitro* biochemical studies failed to interpret the action of EthA on ETH (Andrea DeBarber et al., 2000; Tommaso Vannelli et al., 2002), a whole-cell

based activation strategy and the subsequent biophysical analyses have delineated the bioactive form of ETH(Feng Wang et al., 2007b). In this study, *M. tuberculosis* EthA and InhA are co-expressed by *E. coli* in presence of ETH. The following mass spectra and a 2.2 Å-resolution crystallography clearly show that the purified InhA is complexed to ethyl isonicatinoyl-NAD (ETH-NAD) in a way similar to the binding to isonicatinoyl-NAD (INH-NAD). The isolated ETH-NAD compound exhibits potent inhibition to native InhA ($K_i = 7$ nM), which has further established itself as the bioactive metabolite of ETH.

The active forms of INH and ETH have been defined, still there are contradictions regarding their intracellular action and metabolism. For INH, though “genetic and biochemical studies have provided convincing evidence that InhA is the primary target of INH(Amalio Telenti, 1998; Hongling Guo et al., 2006), other putative targets of INH have also been proposed(Graham Timmins et al., 2004; Khisimuzi Mdluli et al., 1998). Recently, 17 proteins other than InhA were identified from *M. tuberculosis* lysate that could tightly bind to an affinity matrix derived from INH-NADP or INH-NAD adducts by proteomic analysis(Argyrides Argyrou et al., 2006a). Among these proteins, *M. tuberculosis* dihydrofolate reductase (DhfR) was shown to be strongly inhibited by an INH-NADP adduct in vitro ($K_{iapp} = 1$ nM) in a separate study(Argyrides Argyrou et al., 2006b). This INH-NADP adduct was synthesized by incubating INH and $NADP^+$ in the presence of Mn(III) as a catalyst. The crystal structure of the complex indicated that an acyclic 4R INH-NADP adduct was selectively bound in the active site of DhfR. In addition, overexpression of *dfrA* in *M. smegmatis* caused a 2-fold increase

of resistance to INH compared to the wild-type (Argyrides Argyrou et al., 2006b). These observations were taken to suggest that *M. tuberculosis* DhfR is also a target of INH (Argyrides Argyrou et al., 2006a; Argyrides Argyrou et al., 2006b).

For ETH, it is puzzling that its activation is only feasible *in vivo*, while *in vitro* incubation with EthA only resulted in a number of inactive metabolites (Alain Baulard et al., 2000; Andrea DeBarber et al., 2000; Marco Fraaije et al., 2004). This is consistent with the unusually low *in vitro* activity of EthA (Marco Fraaije et al., 2004), which suggests the presence of other cellular factors essential for the function of EthA or the formation of ETH-NAD.

Understanding the prodrug action is critical for designing more potent inhibitors and strategies to resolve the drug resistance issues. Therefore, together with collaborators, we have (i) confirmed that InhA rather than DhfR is the cellular target responsible for the antitubercular activity of INH (Feng Wang et al., 2010); (ii) discovered that mycothiol is essential for ETH susceptibility in *M. tuberculosis* (Catherine Vilchèze et al., 2008). These are demonstrated by multiple genetic and biochemical evidence, among which structural biology has played an important role. To determine whether InhA or DhfR is a molecular target of INH, we activated the pro-drug in whole-cell based system and observed that only InhA was complexed with the INH-NAD adduct using X-ray crystallography. To validate the correlation between mycothiol and ETH susceptibility, we interpreted the rationale for the inactivation of mycothiol biosynthesis in the spontaneous mutants by homology modeling, and we also examined the effect of mycothiol on EthA activity.

Results and Discussion

INH-NADP adduct formation was not observed in an E. coli-based activation system coexpressing katG and dhfR.

In the previous study, a synthetic INH-NADP adduct derived from INH demonstrated strong inhibition of *M. tuberculosis* DhfR in vitro ($K_{iapp} = 1$ nM)(Argyrides Argyrou et al., 2006b). However, the INH-NADP adduct was synthesized by using an inorganic catalyst, Mn(III). Thus, the yield of adduct generated from this approach might not truly reflect an enzyme-mediated process inside the cell. To better mimic the in vivo activation of INH, a cell-based activation system was designed to examine the KatG-catalyzed adduct formation and the inhibition of DhfR by the adduct. This *E. coli*-based activation system is similar to the one used previously to activate the prodrugs ETH and prothionamide (PTH)(Feng Wang et al., 2007b). In this system, *katG* and *dfrA* were coexpressed in *E. coli* in the presence of INH to investigate whether the activated drug would inhibit DhfR. To construct this system, *katG* and *dfrA* were cotransformed into the *E. coli* BL21(DE3) strain and selected on 50 µg of kanamycin and carbenicillin/ml. The *E. coli* strain containing *katG* and *dfrA* genes was grown and induced in the presence and absence of INH, respectively. After the coexpression of both genes was confirmed by SDS-PAGE, recombinant KatG and DhfR proteins were readily purified.

An enzyme assay was performed to determine the activity of purified DhfR. DhfR isolated from the experimental sample was found to be fully active (specific activity of $12 \mu\text{mol mg}^{-1} \text{min}^{-1}$) compared to the enzyme purified from expression in the

absence of INH. Since the acyclic 4R INH-NADP adduct is extremely potent against Dhfr in vitro, it would tightly bind to Dhfr if the adduct is indeed generated by KatG catalysis inside the cell. However, both the activity assay result and the mass analysis indicated that no detectable amount of the INH-NADP adduct had bound to Dhfr. The coexpressed KatG from the same experimental sample was purified and assayed for its activity in vitro. The specific catalase activity of isolated KatG was $17 \text{ mol mg}^{-1} \text{ min}^{-1}$, a finding comparable to published data ($21 \text{ mol mg}^{-1} \text{ min}^{-1}$)(Benfang Lei et al., 2000), which confirmed that the lack of the INH-NADP adduct did not result from the absence of KatG activity. Therefore, the acyclic 4R INH-NADP adduct is not an activated INH product generated by KatG catalysis inside the *E. coli* cell-based system.

INH-NAD adduct was detected in the E. coli based activation system co-expressing katG and inhA.

It has been shown that KatG activates INH and catalyzes the formation of an INH-NAD adduct in vitro(Graham Timmins and Vojo Deretic, 2006; Martin Wilming and Kai Johnsson, 1999). In order to demonstrate that this KatG-catalyzed INH-NAD adduct formation and its inhibition of InhA can be reproduced in the *E. coli*-based system, both *katG* and *inhA* were transformed into BL21(DE3) cells and coexpressed in the presence of INH. InhA was rapidly purified by a Ni-NTA affinity column, and an in vitro enzyme assay was performed. InhA isolated from the experimental sample had <15% of the specific activity of InhA purified without the addition of INH under the same assay condition. The bound inhibitor was isolated by denaturing the InhA purified

from the experimental sample, and a 1 μM concentration of the inhibitor led to complete inhibition of native InhA. The crystal structure of InhA in complex with the inhibitor was solved to 2.4-Å resolution (Table 3-1). In the active site of InhA, an unbiased electron density map (Figure 3-1) clearly indicated the presence of a modified NAD with an isonicotinic-acyl group covalently attached to the 4-position of the nicotinamide ring in a 4S configuration, which is consistent with the previously identified INH-NAD adduct (Denise Rozwarski et al., 1998). This is the first time that the activation of INH by KatG and the formation of the INH-NAD adduct has been demonstrated in a whole-cell environment. This confirms that our *E. coli* cell-based system is capable of activating the pro-drug INH.

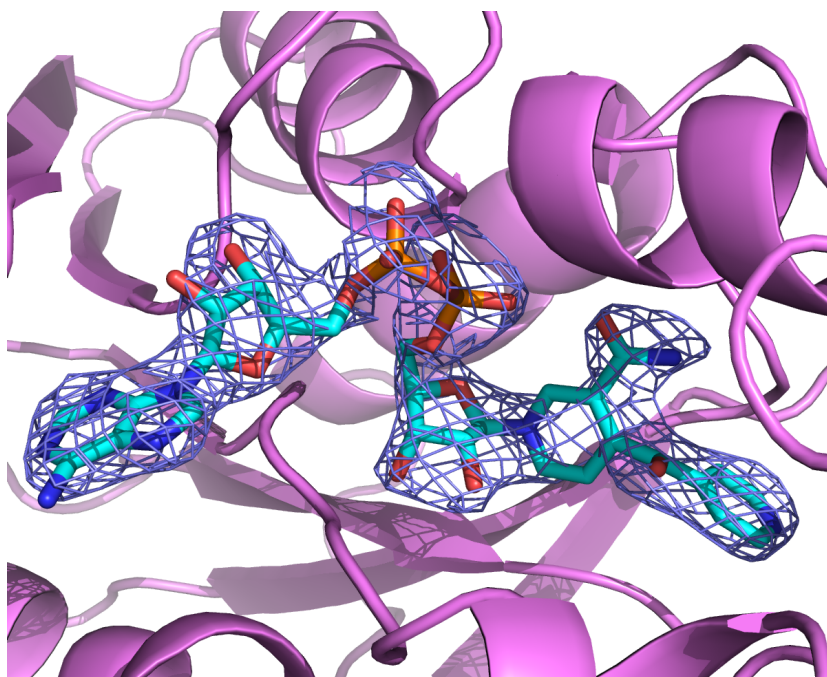


Figure 3-1. The $F_o - F_c$ map that is used to model the INH-NAD adduct (cyan) into the active site of InhA (pink). The difference map is contoured at 3 sigma level.

Table 3-1. Data collection and refinement statistics for InhA in complex with INH-NAD.

Data collection	
Space group	P6 ₂ 22
Unit cell dimensions	a=b=98.85Å, c=138.84Å $\alpha=\beta=90.0^\circ$, $\gamma=120.0^\circ$
Molecules/ASU	1
Wavelength (Å)	1.542
Resolution (Å)	50-2.44
Completeness (%) ¹	99.9 (99.5)
No. of reflections	15560
I/ σ I*	41.02 (5.46)
R _{sym} *	0.0157 (0.1915)
Refinement statistics	
Resolution (Å)	26.96-2.43
No. of reflection work	15675
No. of protein atoms	1994
No. of water molecules	169
No. of heteroatoms	52
R _{cryst} (%)	20.84
R _{free} (%)	25.62
RMSD bond length (Å)	0.01
RMSD angle (°)	1.47
Mean temperature factor (Å ²)	55.27

*. Numbers in parenthesis indicate data for highest-resolution shell.

Spontaneous mutants of M. tuberculosis, co-resistant to INH and ETH, map to mshA

Table 3-2. Point mutations in and deletion of *mshA* cause different levels of resistance to INH and ETH in *M. tuberculosis*.(Catherine Vilchèze et al., 2008)

Parent strain	Mutant	<i>mshA</i> mutation		MIC (mg/l)		MIC (mg/l) pMV361:: <i>mshA</i>	
		Nucleotide	Amino acid	INH	ETH	INH	ETH
H37Rv		-	-	0.06	2.5	0.06	2.5
	mc ² 4930	a124del	Stop codon	0.5	20	0.12	2.5
	mc ² 4931	c382t	Stop codon	0.6	20	0.06	2.5
	mc ² 4932	c817t	R273C	0.4	10	0.06	2.5
	mc ² 4933	g985t	G299C	0.6	20	0.12	2.5
	mc ² 4934	c991t	Stop codon	1	10	0.5	2.5
	mc ² 4935	g1071a	G356D	1	10	0.06	2.5
	mc ² 4936	a1082c	E361A	0.25	20	0.06	2.5
	mc ² 4937	c1265del	Frameshift	1	10	0.25	7.5
	mc ² 4938	$\Delta mshA$		0.06	> 20	0.06	2.5

Numerous studies have demonstrated that there exist strains of *M. tuberculosis* that are resistant to INH and do not have mutations in the genes associated with INH resistance (*katG*, *inhA* structural gene and promoter, *ndh*)(Amy Piatek et al., 2000; Hazbon et al., 2006; Rosilene Fressatti Cardoso et al., 2004; Srinivas Ramaswamy et al., 2003; Telenti et al., 1997). To eliminate the majority of spontaneous mutants of *M. tuberculosis* that are singly resistant to INH and map to *katG*, we chose to isolate mutants that were co-resistant to INH and its structural analogue ETH. Samples of three

independent *M. tuberculosis* H37Rv cultures were plated on media containing low concentrations of both INH and ETH [\leq 4-fold the minimum inhibitory concentration (MIC)]. Seven mutants were isolated at low frequencies ($1-4 \times 10^{-8}$). DNA sequence analysis of targeted genes in these seven strains revealed the absence of mutations in the genes known to mediate co-resistance to INH and ETH, namely *inhA* (the gene or its promoter region) and *ndh*. This analysis provided the evidence that these strains possessed mutations that conferred INH and ETH resistance and had not been previously identified in *M. tuberculosis*. The mutants were transformed with a cosmid genomic library of the drug-susceptible *M. tuberculosis* parent. The frequency of transformation was extremely low for most of the mutants (less than 100 transformants per transformation), and only one mutant, mc²4936, which had the lowest level of INH resistance, yielded more than 1000 transformants. The cosmid transformants were screened for restoration of INH and ETH susceptibility. One potential complementing cosmid was isolated, sequenced and shown to contain the *mshA* gene, a gene characterized as mediating the first step in the biosynthesis of mycothiol (Gerald Newton et al., 2006; Gerald Newton et al., 2003), a key thiol in the family of *Actinomycetes* bacteria (Newton et al., 1996). A link between mycothiol biosynthesis and resistance to INH and ETH had been previously established in *Mycobacterium smegmatis* when transposon mutants in *mshA* were found to be resistant to INH (more than 25-fold) and ETH (sixfold) (Gerald Newton et al., 1999; Gerald Newton et al., 2003; Mamta Rawat et al., 2003). Subsequent sequence analysis of mc²4936 and the other mutants showed that all the *M. tuberculosis* H37Rv mutants had missense, nonsense or frameshift mutations

in *mshA* (Table 3-2). The *mshA* mutants had various levels of resistance to INH (2- to 16-fold) and ETH (four- to eightfold). This is the first report that *mshA* mutations confer co-resistance to INH and ETH in *M. tuberculosis*.

Comparison of the MshA structures of M. tuberculosis and Corynebacterium glutamicum establishes a rationale for the inactivation of MshA in the mutants

The *mshA* mutant strains used in this study are found to be defective in the synthesis of mycothiol. This can be explained by that the mutations lead to the loss of MshA function based on our modeling studies. “Given the sequence identity (45.9%) between *M. tuberculosis* MshA and *Corynebacterium glutamicum* MshA (CgMshA) whose structure was recently determined (Matthew Vetting et al., 2008), the monomeric homology model of *M. tuberculosis* MshA was created using CPHmodels 2.0 (O. Lund et al., 2002) with the UDP-complexed CgMshA (PDB code 3C4Q) as template. Superimposition of the model of *M. tuberculosis* MshA (consisting of Arg46–Ile445) and the chain B from UDP/inositol-phosphate-bound CgMshA (PDB code 3C4V) yields an RMSD of 0.65 Å, indicating a high homology between each other (Figure 3-2 A).

Four of the *mshA* mutants have single amino acid mutation (Table 3-2). These four amino acids (Arg273, Gly299, Gly356 and Glu361) are conserved in CgMshA (as Arg231, Gly263, Gly319 and Glu324) (Figure 3-2 A and B). Each of these amino acids plays an important role in either the substrate binding or the domain interaction (Figure 3-2 B). The side-chain amines of Arg273 interact with the β -phosphate of UDP via hydrogen bonding. This arginine is also one of the major determinants of the orientation

of the inositol-phosphate as its side-chain lies against the face of inositol. Gly299 is not in the vicinity of the active site, but should be important for the protein stability as the next residue, Gly300, forms the only interdomain hydrogen bond with Gly61. Although not directly seen in the model, Gly356 was proposed to be involved in the binding of the *N*-acetyl-glucosamine moiety which shall be transferred from UDP to inositol (Matthew Vetting et al., 2008). In *mc*²4936, the Glu361Ala mutation removes the side-chain carboxylate that forms hydrogen bonds with the 2'- and 3'-hydroxyls from the ribose moiety of UDP, which could result in the inactivation of MshA.

The other *mshA* mutants had either nonsense or frameshift mutations (Figure 3-2 C). In *mc*²4931 and *mc*²4934, the nonsense mutations caused the loss of active-site elements. In *mc*²4937, the truncation of the protein was close to the C-terminus and the active site was unlikely to be affected. Herein the inactivation of MshA could be explained by the protein's characteristic folding. Based on the homology model of MshA, each monomer is composed of N-terminal and C-terminal domains. Towards the end of C-terminus, a large α -helix spanning Cys409 to Ile445 crosses back to the N-terminal, which is likely to stabilize the overall folding of the protein. Therefore the mutations within this α -helix, such as in *mc*²4937, would detrimentally affect the conformation of MshA leading to its inactivation.

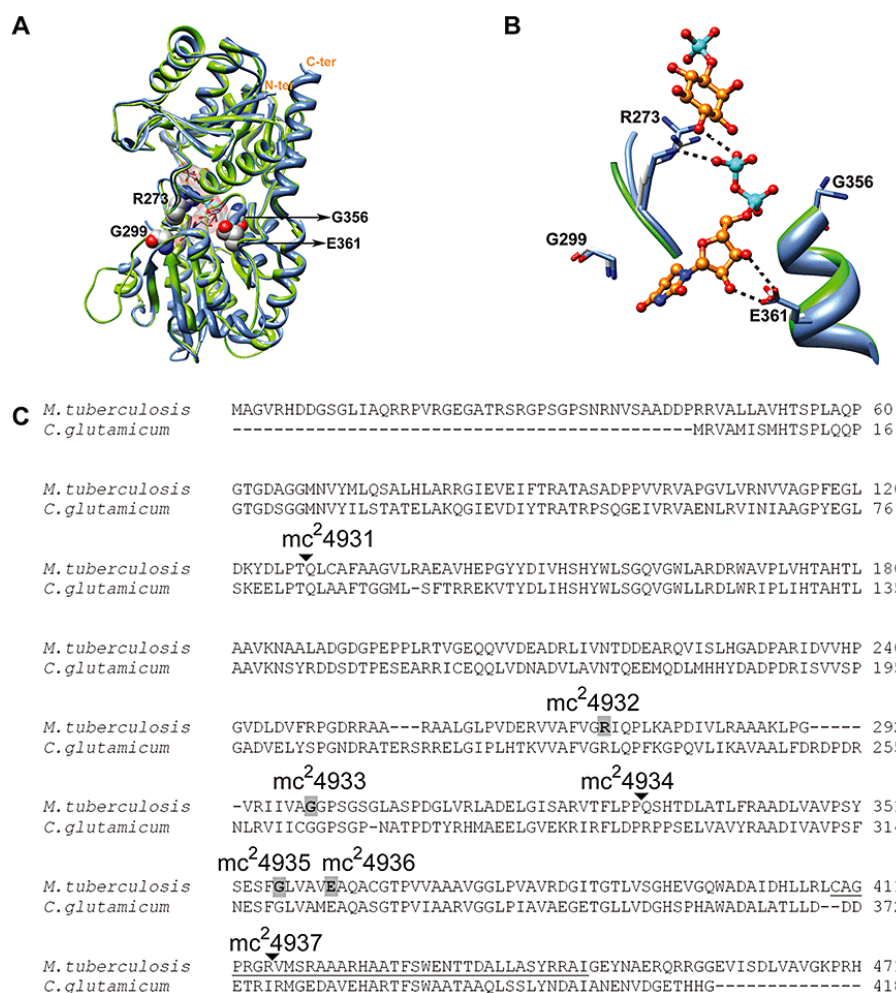


Figure 3-2. Comparison of the MshA structures of *M. tuberculosis* and *Corynebacterium glutamicum* establishes a rationale for the inactivation of MshA in the mutants.(Catherine Vilchèze et al., 2008)

(A) Ribbon representation of the superimposed *M. tuberculosis* MshA model (green) and CgMshA structure (blue) complexed with UDP/inositol-phosphate. Both UDP and inositol-phosphate are shown as stick with transparent surface. Four amino acids, whose mutation led to *M. tuberculosis* MshA inactivation, are represented as CPK structures and labeled accordingly.

(B) Active-site architecture of the superimposed MshA structures shown in (A). UDP and inositol-phosphate are shown as ball and stick. The four amino acid mutations R273, G299, G356 and E361, highlighted in (A), are shown as stick in white scheme, and the conserved residues in CgMshA are in blue scheme. Hydrogen bonds between the side-chain amines of Arg273 and the β -phosphate of UDP, as well as those between the side-chain carboxylate of Glu361 and the ribosyl hydroxyl groups of UDP are shown as black dotted lines. The residue numbers are for *M. tuberculosis* MshA.

(C) Alignment of the *M. tuberculosis* and *C. glutamicum* *mshA* sequences. The mutations identified in the *M. tuberculosis* *mshA* mutants are indicated. The four amino acid changes are in bold. The stop codons or frameshift are pointed by arrows. The residues in the α -helix crossing from C-terminal to N-terminal domain are underlined.

Mycothioli promotes ETH activation by the ethA-encoded mono-oxygenase

As the null mutants showed low (twofold the MIC) to no resistance to INH but showed a high level of resistance to ETH (≥ 6 -fold the MIC), we therefore postulated that mycothiol could be involved in either ETH activation or ETH-NAD adduct formation in *M. tuberculosis*. ETH is activated by the NADPH-specific FAD-containing mono-oxygenase EthA (Alain Baulard et al., 2000; Andrea DeBarber et al., 2000; Tommaso Vannelli et al., 2002).” The activity can be evaluated by monitoring the oxidation of NADPH aerobically (Figure 3-3 A). We have found a higher activity of EthA in the presence of mycothiol (Figure 3-3 B), and observed “an increase in the reaction rate directly proportional to the increase in mycothiol concentration (Table 3-3), suggesting that mycothiol plays a role in the activation steps rather than in the formation of the ETH-NAD adduct. Furthermore, replacing mycothiol by a different thiol, such as reduced glutathione, had no effect on the oxidation rate of NADPH (data not shown). This suggests that the increase in EthA activity upon the addition of mycothiol is specific to mycothiol, and does not occur in the presence of another thiol. To test if mycothiol was also required for the formation of the ETH-NAD adduct, the rate of inhibition of InhA by ETH in the presence of NAD^+ , NADPH, EthA and mycothiol was also measured. No formation of the ETH-NAD adduct was observed in these conditions (data not shown), which suggests that mycothiol is not involved in the formation of the ETH-NAD adduct. Two other anti-TB drugs, isoxyl and thiacetazone, are also activated by EthA (Lynn Dover et al., 2007). We therefore tested if the *mshA* mutants (null and point mutants) were also resistant to isoxyl and thiacetazone and found that they were

fully sensitive to both drugs (data not shown). This implies that mycothiol is solely involved in the activation of ETH. We could hypothesize that mycothiol either stabilizes the intermediates formed upon activation of ETH or forms a complex with the active form of ETH, which allows for the formation of the ETH-NAD adduct. More in-depth studies are necessary to fully understand which role mycothiol plays in the activation step.

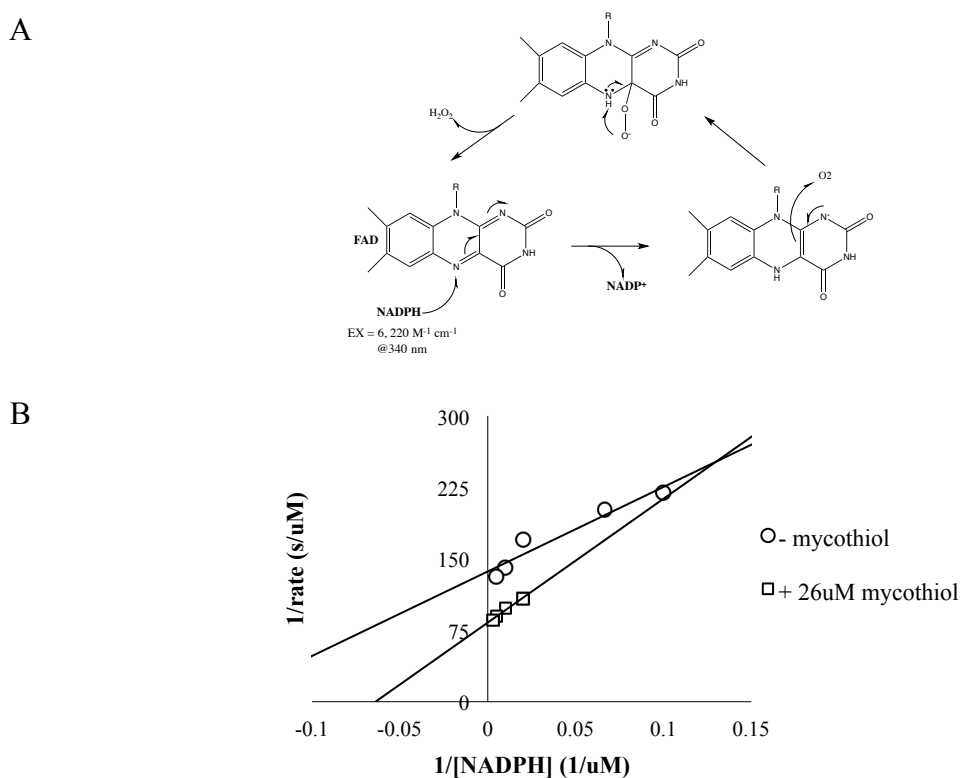


Figure 3-3. Mycothiol promotes ETH activation by the *ethA*-encoded mono-oxygenase. (A) EthA mediated NADPH oxidation aerobically (Bruce Palfey and Claudia McDonald, 2010). (B) Lineweaver–Burk plots for the NADPH oxidation catalyzed by EthA in the absence or presence of mycothiol. Without the additive, $k_{cat} = 0.0063 \text{ s}^{-1}$ which was comparable with the previous report (Marco Fraaije et al., 2004). When $26 \mu\text{M}$ mycothiol was added in the reaction, the k_{cat} was increased to 0.0115 s^{-1} .

Table 3-3. The effect of mycothiol on EthA activity.(Catherine Vilchèze et al., 2008)

[mycothiol] (μM)	[NADPH]/s ($\mu\text{M} /\text{s}$)	NADPH/EthA (mmol/s/mg protein)
0	0.0071	$1.24 \cdot 10^{-4}$
4.38	0.0074	$1.29 \cdot 10^{-4}$
17.5	0.0094	$1.64 \cdot 10^{-4}$
26.2	0.0111	$1.94 \cdot 10^{-4}$
43.8	0.0127	$2.23 \cdot 10^{-4}$

Experimental Procedure

Cloning, expression, and purification

The *M. tuberculosis dfrA* and *katG* genes were cloned as previously described (Argyrides Argyrou et al., 2006b). The plasmids of *M. tuberculosis katG* and *dfrA* were singly and doubly transformed into *E. coli* BL21(DE3) (EMD Bioscience, catalog no. 69387-3). The strain containing plasmids of *katG* and *dfrA* was cultured in LB-Miller medium containing 50 μg of kanamycin/ml and 50 μg of carbenicillin/ml at 37°C until the optical density (OD) at 600 nm reached 0.5. Expression of both genes was carried out by induction for 20 h at 18°C by the addition of 1 mM IPTG. At the same time of induction, 100 μg of INH/ml was also added to the culture. The same protocol was used for the strain containing just the *dfrA* plasmid. Recombinant *M. tuberculosis* DhfR was purified according to a previously described method (John Belisle et al., 1997).

The *M. tuberculosis inhA* and *katG* genes were cloned into pET30b and pDEST17 vectors, respectively, and then co-transformed into *E. coli* BL21(DE3). The strain containing both plasmids was cultured in LB medium containing 50 μg of

kanamycin/ml and 50 µg of carbenicillin/ml at 37°C until OD₆₀₀ reached 0.5. Expression of both genes was carried out by induction for 20 h at 18°C by the addition of 1 mM IPTG. At the same time of induction, 100 µg of INH/ml was also added to the culture. The proteins of InhA and KatG were co-purified by Ni-column followed by octyl sepharose hydrophobic column.

Enzymatic assays

All assays were carried out on a Cary 100 Bio Spectrophotometer at 25°C. Dhfr assays are performed by monitoring the oxidation of NADPH and reduction of dihydrofolate (DHF) at 340 nm. Reactions were initiated by adding Dhfr (10 nM) to assay mixtures containing NADPH (10 µM), DHF (4.5 µM), and phosphate buffer (pH 7.5, 50 mM). The KatG activity was assayed as previously described(Xiangbo Zhao et al., 2006). The InhA activity was assayed as previously described(Feng Wang et al., 2007b).

Mass spectroscopy analysis

Purified DHFR was heated for 60 s at 100°C. After the heat treatment, denatured enzyme was separated by filtration, using a Centricon (cutoff, 3 kDa). The filtrate was used for mass analysis. The matrix-assisted laser desorption ionization (MALDI) mass spectrometry experiment was carried out on an ABI Voyager-DE STR.

Crystallization of InhA in complex with INH-NAD adduct and data collection

Crystallization was accomplished by the hanging-drop vapor diffusion method. *M. tuberculosis* InhA in complex with INH-NAD was obtained in hanging droplets containing 2 μ l of protein solution at 10 mg/ml and with 2 μ l of buffer (12% 2-methyl-2,4-pentanediol, 4% dimethyl sulfoxide, 0.1 M HEPES, and 0.025 M sodium citrate) at 16°C in Linbro plates against 1 ml of the same buffer. To obtain a good occupancy of the INH-NAD adduct, 500 μ L of InhA (10 mg/mL) co-expressed with KatG was denatured by heating to release INH-NAD. The denatured proteins were removed by centrifugation. The resulted INH-NAD solution was incubated with 50 μ L InhA (10 mg/mL) on ice for 30 min, and the mixture was concentrated to a volume of 50 μ L for purpose of crystallization. Diamond shaped protein crystals formed about 4 days later.

Diffraction data of single InhA crystal was collected to at the wavelength of 1.542 Å using Rigaku R-Axis IV++ at home source. All the data were processed and reduced using HKL2000(Zbyszek Otwinowski and Wladek Minor, 1997). It is in the space group P6₂22, with one molecule in each asymmetric unit (Table 3-1).

Structure determination and model refinement

The structure of InhA was solved by molecular replacement using Molrep(Alexei Vagin and Alexei Teplyakov, 1997) in CCP4. InhA (PDB code 1ZID) with all nonprotein molecules removed, was used as the search model. A single solution for the molecular replacement was obtained. Isonicotinoyl-NAD (INH-NAD) was manually built in the active site of the model by examining the $F_o - F_c$ map in Coot(Paul Emsleya

and Kevin Cowtan, 2004). The final model containing residues 2–269 as well as 16 water molecules was obtained after further cycles of model building and PHENIX refinement (Afonine et al., 2005) yielding R factors of 20.8% and 25.6%. The full crystallization statistics are given in Table 3-1.

Isolation of INH- and ETH-resistant spontaneous mutants

Mycobacterium tuberculosis H37Rv mutants were isolated from non-mutagenized cultures grown in the media described above. The cultures were incubated by shaking at 37°C to late log phase. Ten-fold serial dilutions were then plated on agar plates (media described above) containing INH (0.2 $\mu\text{g ml}^{-1}$) and ETH (5 or 10 $\mu\text{g ml}^{-1}$). The plates were then incubated at 37°C for 6 weeks.

MIC determination

The strains were grown to an $\text{OD}_{600} \approx 1.0$. Ten-fold serial dilutions were plated on plates containing INH (0, 0.1, 0.2, 0.25, 0.3, 0.4, 0.5, 0.6, 0.8, 1 $\mu\text{g ml}^{-1}$) or ETH (0, 2.5, 5, 10, 15, 20 $\mu\text{g ml}^{-1}$). The MIC was determined as the concentration of drug that reduced the number of colony-forming units (cfu) ml^{-1} by 99%. MICs were also determined using the MTT assay (Martin et al., 2005).

EthA enzymatic activity assay

The his-tagged EthA was produced, as previously described (Lynn Dover et al., 2007). The activity of EthA was determined by monitoring the absorbance decrease of

NADPH at 340 nm ($\epsilon_{340\text{ nm}} = 6.22\text{ mM}^{-1}\text{ cm}^{-1}$). All the reactions were catalysed by $\sim 1\text{ }\mu\text{M}$ EthA and performed in 50 mM Tris/HCl, pH 7.5. Double reciprocal plots were used to determine the k_{cat} of the oxidation of NADPH. For measuring the effect of mycothiol, reaction mixtures contained 200 μM NADPH and varying mycothiol concentrations.

CHAPTER IV

STRUCTURES OF MYCOBACTERIUM TUBERCULOSIS FADD10 PROTEIN

REVEAL A NEW TYPE OF ADENYLATE-FORMING ENZYME*

Summary

Mycobacterium tuberculosis has a group of 34 FadD proteins that belong to the adenylate-forming superfamily. They are classified as either fatty acyl-AMP ligases (FAALs) or fatty acyl-CoA ligases (FACLs) based on sequence analysis. FadD10, involved in the synthesis of a virulence-related lipopeptide, was mis-annotated as a FACL, however, it is in fact a FAAL that transfers fatty acids to an acyl carrier protein (Rv0100). In this study, we have determined the structures of FadD10 in both the apo and the complexed form with dodecanoyl-AMP, where we see for the first time an adenylate-forming enzyme that does not adopt a closed conformation for catalysis. Indeed, this novel conformation of FadD10, facilitated by its unique inter-domain and intermolecular interactions, is critical for the enzyme to carry out the acyl transfer onto Rv0100 rather than Coenzyme A. This contradicts the existing model of FAALs that rely on an insertion motif for the acyl transferase specificity, and thus makes FadD10 a new type of FAAL. We have also characterized the fatty acid preference of FadD10 through

* This work has been published in and is reprinted with permission from: Zhen Liu, Thomas Ioerger, Feng Wang, and James Sacchettini. "Structures of *Mycobacterium tuberculosis* FadD10 protein reveal a new type of adenylate-forming enzyme" *The Journal of Biological Chemistry* 2013, 288 (25): 18473-83 Copyright 2013 (American Society for Biochemistry and Molecular Biology).

biological and structural analyses, and the data indicate long chain saturated fatty acids as the biological substrates of the enzyme.

Introduction

Adenylate-forming enzymes are found in a variety of important biological processes in both eukaryotes and prokaryotes (Stefan Schmelz and James Naismith, 2009). They show wide diversity in their catalytic activities and biological functions. The adenylate-forming superfamily of enzymes is composed of luciferases, amino acid adenylation domains of non-ribosomal peptide synthetases (NRPSs), acyl-Coenzyme A (acyl-CoA) synthetases, and acyl-acyl carrier protein (acyl-ACP) synthetases. These enzymes first use ATP to adenylate the carboxylate group of the cognate substrate, which is then followed by the transfer of the acyl moieties to the corresponding acceptors, for example, luciferyl to oxygen, amino acyl to peptidyl carrier protein (PCP) domains, and fatty acyl to CoA or ACPs. The fatty acyl-CoA synthetases (EC 6.2.1.3) and fatty acyl-ACP synthetases (EC 6.2.1.20) have also been referred to as fatty acyl-CoA ligases (FACLs) and fatty acyl-AMP ligases (FAALs), respectively (Benjamin Duckworth et al., 2012; Omita Trivedi et al., 2004; Pooja Arora et al., 2009; Zhening Zhang et al., 2011). Both enzymes have acyl-AMP ligase activity. However, FACLs transfer fatty acyl chains to Coenzyme A, while FAALs transfer fatty acyl chains to ACPs.

Within the genome of *Mycobacterium tuberculosis* (*M. tuberculosis*), there are 34 *fadD* genes that have been annotated to be members of the adenylate-forming

superfamily(Jean-Christophe Camus et al., 2002). Although the precise functions of most are unclear, several have been shown to be involved in the synthesis of bioactive lipids that are essential for bacterial survival or virulence(Israël Casabon et al., 2012; Kathleen Y. Dunphy et al., 2010; Laura Rindi et al., 2004; Roxane Siméone et al., 2010), and thus represent potential targets for drug discovery. Multi-sequence alignment of the 34 *M. tuberculosis* FadDs revealed two subclasses: 12 FAALs and 22 FACLs(Omita Trivedi et al., 2004). The 12 FAALs share a much higher sequence homology (70%-80% identity) than the FACLs (20%-30% identity). Interestingly, 10 of the 12 *M. tuberculosis* FAAL-encoding genes are located in close proximity to multienzyme polyketide synthases. Biochemical studies have shown that three of the FAALs (FAAL26, FAAL30, and FAAL32) transfer long chain fatty acyl moieties to the polyketide synthases: PpsA, PKS6, and PKS13, respectively(Mathieu Léger et al., 2009; Omita Trivedi et al., 2004; Sabine Gavalda et al., 2009). Therefore, it has been suggested that FAAL enzymes activate fatty acids as adenylate derivatives and sequentially transfer acyl moieties to cognate modular enzymes, particularly their ACP domains, to be further processed into complex lipids(Omita Trivedi et al., 2004; Pooja Arora et al., 2009). Recent structural and biochemical studies of *M. tuberculosis* FAAL28(Pooja Arora et al., 2009) and FAALs from *E. coli*, and *L. pneumophila*(Zhening Zhang et al., 2011) have provided a molecular basis for their catalytic mechanism. These studies have identified a signature sequence motif, consisting of an insertion of about 20 amino acids, that defines the function of this newly recognized subclass of the adenylate-forming

superfamily and distinguishes them from FACLs(Aneesh Goyal et al., 2011; Pooja Arora et al., 2009).

FadD10 (Rv0099) is present on an operon consisting of *Rv0096 – Rv0101*. The operon has been the subject of many studies(Arush Chhabra et al., 2012; Feng Wang et al., 2007a; Grant Hotter et al., 2005) because it is involved in making a virulence-essential lipopeptide using an NRPS (Rv0101, *nrp*). *M. smegmatis* has a similar NPRS, called *mps*, which synthesizes a glycopeptidolipid(Helen Billman-Jacobe et al., 1999). We have shown that Rv0098(Feng Wang et al., 2007a) is a fatty acyl-CoA thioesterase. While the identity of the lipopeptide produced by *M. tuberculosis Rv0096-Rv0101* operon is not known, its biological significance was indicated in several studies. For example, *Rv0096* was demonstrated to be required for *M. tuberculosis* survival in mouse macrophages(Jyothi Rengarajan et al., 2005), and *Rv0098-Rv0101* were predicted, using transposon site hybridization, to be required for *M. tuberculosis* survival in a mouse model of infection(Christopher Sassetti and Eric Rubin, 2003). It has been suggested that the products of the operon repressed the *SigM* factor that further regulates a series of metabolic pathways and modulates the host-bacteria interactions(Sahadevan Raman et al., 2006). In spite of the biological significance of the lipopeptide produced by the *Rv0096-Rv0101* operon, neither the isolation nor the identity of this lipopeptide have been reported; therefore, an alternative approach to define its chemical structure is to characterize the function and mechanism of the individual proteins involved in its synthesis.

Rv0098-Rv0101 are essential for *M. tuberculosis* survival in the mouse model of infection(Christopher Sassetti and Eric Rubin, 2003). Hence they likely to have direct enzymatic roles in the synthesis of the virulence-related lipopeptide product of the operon. As mentioned above, our biochemical and structural characterization of *Rv0098* has shown that it encodes a thioesterase capable of hydrolyzing a long chain fatty acyl-CoA to release a fatty acid and Coenzyme A(Feng Wang et al., 2007a). Rv0100 is clearly an ACP according to sequence analysis, and it shares 24.4% sequence identity to the primary *M. tuberculosis* ACP (Rv0033) involved in type II fatty acid biosynthesis. Rv0101 is a two-module NRPS, with the first module of an undefined amino acid specificity and the second module to incorporate phenylalanine(Marc Röttig et al., 2011). *M. tuberculosis* FadD10 (Rv0099) was designated as an FAAL based on sequence analysis(Omita Trivedi et al., 2004). However, the presence of a thioesterase (*Rv0098*) immediately upstream suggests that *fadD10* is unlikely to function as an acyl-CoA synthetase because this would put two enzymes with opposing functions next to each other in the operon. Indeed, the fact that *fadD10* is located in close proximity with a multi-function enzyme (*Rv0101*) is analogous to the *M. tuberculosis* FAALs. These findings suggest that *M. tuberculosis* FadD10 activates and transfers the fatty acyl chain to the cognate ACP - Rv0100. Chhabraa *et al.* recently showed that FadD10 does not acylate CoA, but is able to transfer a radioactively labeled dodecanoyl moiety to Rv0100 *in vitro*(Arush Chhabraa et al., 2012). This suggests that FadD10 has FAAL activity even though it has a primary sequence more similar to FAALs. FadD10 has much lower sequence similarity to the members of the *M. tuberculosis* FAALs cluster and moreover

lacks the signature motif critical for FAAL activity (Figure 4-1); hence, it is intriguing to delineate the molecular basis underlying this discrepancy.

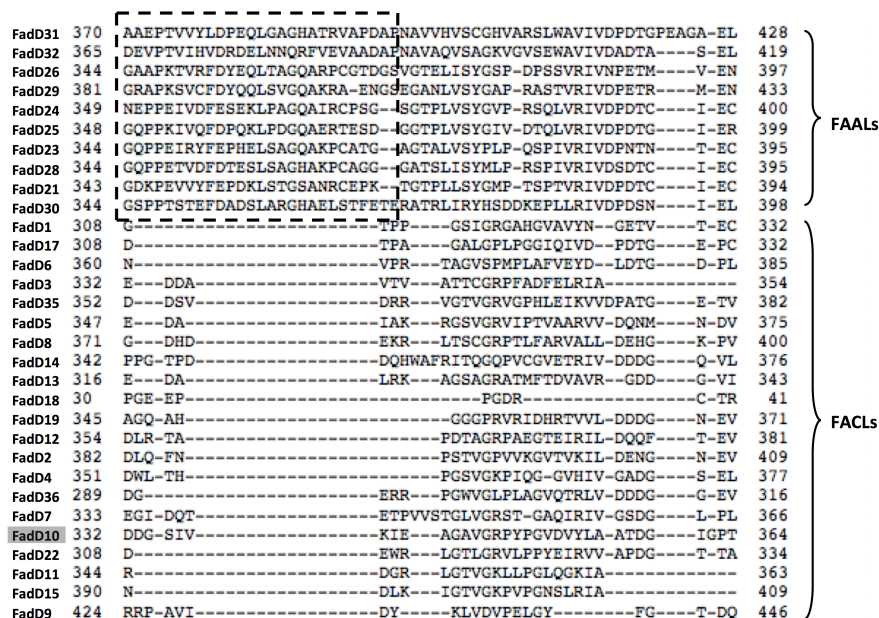


Figure 4-1. Mutisequence-alignment of *M. tuberculosis* FadDs reveals a signature insertion (boxed) for FAALs cluster.

In this study, we have solved the structures of both apo and dodencanoyl-AMP bound *M. tuberculosis* FadD10, leading to the characterization of a novel ligand bound conformation for the adenylate-forming superfamily. Instead of undergoing conformational rearrangement between the N- and C-terminal domains, as observed in all the other reported adenylate-forming homologues(Andrew Gulick, 2009), FadD10 retains a single open conformational state for both the apo- and ligand-bound forms. We find that FadD10's FAAL activity can be explained by its unique inter-domain and

intermolecular interactions, a mechanism distinct from that known for the other FAALs. Our modeling studies identify the binding site of the ACP (Rv0100) onto FadD10 in the acyl transfer reaction. Also, our studies provide a structural basis for the fatty acid preference of *M. tuberculosis* FadD10, which may eventually aid in elucidating the chemical structure of the virulence-related lipopeptide produced by *the Rv0096-Rv0101* operon.

Results and Discussion

Crystal structures of M. tuberculosis FadD10 subunit

In order to understand the molecular basis of the FAAL activity of FadD10 arising from a primary sequence more similar to FAALs, we have determined the structures of FadD10 in both apo and complexed forms. The full-length apo *M. tuberculosis* FadD10 crystallized in space group P2₁ and its structure was solved using Selenium-Single-wavelength Anomalous Dispersion. The asymmetric unit contains a dimer (Figure 4-2 A), consistent with the gel filtration analysis. The two subunits are very similar with an RMSD of 0.68 Å for 491 α carbons after superimposition (Figure 4-2 C). For the chains designated as A and B, a total of 508 and 502 out of 540 residues, respectively, were visible and built into the electron density. Residues S178, T181, E183, and K185 of chain A and residues E426, R451, S474, E476, and L477 of chain B were built as alanine due to ambiguous side chain electron density. The structure was refined to 2.2 Å resolution with a final R-factor of 22.7% and a R-free of 27.3%. Statistics of the refined structures are listed in Table 1.

FadD10 complexed with the half-reaction product dodecanoyl-AMP crystallized in space group $P3_121$. Its structure was solved by molecular replacement using chain A of our refined apo structure as the search model. Dodecanoyl-AMP was built into a clear electron density ($F_o - F_c$ map) located at the active site (Figure 4-2 B). In this crystal, *M. tuberculosis* FadD10 packed with one molecule per asymmetric unit, and the two subunits of the dimer are related to each other by a crystallographic 2-fold symmetry. The structure, with 508 residues built into the electron density, was refined to 2.8 Å resolution with a R-factor of 22.6% and a R-free of 27.9%. Superposition of the complexed *M. tuberculosis* FadD10 subunit with the chain A and chain B from the apo crystal yields an RMSD of 0.596 Å and 0.637 Å, respectively, for the α -carbons (Figure 4-2 C).

Each subunit of *M. tuberculosis* FadD10 is composed of two domains (Figure 4-2 D). The N-terminal domain consists of 420 amino acids (residue 1-420), forming a central α/β structure surrounded by a distorted β -sheet on one side and three β -strands with intervening α -helices on the other side. The loop containing the residues ⁴²¹KGRSS⁴²⁵ extends from the β -strand B15 and continues into the C-terminal domain, consisting of 115 amino acids (residue 426-540). This domain is composed of three β -strands surrounded by two α -helices and a pair of short anti-parallel β -strands at the beginning of the domain.

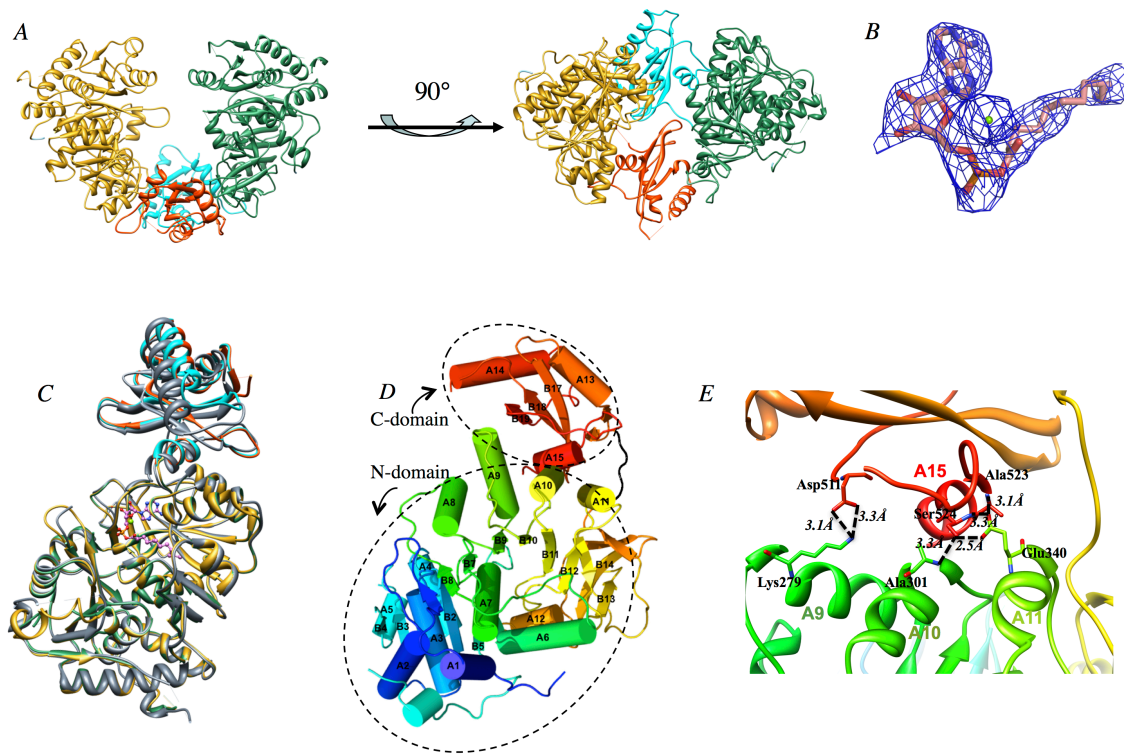


Figure 4-2. The structures of apo- and complexed FadD10 with dodecanoyl-AMP. (A) Ribbon representation of the dimeric FadD10. The N-terminal domains of the two subunits, designated as A and B, are colored yellow and green, while the corresponding C-terminal domains are colored orange and cyan, respectively. (B) $F_o - F_c$ map is calculated when dodecanoyl-AMP and magnesium ion are omitted from the model, and is contoured at 2 sigma level. (C) FadD10 (grey) in complex with dodecanoyl-AMP (pink) is superimposed with the two subunits (colored as in Figure 2A) from the apo structure. (D) Cylinder representation of FadD10 that demonstrates the 2-domain organization and the secondary structure elements of each subunit. The inter-domain loop is colored in black. (E) The inter-domain hydrogen bonds shown as dotted lines. The residues involved in the interactions are shown in stick. The identity of the helices involved in forming the hydrogen bonds is marked in color.

Analysis of the complexed FadD10 subunit structure using VAST (Vector Alignment Search Tool)(Jean-Francois Gibrata et al., 1996) revealed that the highest structural similarity was with adenylate-forming enzymes, namely *Alcaligenes sp.* 4-chlorobenzoate-CoA synthetase (CBL), the *M. tuberculosis* very-long-chain fatty acyl-

CoA synthetase FACL13, and the *N. lolii* NRPS activation domain SidNA3.

Superposition of the full-length *M. tuberculosis* FadD10 with these structures yielded fairly poor alignments. For instance, superposition between *M. tuberculosis* FadD10 and FACL13 (PDB ID: 3R44) showed an alignment with only part (301 out of 420 α -carbons) of the N-terminal domain (RMSD 2.61 Å). When the N-terminal domains were aligned, the C-terminal domains were found to be in a completely different orientation, even though the secondary structural elements of their C-terminal domains were quite similar. Indeed, dividing FadD10 into N-terminal and C-terminal domains allowed 80% of its N-terminal structure and 70% of the C-terminal structure to align with FACL13, yielding RMSD of 2.80 Å for 345 N-terminal domain α -carbons and 4.24 Å for 101 C-terminal domain α -carbons. A similar result was observed when *M. tuberculosis* FadD10 was compared with the other adenylate-forming homologues identified by VAST, i. e. structural superposition could only be obtained when the N-terminal and C-terminal domains were overlaid independently. While all of the adenylate-forming enzymes complexed with adenylate (including analogs) share a similar inter-domain orientation, *M. tuberculosis* FadD10 adopts a distinctive inter-domain conformation (Figure 4-3 A). As expected, similar alignments were obtained with the apo structure of FadD10.

The adenylate-forming superfamily of proteins that have been structurally characterized revealed remarkable conformational flexibility between the N- and C-terminal domains (Andrew Gulick et al., 2004; Charlotta S. Andersson et al., 2012; Elena Conti et al., 1996; Grazyna Kochan et al., 2009; Jurgen May et al., 2002; Manish Shah et al., 2009; Yuko Hisanaga et al., 2004). The inter-domain orientations of these proteins

vary noticeably among the apo structures as well as between the apo and the respective ligand bound structures of the individual proteins. Such variations are not correlated to the functions of different subclasses. They likely arise because the two domains form no significant protein-protein inter-domain contacts and are connected by only a flexible loop. This feature allows the two domains to rearrange upon substrates binding in order to desolvate the active site, a process that has been referred to as the “domain alternation” mechanism for the adenylate-forming superfamily(Andrew Gulick, 2009). This mode of ligand binding is exemplified by the *Thermus thermophilus* long chain fatty acyl-CoA synthetase (LC-FACS)(Yuko Hisanaga et al., 2004). When this protein binds AMPPNP or myristyl-AMP, its C-terminal domain rotates almost 180° relative to the inter-domain linkage loop (⁴³²DRLK⁴³⁵) and moves towards the N-terminal domain forming a lid over the active site. A similar rearrangement, with varying extents of rotation, has also been observed for *P. pyralis* luciferase(Elena Conti et al., 1996), the aryl acid adenylation domain of bacillibactin synthetase (DhbE)(Jurgen May et al., 2002), *Alcaligenes sp.* CBL(Andrew Gulick et al., 2004), and *H. sapiens* medium chain acyl-CoA synthetase(Grazyna Kochan et al., 2009), for which both apo and ligand-bound structures are available. Thus, the closure of the C-terminal domain toward the N-terminal domain is believed to be a common substrate binding event for the adenylate-forming superfamily. In this respect, *M. tuberculosis* FadD10 is clearly unique in comparison to other homologous adenylate-forming proteins, as it maintains an “open” conformation for the apo structure, as well as for FadD10 complexed to the half-reaction product dodecanoyl-AMP.

A novel ligand-bound conformation of M. tuberculosis FadD10

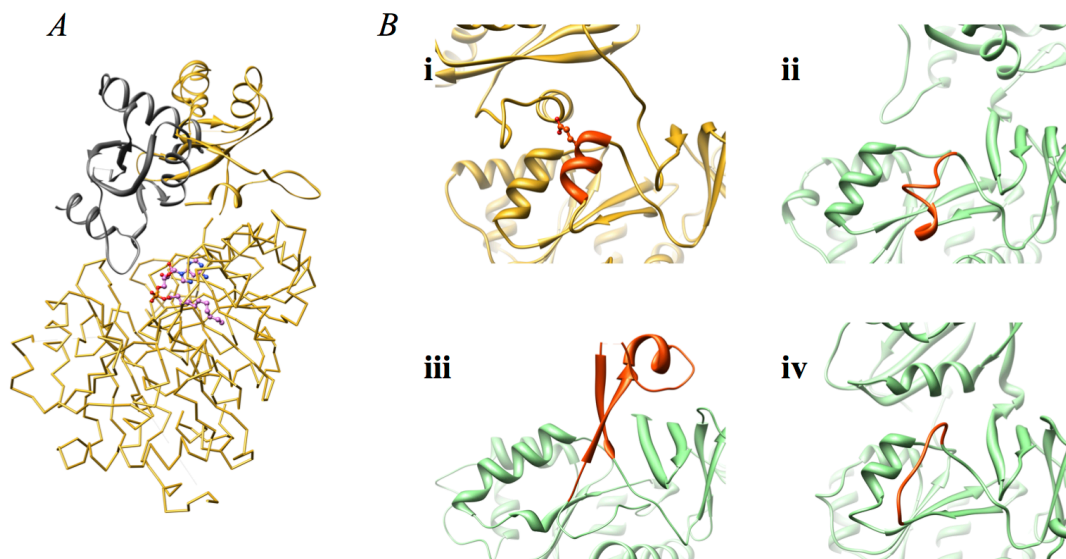


Figure 4-3. The unique inter-domain interaction of FadD10 contributes to the conformational maintenance.

(A) FadD10 (yellow) complexed with dodecanoyl-AMP (ball and stick) is aligned with human medium chain acyl-CoA synthetase (gray, PDB ID: 3DAY) at their N-terminal domains. The latter is shown only the C-terminal domain, and the N-terminal domain of FadD10 is shown in carbon trace for clarity.

(B) The variation of the secondary structure equivalent to FadD10 helix A11 (i), among adenylate-forming enzymes, is exemplified by ii. *M. tuberculosis* FACL13 (PDB ID: 3R44), iii. *M. tuberculosis* FAAL28 (PDB ID: 3E53), and iv. *B. brevis* PheA (PDB ID: 1AMU). E340 in FadD10 is shown as ball and stick. A11 and its equivalents are colored red.

The apo and complexed structures of *M. tuberculosis* FadD10 have provided several insights into the structural determinants for its unique “open” ligand bound conformation. The first factor that contributes to the maintenance of the open conformation in the *M. tuberculosis* FadD10 structures is the inter-domain interactions between the α -helix A15 from the C-terminal domain and the three-helix (A9, A10,

A11) cluster from the N-terminal domain (Figure 4-2 E). Specifically, the side-chain oxygen of Ser524 forms hydrogen bonds with both the side-chain oxygen of Glu340 (2.5 Å) and the backbone nitrogen of Ala301 (3.3 Å). More inter-domain hydrogen bonds are formed by the backbone nitrogens of Ala523 (3.1 Å) and Ser524 (3.3 Å) with the side-chain carboxylate of Glu340, as well as between the side-chain amine of Lys279 and the side-chain oxygen atoms of Asp511 (3.1 Å and 3.3 Å). These interactions are maintained in both the apo *M. tuberculosis* FadD10 structure and the complexed structure with dodecanoyl-AMP, which greatly limits the inter-domain movement of the protein. A similar inter-domain contact has not been observed in the other adenylate-forming proteins. The reason is likely due to the absence of the structural elements found in *M. tuberculosis* FadD10 accounting for this interaction. While A9, A10, and A15 are structurally conserved, the structural equivalent to helix A11 of FadD10 (Figure 4-3 B i) notably varies among adenylate-forming proteins. A short helix equivalent to A11 is found present in only four members, including the adenylation domains DhbE(Jurgen May et al., 2002) and DltA(Huma Yonus et al., 2008), as well as the acyl-CoA synthetases LC-FACS(Yuko Hisanaga et al., 2004) and *M. tuberculosis* FAAL13(Charlotta S. Andersson et al., 2012). However, the glutamate residue (E340) essential to forming inter-domain hydrogen bonds in *M. tuberculosis* FadD10 is replaced by non-polar residues in these four homologous proteins (Figure 4-3 B ii). A significant structural alteration of A11 is observed in FAALs, including the N-terminal domain of *M. tuberculosis* FAAL28(Pooja Arora et al., 2009), the full-length *E. coli*, and *L. pneumophila* FAALs(Zhening Zhang et al., 2011), where the helix A11 is replaced by a

β -strand followed by an α -helix or a loop (Figure 4-3 B iii). This is the location where the ~20-amino-acid insertion motif occurs in FAALs, which has been implicated in determining FAAL activity. In all of the other structures that have been determined for the adenylate-forming superfamily, the region equivalent to the helix A11 is disordered (Figure 4-3 B iv).

The second factor contributing to the rigidity of *M. tuberculosis* FadD10 open conformation arises from the quaternary organization of the dimer. According to the current understanding of adenylate-forming proteins, most of them, including FAALs (Zhening Zhang et al., 2011), are functional as monomers. The only subclass that can form dimers are the acyl-CoA synthetases, and for these proteins the dimerization interface is always limited to the N-terminal domains. This observation is consistent with the acyl-CoA synthetic mechanism, which requires the C-terminal domain to move freely relative to the N-terminal domain in order to bind ATP and then Coenzyme A in the step-wise reactions. *M. tuberculosis* FadD10 is also shown to be a dimer in solution based on both gel filtration analysis (data not shown), and PISA (Protein Interfaces, Surfaces and Assemblies) calculation (Evgeny Krissinel and Kim Henrick, 2007). In both the apo structure of *M. tuberculosis* FadD10 and its complexed structure with dodecanoyl-AMP, the two subunits of the dimer form an extensive network of intermolecular interactions, including 8 hydrogen bonds and many van der Waals interactions. All of the hydrogen bonds and most of the van der Waals interactions are between residues from the C-terminal domain of one subunit and residues from the N-terminal domain of the other subunit. This confers a contact area of about 1600 Å² per

22000 Å² for each subunit. FadD10 is the first adenylate forming enzyme other than acyl-CoA synthetases, to be identified as a dimer. More importantly, the two subunits of the dimer interact in a manner which was previously unseen in the other homologs, and we propose this dimerization mode has played a role in maintaining the “open” conformation of *M. tuberculosis* FadD10 upon binding dodecanoyl-AMP.

The conformation of M. tuberculosis FadD10 prevents Coenzyme A binding

The adenylate-forming proteins, as a superfamily, share 10 conserved sequence motifs (Mohamed Marahiel et al., 1997), a similar structural scaffold (Andrew Gulick, 2009), and a common half reaction -the adenylation of the carboxylate group of a substrate. Moreover, structural characterization of the superfamily revealed that a phosphopantetheine binding cavity is structurally conserved in the N-terminal domain. This is consistent with the notion of an evolutionary relationship within the adenylate-forming superfamily, and strongly argues that the ubiquitous acyl-CoA synthetases are likely to be ancestral (Aneesh Goyal et al., 2011; Hugo Fraga et al., 2004; Uwe Linnea et al., 2007). Functional conservation of acyl-CoA synthesis activity has also been reported in other sub-classes of the adenylate-forming superfamily. For example, firefly luciferase (Hugo Fraga et al., 2004) as well as five different adenylation domains of NRPSs (Uwe Linnea et al., 2007) were shown to synthesize luciferyl-CoA and aminoacyl-CoAs, respectively, when their genuine acyl acceptors were absent and Coenzyme A was added as substrate. In contrast, *M. tuberculosis* FAALs (acyl-ACP synthetases) that have been studied, to date, which have also been proposed to be

descendants of acyl-CoA synthetases, lack acyl-CoA synthesis activity(Aneesh Goyal et al., 2011; Pooja Arora et al., 2009), even though they retain the binding elements of phosphopantetheine. This was demonstrated as well for FadD10.

Structural comparison and analyses of relative domain orientation of FAALs and FadD10 with acyl-CoA synthetases provides a plausible explanation to their inability to turnover acyl-CoA. The structures of three acyl-CoA synthetases, *Alcaligenes sp.* CBL, human medium chain fatty acyl-CoA synthetase, and *E. coli* acetyl-CoA synthetase have all been reported in complex with Coenzyme A or derivatives(Andrew Gulick et al., 2003; Andrew Gulick et al., 2004; Grazyna Kochan et al., 2009). When these proteins bind to Coenzyme A, their C-terminal domains all rotate about 140° relative to the position in the adenylate bound form. Also, for all of these proteins, the C-terminal domain is explicitly engaged in the binding of Coenzyme A through hydrophobic interactions with its nucleotide moiety. This domain reorganization is believed to be requisite for Coenzyme A binding by the adenylate-forming enzymes, and hence for the formation of acyl-CoA.

Sequence analysis of *M. tuberculosis* FadD proteins reveals an N-terminal domain insertion of 10 to 24 amino acids only present in the FAAL cluster (Figure 4-1). Using the sequence insertion as an indicator, a number of putative FAALs can be identified in various organisms. Structural studies of *E. coli* FAAL, *L. pneumophila* FAAL(Zhening Zhang et al., 2011), and the N-terminal domain of *M. tuberculosis* FAAL28(Pooja Arora et al., 2009) indicate that the inserted sequence flanks the interface of the two domains. In *M. tuberculosis* FadD28 and *E. coli* FAAL, the insertion

folds into a β -strand followed by a short α -helix and a short extension of β -strand; in *L. pneumophila* FAAL, the insertion folds into a β -strand and then a loop. The structural insertion does not appear to interfere with the closure of the C-terminal domain to form the adenylate bound conformation (Zhening Zhang et al., 2011). However, it prevents the FAALs from undergoing the large-scale inter-domain rotation associated with Coenzyme A binding. The functional role of the insertion was further established, by showing that its deletion and addition manipulated the gain and loss of acyl-CoA synthesis activity in *M. tuberculosis* FAALs and FACLs, respectively (Aneesh Goyal et al., 2011; Pooja Arora et al., 2009).

M. tuberculosis FadD10 does not have the FAALs insertion; therefore, the lack of acyl CoA synthesis activity for *M. tuberculosis* FadD10 must be based on a different mechanism. We propose that it is the unique inter-domain and intermolecular interactions of FadD10, as described above, that prevent the required inter-domain rearrangement for Coenzyme A binding. The introduction of an acyl moiety into a natural product made by a PKS or NRPS is a well-recognized function of the acyl-CoA synthetases. While the acyl-CoA synthetases have been extensively studied, the CoA independent acyl transfer function has only been recently discovered and the understanding of its mechanism is limited to FAALs (Debasisa Mohanty et al., 2011). Functionally analogous to FAALs, *M. tuberculosis* FadD10 has revealed a distinct strategy to prevent acyl-CoA synthesis. It contradicts the existing model for the catalysis of FAALs dependent on an insertion motif, therefore establishes *M. tuberculosis* FadD10 as a new type of FAAL.

Modeling studies of the interactions between M. tuberculosis FadD10 and Rv0100

We have identified the likely binding interface for ACP (Rv0100) on FadD10. Because the transfer of a fatty acyl chain to the ACP by FadD10 is analogous to the transfer of amino acyl groups to peptidyl carrier proteins by NRPS adenylation domains, we have compared FadD10 with the structure of *P. aeruginosa* PA1221, which is a didomain construct containing an adenylation domain and a peptidyl carrier protein (Carter Mitchell et al., 2012). When the N-terminal domains of FadD10 and PA1221 adenylation domain (21% identity) are superimposed, their C-terminal domains are in different orientations as expected. Interestingly, the peptidyl carrier protein of the didomain structure is positioned in an orientation poised for the FadD10 substrate to bind. Specifically, the side chain of the active site serine residue of the peptidyl carrier protein is directed toward and is approximately the correct distance to the phosphopantetheine binding cavity of FadD10 (Figure 4-4 A). When the interaction between FadD10 and the PA1221 peptidyl carrier protein is examined over the surface of the FadD10 dimer, we observe a relatively good fit of the carrier protein onto the intermolecular space of the dimer. Because ACPs are highly functionally and structurally homologous to the peptidyl carrier proteins, we have generated a homology model of Rv0100 based on the structure of PA1221 peptidyl carrier protein (19% identity) (Christophe Lambert et al., 2002). When the ACP model is overlaid on top of the superposition of FadD10 and PA1221, the interaction of ACP to FadD10 is similar to that of the PA1221 peptidyl carrier protein to FadD10 (Figure 4-4B), which suggests that

the open conformation of FadD10 has room for the ACP (Rv0100) to bind for acyl transfer.

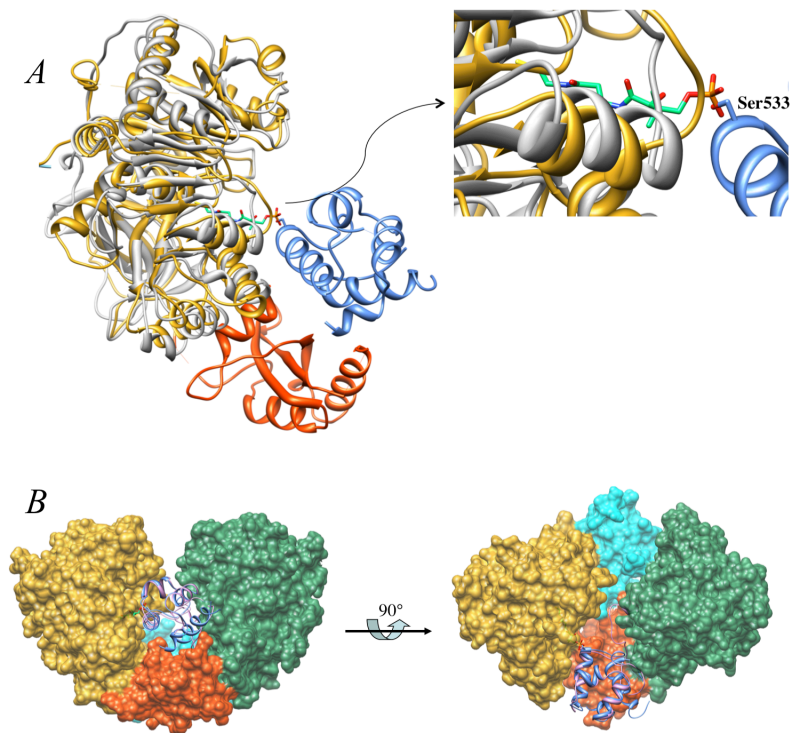


Figure 4-4. Modeling studies of the interactions between *M. tuberculosis* FadD10 and Rv0100. (A) Ribbon representation of the superposition of FadD10 subunit A with the didomain structure of PA1221 (PDB ID: 4DG9). The N-terminal and C-terminal domains of FadD10 are colored in yellow and orange, respectively. The N-terminal domain of the PA1221 adenylation domain is colored in white and its C-terminal domain is hidden for clarity. The PA1221 peptidyl carrier protein is colored in blue and its active site residue Ser533 is shown in stick. Phosphopantetheine, shown in green stick, is modeled based on comparison with human medium chain fatty acyl synthetase in complex with butyl-CoA (PDB ID: 3EQ6). (B) Surface representation of the interaction between the ACP (Rv0100) and FadD10 dimer. The subunit A of FadD10 dimer and PA1221 peptidyl carrier protein are colored as in panel A. The N-terminal and C-terminal domains of the FadD10 subunit B are colored in green and cyan, respectively. The Rv0100 model is shown as pink ribbon.

Substrate binding site of M. tuberculosis FadD10

Several structures of adenylate-forming proteins in complex with adenylated derivatives (including three proteins bound to different long chain acyl-AMPs (Yuko Hisanaga et al., 2004; Zhening Zhang et al., 2011)) have been reported, wherein multiple residues from both the N-terminal and C-terminal domains are involved in the binding of adenylate moiety. However, the interactions between the amino acids of the C-terminal domain to the adenylate moiety are missing in *M. tuberculosis* FadD10, due to its open conformation. Conserved between FadD10 and the other homologous structures are primarily the interactions between the residues from the N-terminal domain of the enzyme and the adenylate group. The adenosine moiety, which is coordinated by a network of both hydrophobic interactions and hydrogen bonding (Figure 4-5 A), sits at the entrance to the catalytic cavity. The planar adenine is sandwiched by the hydrophobic side-chains of Tyr317 and Val344 on one side, and the backbone atoms of ²⁹⁴GGSR²⁹⁷ on the other side. The exocyclic nitrogen forms hydrogen bonds with the side-chain oxygen of Gln315 (3.2 Å) and the backbone oxygen of Val316 (3.2 Å). The major binding determinants of ribose are Gly295 and Asp408. Specifically, the backbone oxygen of the former forms hydrogen bond (3.3 Å) with the ribose ring oxygen, and a side chain oxygen of the latter interacts with the 3' (3.2 Å) ribosyl hydroxyl via hydrogen bond. The α -phosphate of AMP interacts with Ser320 by forming hydrogen bonds between the O2 of the phosphate and the backbone nitrogen (3.3 Å) of this residue.

The dodecanoyl aliphatic chain is buried inside a preformed narrow closed-end tunnel by β -strands B9, B10, B11, and α -helix A7 (Figure 4-5 B). In the apo structure of FadD10, this fatty acyl binding cavity is vacant. The tunnel that contains the aliphatic chain is lined primarily by the backbone atoms of B9, B10, and B11 (i.e. ²⁶⁴TCLV²⁶⁷, ²⁹¹VGYGG²⁹⁵, and ³¹⁷YG³¹⁸), while only three hydrophobic side chains, Val316, Ile226, and Trp231, are within van der Waal's distance to the aliphatic chain. Approximately 11 Å from the portal of the fatty acyl binding cavity, which is near the C12 of the dodecanoyl chain, the tunnel splits into two directions. In one direction, it extends along strand B9 to Leu290, whose dimethyl carbons are 5.5 Å from C12 of the dodecanoyl chain. In the other direction, it bends into a highly hydrophobic groove made by the side-chains of Leu201, Val209, Trp211, Trp230, and Tyr348. At the distal end, it is terminated by the side chains of Val197 and Pro198. The bottom of this groove is about 9.4 Å from C12 of the dodecanoyl chain, raising the possibility that the enzyme could accommodate a longer fatty acid substrate. We compared the fatty acid binding tunnels of the very long chain fatty acyl-CoA synthetase *M. tuberculosis* FACL13 (active on fatty acid with up to 26 carbons)(Charlotta S. Andersson et al., 2012), FadD10, and the human medium chain fatty acyl-CoA synthetase (active on fatty acid with up to 10 carbons)(Grazyna Kochan et al., 2009). The linear distance between the distal end and the portal of their fatty acyl binding tunnels are approximately 17 Å, 14 Å, and 10 Å, respectively, which indicates that the biological substrate of FadD10 is probably a long chain fatty acid. Based on the geometric modeling and taking into account of the contact

distance associated with atomic van der Waals radii, the fatty acid binding tunnel in FadD10 could accommodate at most 16 carbons (i. e. hexadecanoic acid).

To further determine the fatty acid specificity of FadD10, we incubated *M. tuberculosis* FadD10 and the holo-ACP (Rv0100), with fatty acids of varying chain length and degree of saturation, and then analyzed the results for the acylation of ACP (Rv0100) using ESI-QTOF mass spectrometry. We observed acylated ACP even when hexadecanoic acid was used as a substrate (Figure 4-5 C). This is consistent with the modeling study that shows a hexadecyl chain can be accommodated in the fatty acid binding tunnel of FadD10, and Chhabraa *et al.*'s study (Arush Chhabraa et al., 2012) showing that FadD10 could utilize fatty acids with up to 16 carbons in the adenylation reaction. The lower product yield for hexadecanoic acid could reflect differences in solubility or affinity. We have also observed a higher activity of FadD10 with hexadecanoic acid than 2-trans-hexadecenoic acid, which suggests that FadD10 prefers saturated fatty acid substrates. We previously identified Rv0098 as a long chain (C12-C18) fatty acyl-CoA thioesterase. It, taken together with the structural analyses and enzymatic characterization of FadD10 (Rv0099), suggests that the lipopeptide produced by the *M. tuberculosis* Rv0096-Rv0101 operon incorporates a long chain fatty acid, particularly tetradecanoic acid that demonstrated the highest activity to acylate the ACP (Rv0100).

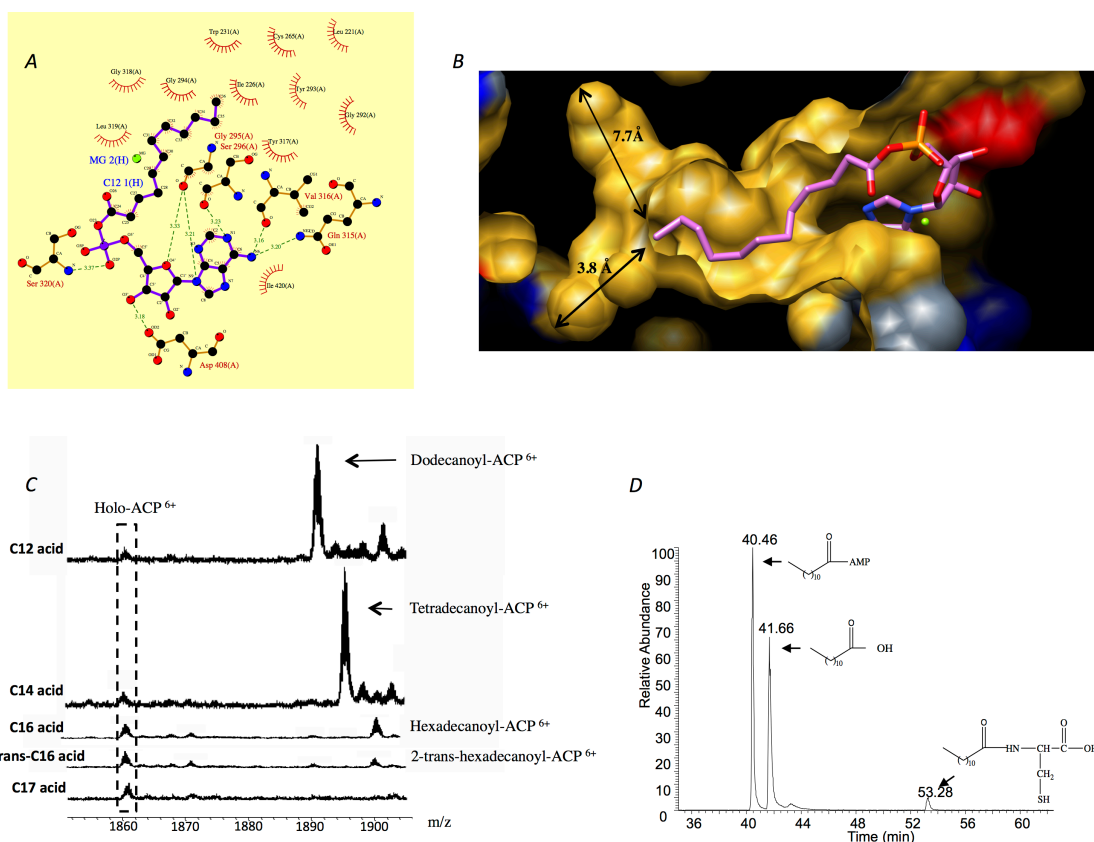


Figure 4-5. Biochemical and structural analyses suggest the biological substrate of FaddD10. (A) Schematic representation of the hydrogen bonds (dotted lines) and hydrophobic interactions (bows) between dodecanoyl-AMP and FaddD10. (B) The fatty acid binding tunnel of *M. tuberculosis* FaddD10. The hydrophobic, positive, negative, and neutral surfaces of FaddD10 are colored yellow, blue, red, and grey, respectively. Dodecanoyl-AMP is shown in stick and colored in pink. The arrows indicate the distance from the terminal carbon of dodecanoyl chain to the molecular surface of the binding tunnel, taking into account of atomic van der Waals radii. (C) ESI-QTOF mass spectrometry of the holo-ACP (Rv0100) acylated by *M. tuberculosis* FaddD10, in addition of fatty acids with varying chain length and degree of saturation. The ratio of abundance between the unreacted holo-ACP and the acylated ACP is approximately 1:5.5, 1:6.9, 1:1.5, 1:0.6, and 1:0, respectively, for C12, C14, C16, 2-trans-C16, and C17 fatty acid. (D) FaddD10 was incubated with dodecanoic acid, ATP, and cysteine, and then analyzed by LC-MS. The result is simplified for clarity by only showing the elution of dodecanoic acid, dodecanoyl-AMP, and dodecanoyl-cysteine.

ATP-dependent amide bond synthesis activity has been previously reported for the short chain acyl-CoA synthetases as well as for firefly luciferase (Tomoko Abe et al., 2008). Specifically, this was observed when cysteine analogues, including D-cysteine, homocysteine, and L-cysteine, were used as substrates to react with the preferred acid substrate of each enzyme. N-acylated cysteine derivatives were detected (Tomoko Abe et al., 2008). We have observed a similar activity in FadD10 using cysteine as a substrate (Figure 4-5 D). Unlike the side reactions observed in short chain acyl-CoA synthetases and firefly luciferase, whose amide forming activity is limited to cysteine analogues (Tomoko Abe et al., 2008), FadD10 is promiscuous with respect to other amino acids, specifically histidine, aspartate, glycine, and phenylalanine as we have tested (data not shown). Other amide synthetases belonging to the adenylate-forming superfamily have been reported. NovL, CloL, CouL, and SimL involved in novobiocin, chlorobiocin, coumermycin A1, and simocyclinone D8 synthesis, respectively, can catalyze the formation of an amide bond between the amino group on the aminocoumarin ring and a carboxylate moiety through forming an adenylated intermediate (Elisabeth Schmutz et al., 2003; Florence Pojer et al., 2002; Marion Steffensky et al., 2000; Thomas Luft et al., 2005). Similar to *fadD10*, these four enzymes are in proximity to and cooperate with NRPS encoding genes. This suggests that amide formation, a side reaction to thioesterification of adenylate-forming enzymes, may evolve into a major biological function.

Superposition of FadD10 with acyl-CoA synthetase complexed with Coenzyme A derivatives shows that the phosphopantetheine binding cavity is in the N-terminal

domain of FadD10. In our two structures, the continuity between the phosphopantetheine cavity and the fatty acyl binding tunnel is blocked by the side-chain of H225. A conserved aromatic residue (either histidine, phenylalanine, or tryptophan), equivalent to H225 in FadD10, is found in the sequences of all of the adenylate-forming enzymes. It is thought to function in the proper positioning of a fatty acid substrate into its cognate binding tunnel instead of extending into the phosphopantetheine binding site. More clearly described in the human medium chain fatty acyl CoA synthase (Grazyna Kochan et al., 2009), the indole ring of W265 (equivalent to H225 in FadD10) rotates about 180 degrees relative to the main chain in the ATP or Coenzyme A binding state. This action switches off and on the connection between the fatty acid binding tunnel and the phosphopantetheine binding cavity. FadD10 should adopt a similar scheme to reorient H225 in the context of the overall reaction in order to allow for the extension of the phosphopantetheine terminus of the ACP (Rv0100) into the fatty acid binding site.

Conclusion

We have determined the apo and dodecanoyl-AMP bound structures of *M. tuberculosis* FadD10, leading to the characterization of a new type of adenylate-forming enzyme. FadD10, independent of the presence of ligand, adopts and maintains an “open” conformation wherein the inter-domain orientation prevents the binding of Coenzyme A. Although *M. tuberculosis* FadD10 has a primary sequence similar to FAALs, we have clearly shown that it is indeed an FAAL that is only able to acylate an ACP (Rv0100) rather than Coenzyme A. This activity is consistent with the structural features of

FadD10; and is in agreement with the operon organization of *M. tuberculosis* Rv0099 (*FadD10*) – Rv0101 (*nrp*), an assembly line for the production of lipopeptide(s).

Because many similar gene clusters, involving an FAAL, an ACP, and an NRPS, have been observed in the synthetic pathways for bioactive lipopeptides (Darren Hansen et al., 2007; Erwin Duitman et al., 1999; Eva Heinzelmann et al., 2005; Richard Baltz et al., 2006), therefore it is very likely that enzymes with similar mechanisms and structures to *M. tuberculosis* FadD10 will be discovered in nature.

Experimental Procedure

Cloning, protein expression, and purification

The *M. tuberculosis fadD10* (Rv0099) gene was amplified by PCR, incorporated into the pDEST17 vector by gateway cloning (Invitrogen), and then transformed into either Novagen BL21(DE3)pLys *E. coli* cells for expression of native protein or Novagen B834(DE3)pLys cells for selenomethionine-incorporated protein expression.

The cells were cultured at 37 °C until an OD₆₀₀ of 0.8 was reached. For native protein expression, 1mM isopropyl-1-thio-β-D-galactopyranoside (IPTG) was added to induce expression and the cells were grown overnight at 20 °C. For selenomethionine-incorporated protein expression, the cells were collected at an OD₆₀₀ of 0.8, centrifuged, then resuspended and transferred into minimal media with selenomethionine. Induction of expression and growth were the same as for the native protein.

After harvesting, the cells were resuspended in 25 mM Tris (pH 8.0), 500 mM NaCl and 2 mM β-mercaptoethanol, and lysed by French press. Recombinant FadD10

with an N-terminal poly-His tag was purified by nickel affinity chromatography followed by gel filtration. The His₆ tag was then cleaved by TEV protease and the untagged protein was passed through another nickel column in 25 mM Tris (pH 8.0), 100 mM NaCl and 2 mM β-mercaptoethanol. It was then concentrated to 15 mg mL⁻¹, flash-frozen, and stored at -80 °C.

The *M. tuberculosis Rv0100* gene was amplified by PCR, ligated into the Novagen pET28b vector. The *E. coli* phosphopantetheine transferase *Sfp* was cloned into Novagen pETduet-1 vector. The plasmids containing *Rv0100* and *Sfp*, respectively, were co-transformed into Novagen BL21(DE3) *E. coli* cells, and then expressed as described for the native FadD10. Recombinant holo-Rv0100 with a His₆ tag was purified by nickel affinity chromatography in 25 mM Tris (pH 8.0), 100 mM NaCl and 2 mM β-mercaptoethanol.

Crystallization

Crystals of Se-FadD10 (selenomethionine incorporated) were grown at 18 °C by hanging drop vapor diffusion. Each drop contained an equal volume of the protein solution and reservoir solution (0.32-0.36 mM LiSO₄ and 15-30% polyethylene glycol 6000).

FadD10 in complex with dodecanoyl-AMP was obtained by incubating the protein solution for one hour with the reaction mixture in a 10:1 volume ratio. The reaction mixture was made by incubating 10 μM FadD10 with 2.5 mM ATP, 10 mM MgCl₂, and 1 mM dodecanoic acid for one hour at 37 °C, then filtering out the protein

and concentrating the mixture ten-fold. Crystals formed in hanging drops after four days in 4 M potassium formate.

Data collection and processing

Diffraction data from a single apo Se-FadD10 crystal was collected at 120 K using a cryo-protection solution consisting of the crystallization condition with the addition of 30% glycerol. Crystals diffracted to 2.20 Å at beam line 5.0.2 at the Advanced Light Source (ALS). A total of 180° diffraction data were collected at the wavelength of 0.9795 Å, which is the absorption peak of Se-FadD10 crystals.

Diffraction data of FadD10 in complex with dodecanoyl-AMP were collected to 2.44 Å at the wavelength of 1.542 Å using Rigaku R-Axis IV++ at home source. All the data were processed and reduced using HKL2000 (Zbyszek Otwinowski and Wladek Minor, 1997). The crystals of apo Se-FadD10 are in the space group $P2_1$, with two molecules in each asymmetric unit. The crystals of FadD10 binding dodecanoyl-AMP are in the space group $P3_121$, with one molecule in each asymmetric unit (Table 4-1).

Table 4-1. Data collection and refinement statistics for FadD10 structures.

PDB ID	4ISB	4IR7
Crystal	Se-FadD10	C12-FadD10
Ligands	SO42-	dodecanoyl-AMP
		Mg2+
Data collection		
Space group	P21	P3121
Unit cell dimensions	a=57.32Å, b=107.91Å, c=85.69Å a=90.0°, b=106.9°, g=90.0°	a=b=138.16Å, c=82.47Å a=b=90.0°, g=120.0°
Molecules/ASU	2	1
Wavelength (Å)	0.9795	1.542
Resolution (Å)	48.57-2.20	39.84-2.80
Completeness (%) ¹	99.3 (98.9)	100.0 (99.7)
No. of reflections	49204	24707
I/σI [*]	9.50 (1.94)	14.01 (2.15)
Rsym [*]	0.103 (0.703)	0.0567 (0.504)
Refinement statistics		
Resolution (Å)	48.50-2.20	39.03-2.80
No. of reflection work	49014	22632
No. of protein atoms	7422	3734
No. of water molecules	59	32
No. of heteroatoms	20	36
Rcryst (%)	22.69	22.61
Rfree (%)	27.28	27.95
RMSD bond length (Å)	0.01	0.002
RMSD angle (°)	1.26	0.60
Mean temperature factor (Å ²)	25.5	62.0

*. Numbers in parenthesis indicate data for highest-resolution shell.

Structure determination and model refinement

The phase of Se-FadD10 was determined by single-wavelength anomalous dispersion using Autosol in PHENIX (Paul Adams et al., 2010). Twenty-two selenium atoms were located and refined per asymmetric unit till the overall figure of merit reaches 0.32. An initial model was built by Autobuild in PHENIX (Paul Adams et al., 2010). Manual rebuilding was then performed to improve the model using Coot (Paul Emsley and Kevin Cowtan, 2004). The final model was obtained after further cycles of model building and PHENIX refinement yielding R_{cryst} and R_{free} of 22.69% and 27.28%, respectively. There are two subunits, designated as A and B, as well as 4 sulfate ions and 59 water molecules per asymmetric unit in the refined model. A total of 508 and 502 out of 540 residues for chain A and B, respectively, were visible and built into the electron density. The missing residues are due to the absence of interpretable electron density. They include the N-terminal residues 1-8, the C-terminal residues 532-540, and the loop residues 145-154, 424, 477-480 of chain A; and the N-terminal residues 1-3, the C-terminal residues 532-540, and the loop residues 125-131, 145-154, 161-164, 179-183 of chain B. Residues S178, T181, E183, and K185 of chain A and residues E426, R451, S474, E476, and L477 of chain B were built as alanine due to ambiguous side chain electron density.

The structure of FadD10 in complex with dodecanoyl-AMP was solved by molecular replacement using MOLREP (Alexei Vagin and Alexei Teplyakov, 1997) in CCP4. A single solution for the molecular replacement was obtained using the chain A of apo FadD10 as the search model. Dodecanoyl-AMP was manually built in the model

by examining the $F_o - F_c$ map in Coot(Paul Emsley and Kevin Cowtan, 2004). The final model was obtained after further cycles of model building and PHENIX refinement, to 2.80 Å, yielding R_{cryst} and R_{free} of 22.61% and 27.95%, respectively. There are one subunit of FadD10, one dodecanoyl-AMP, and 32 water molecules in each asymmetric unit. A total of 508 residues are built into the refined model. The N-terminal residues 1-10, the C-terminal residues 532-540, and the loop residues 124-128, 147-152, 179-180 are missing from the model due to the absence of interpretable electron density. The complete refinement statistics are given in Table 1.

Enzymatic assays to detect acylation of Rv0100

FadD10 (1.5 µM) and Rv0100 (20 µM) were incubated with 2 mM ATP, 5 mM MgCl₂, in presence of 200 µM different fatty acids, in 25 mM ammonium bicarbonate buffer at pH 7.8, for 1 hour. The salts were removed by diluting and concentrating the solutions by 10-fold in 25 mM ammonium bicarbonate buffer, for 3 cycles. The resulted samples were mixed with acetonitrile and formic acid in a ratio of 1:1:0.002, and then analyzed by Bruker microQTOF-QII.

HPLC-MS analysis of dodecanoyl-amino acids

FadD10 (10 µM) was incubated with 2 mM ATP, 8 mM MgCl₂, 200 µM dodecanoic acid, in presence of 2 mM different amino acids, in 50 mM phosphate buffer at pH 6.5, for 1 hour. The macromolecules were removed by passing the solutions through 5 kDa cutoff filters. 100 µL of each reaction product were injected in to HPLC

coupled with ESI-MS analysis. The HPLC was performed with an Atlantis T3 5 μ M column (4.6, 250 mm), using a 5% acetonitrile/0.1% TFA wash for 10 minutes followed by a 5%-80% acetonitrile/0.1% TFA gradient over 1 hour.

Additional Unpublished Results

Kinetics of the adenylation activity of FadD10

The adenylation activity of *M. tuberculosis* FadD10 was monitored by a phosphate detecting enzymatic assay. The enzyme displayed K_m values of 106 μ M (Figure 4-6 A and B) and 46 μ M (Figure 4-6 C) for ATP and dodecanoic acid, respectively. The K_{cat} was determined to be 0.005 s^{-1} (Figure 4-6 B). These kinetic parameters are comparable to those reported for the adenylation reaction catalyzed by FAAL enzymes. For example, *Mycobacterium smegmatis* FAAL32 showed K_m of 20 μ M and 250 μ M for dodecanoic acid and ATP, respectively (Ségolène Galandrin et al., 2013); *E. coli* FAAL showed K_{cat} of 0.001 s^{-1} using octyldecanoic acid as substrate (Zhening Zhang et al., 2011). We have also examined the overall acyl transfer activity of FadD10 by incubating the enzyme, ATP, dodecanoic acid (C12 acid), in addition to both Coenzyme A and the holo-ACP (Rv0100). The resulted adducts were analyzed by ESI-QTOF mass spectrometry, where no dodecanoyl-CoA but only dodecanoyl-ACP was detected (data not shown).

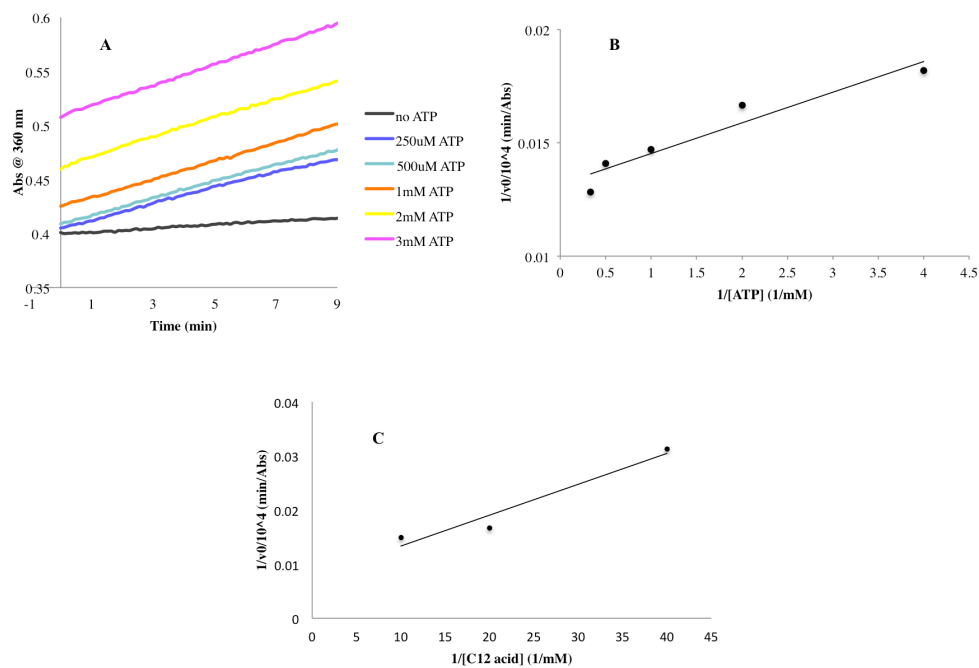


Figure 4-6. Kinetics of the adenylation activity of FadD10. (A) The absorbance spectrometry with 50 μ M dodecanoic acid and varying concentration of ATP. (B) and (C) The Lineweaver-Burk plots to determine the K_m of ATP and dodecanoic acid, respectively.

Gel filtration analysis of the interaction between FadD10 and Rv0100

The interaction between *M. tuberculosis* FadD10 and the ACP (Rv0100) in solution has been examined by gel filtration chromatography using Sephacryl S-200 HR from GE Healthcare. When equimolar mixture of FadD10 (~5 mg/mL) and holo-Rv0100 (~1 mg/mL) was passed through the column, part of Rv0100 was associated to FadD10 (Figure 4-7); but pure holo-ACP only eluted at the volume as observed for the free Rv0100 in Figure 4-7. This confirms our modeling studies of the interaction between the two proteins. The same was observed for apo-Rv0100 (the wide-type Rv0100 without

phosphopantetheination) as well (data not shown), which suggests that the interaction between FadD10 and Rv0100 is likely driven by interactions at the inter-molecular interface or a desolvation process, rather than being determined by phosphopantetheine binding.

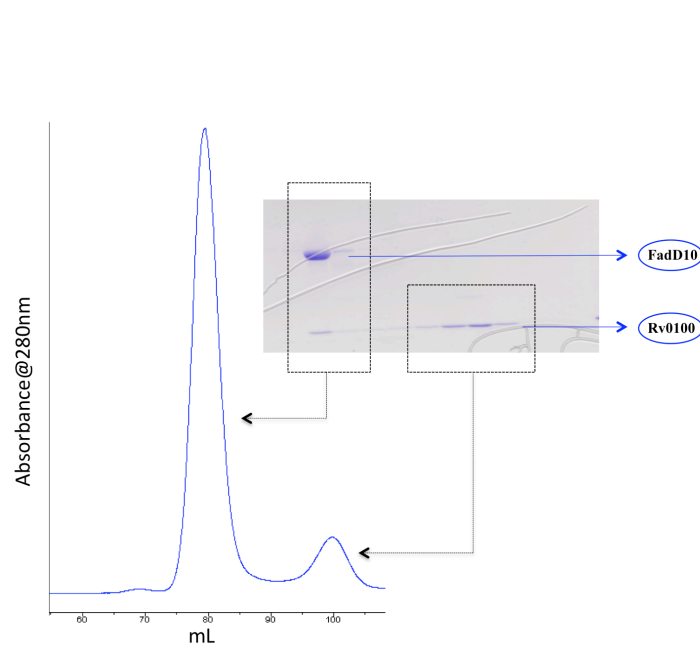


Figure 4-7. Gel filtration analysis of the interaction between FadD10 and Rv0100. The first peak corresponds to FadD10 associated with Rv0100, and the second peak corresponds to free Rv0100.

Additional Unpublished Experimental Procedures

Enzymatic assays for adenylation activity

The adenylation reaction catalyzed by FadD10 is monitored by measuring the released pyrophosphate (Martin Webb, 1992). Each reaction (180 μ L) contained FadD10,

dodecanoic acid, ATP, and 50mM Tris-HCl (pH 7.5), 10 mM MgCl₂, 550 mM 2-amino-6-mercapto-7-methylpurine riboside, which was coupled to 0.1 unit pyrophosphatase (Sigma-Aldrich) and 0.2 unit purine nucleoside phosphorylase (Sigma-Aldrich). The K_m of dodecanoic acid was determined with 7 μM FadD10, 1mM ATP, and dodecanoic acid varying from 0 to 100 μM; and the K_m of ATP was determined with 3.3 μM FadD10, 50 μM dodecanoic acid, and ATP varying from 100 μM to 3 mM. All the reactions were read at 360 nM by Thermo Scientific Multiskan GO microplate spectrophotometer.

CHAPTER V

CONCLUSION

In this thesis, I highlighted my work with peers on the proteins involved in the lipid metabolism of *M. tuberculosis*. In CHAPTER I, I presented the literature review on the physiological significance of lipid metabolism in *M. tuberculosis*, and the prospects of lipid metabolic pathways as targets for anti-tubercular drug design. In CHAPTER II, I characterized the binding of dioctylamine with the methyltransferase CmaA2, designed an enzymatic assay, and demonstrated the inhibition action of dioctylamine on CmaA2 *in vitro*. This work, coupled with my collaborators' *in vivo* examination, showed that dioctylamine had tentative antimicrobial activity and could serve as a framework to design more potent inhibitors. This research also validated the mycobacterial methyltransferases (CmaA2 and homologues) as promising drug targets. In CHAPTER III, I presented my work with peers on the understanding of the action of INH and ETH. They are pro-drugs that are metabolized intracellular and thus the action is largely complicated. Using technologies covering microbiology, structural biology, enzymology, and computation, we confirmed the target of INH and found out a new cellular component to affect ETH susceptibility. In CHAPTER IV, I showed the characterization of the enzyme FadD10. It is virulence associated yet its function was previously mysterious. Through delicate analyses of its sequence, activity, and structure, I identified the enzyme as a fatty acyl-ACP synthetase and elucidated the molecular basis of its action.

Since the bacterium of *M. tuberculosis* was discovered more than a century ago, TB continues to reign as the single leading cause of death by an infectious disease. Instead of being eliminated from the human society, the bacterium has developed into more fatal formats, i. e. MDR- and XDR-TB strains. This is largely due to a chronicle use of a small category of anti-tubercular drugs. Therefore scientists from different fields, such as microbiology, enzymology, biophysics, and informatics, have been thriving to come up with new strategies to fight against this persistent bug. I hope our efforts to try to understand and target the lipid metabolism of *M. tuberculosis* will provide a new perspective in the understanding of infection mechanism, the validation of new drug targets, and the design of new drugs.

REFERENCES

- Tomoko Abe, Yoshiteru Hashimoto, Hideaki Hosaka, Kaori Tomita-Yokotani, and Michihiko Kobayashi (2008). Discovery of amide (peptide) bond synthetic activity in acyl-CoA synthetase. *J Biol Chem* 283, 11312-11322.
- Paul Adams, Pavel Afonine, Gábor Bunkóczi, Vincent Chen, Ian Davis, Nathaniel Echols, Jeffrey Headd, Li-Wei Hung, Gary Kapral, Ralf Grosse-Kunstleve, *et al.* (2010). PHENIX: a comprehensive Python-based system for macromolecular structure solution. *Acta Crystallogr D Biol Crystallogr* 66, 213-222.
- Afonine, P.V., Grosse-Kunstleve, R.W., and Adams, P.D. (2005). The Phenix refinement framework. *CCP4 Newsl* 42.
- Nisheeth Agarwal, Samuel Woolwine, Sandeep Tyagi, and William Bishai (2007). Characterization of the Mycobacterium tuberculosis sigma factor SigM by assessment of virulence and identification of SigM-dependent genes. *Infect Immun* 75, 452-461.
- Anuradha Alahari, Xavier Trivelli, Yann Guérardel, Lynn Dover, Gurdyal Besra, James Sacchettini, Robert Reynolds, Geoffrey Coxon, and Laurent Kremer (2007). Thiacetazone, an antitubercular drug that inhibits cyclopropanation of cell wall mycolic acids in mycobacteria. *Plos One* 12, e1343.
- Anuradha Alahari, Laetitia Alibaud, Xavier Trivelli, Radhika Gupta, Gyanu Lamichhane, Robert Reynolds, William Bishai, Yann Guerardel, and Laurent Kremer (2009). Mycolic acid methyltransferase, MmaA4, is necessary for thiacetazone susceptibility in Mycobacterium tuberculosis. *Mol Microbiol* 71, 1263-1277.
- Charlotta S. Andersson, Camilla A.K. Lundgren, Auður Magnúsdóttir, Changrong Ge, Åke Wieslander, Daniel Martinez Molina, and Martin Högbom (2012). The Mycobacterium tuberculosis very-long-chain fatty acyl-CoA synthetase: structural basis for housing lipid substrates longer than the enzyme. *Structure* 20, 1062-1070.
- Argyrides Argyrou, Lianji Jin, Linda Siconilfi-Baez, Ruth Angeletti, and John Blanchard (2006a). Proteome-wide profiling of isoniazid targets in Mycobacterium tuberculosis. *Biochemistry* 45, 13947-13953.
- Argyrides Argyrou, Matthew Vetting, Bola Aladegbami, and John S Blanchard (2006b). Mycobacterium tuberculosis dihydrofolate reductase is a target for isoniazid. *Nat Struct Mol Biol* 13, 408-413.
- Pooja Arora, Aneesh Goyal, Vivek T Natarajan, Eerappa Rajakumara, Priyanka Verma,

- Radhika Gupta, Malikmohamed Yousuf, Omita A Trivedi, Debasisa Mohanty, Anil Tyagi, *et al.* (2009). Mechanistic and functional insights into fatty acid activation in *Mycobacterium tuberculosis*. *Nature Chem Biol* 5, 166-174.
- Catherine Astarie-Dequeker mail, Laurent Le Guyader, Wladimir Malaga, Fam-Ky Seaphanh, Christian Chalut, André Lopez, and Christophe Guilhot (2009). Phthiocerol dimycocerosates of *M. tuberculosis* participate in macrophage invasion by inducing changes in the organization of plasma membrane lipids. *PLoS Pathog* 5, e1000289.
- Tanjore Balganesh, and B. J. Furr (2007). Molecular approaches to target discovery:-- evaluating targets for anti-tuberculosis drug discovery programmes. *Infect Disord Drug Targets* 7, 120-126.
- Richard Baltz, Paul Brian, Vivian Miao, and Stephen Wrigley (2006). Combinatorial biosynthesis of lipopeptide antibiotics in *Streptomyces roseosporus*. *J Ind Microbiol Biotechnol* 33, 66-74.
- Ashesh Banerjee, Eugenie Dubnau, Annaik Quemard, V. Balasubramanian, Kyung Sun Urn, Theresa Wilson, Des Collins, Geoffrey de Lisle, and William Jacobs Jr. (1994). *InhA*, a gene encoding a target for isoniazid and ethionamide in *Mycobacterium tuberculosis*. *Science* 263, 227-230.
- Xiaoming Bao, Sue Katz, Mike Pollard, and John Ohlrogge (2002). Carbocyclic fatty acids in plants: biochemical and molecular genetic characterization of cyclopropane fatty acid synthesis of *Sterculia foetida*. *P Natl Acad Sci USA* 99, 7172-7177.
- Daniel Barkan, Zhen Liu, James Sacchettini, and Michael Glickman (2009). Mycolic acid cyclopropanation is essential for viability, drug resistance, and cell wall integrity of *Mycobacterium tuberculosis*. *Chem Biol* 16, 499-509.
- Clifton Barry III, Richard Lee, Khisimusi Mdluli, Andrea Sampson, Benjamin Schroeder, Richard Slayden, and Ying Yuan (1998). Mycolic acids: structure, biosynthesis and physiological functions. *Prog Lipid Res* 37, 143-179.
- Alain Baulard, Joanna Betts, Jean Engohang-Ndong, Selwyn Quan, Ruth McAdam, Patrick Brennan, Camille Locht, and Gurdyal Besra (2000). Activation of the pro-drug ethionamide is regulated in mycobacteria. *J Biol Chem* 275, 28326-28331.
- Marcel Behr, Benjamin Schroeder, Jacquelyn Brinkman, Richard Slayden, and Clifton Barry III (2000). A point mutation in the *mma3* gene is responsible for impaired methoxymycolic acid production in *Mycobacterium bovis* BCG strains obtained after 1927. *J Bacteriol* 182, 3394-3399.

- Bekierkunst, A., Levij, I.S., and Yarkoni, E. (1971). Suppression of urethan-induced lung adenomas in mice treated with trehalose-6,6-dimycolate (cord factor) and living bacillus Calmette Guerin. *Science* 174, 1240-1242.
- John Belisle, Varalakshmi Vissa, Todd Sievert, Kuni Takayama, Patrick Brennan, and Gurdyal Besra (1997). Role of the major antigen of Mycobacterium tuberculosis in cell wall biogenesis. *Science* 276, 1420-1422.
- Adam Belley, David Alexander, Tania Di Pietrantonio, Manon Girard, Joses Jones, Erwin Schurr, Jun Liu, David Sherman, and Marcel Behr (2004). Impact of methoxymycolic acid production by Mycobacterium bovis BCG vaccines. *Infect Immun* 72, 2803-2809.
- Apoorva Bhatt, Nagatoshi Fujiwara, Kiranmai Bhatt, Sudagar Gurcha, Laurent Kremer, Bing Chen, John Chan, Steven Porcelli, Kazuo Kobayashi, Gurdyal Besra ||, *et al.* (2007). Deletion of kasB in Mycobacterium tuberculosis causes loss of acid-fastness and subclinical latent tuberculosis in immunocompetent mice. *P Natl Acad Sci USA* 104, 5157-5162.
- Helen Billman-Jacobe, Malcolm McConville, Ruth Haites, Svetozar Kovacevic, and Ross Coppel (1999). Identification of a peptide synthetase involved in the biosynthesis of glycopeptidolipids of Mycobacterium smegmatis. *Mol Microbiol* 33, 1244-1253.
- Fanny Boissier, Fabienne Bardou, Valérie Guillet, Sandrine Uttenweiler-Joseph, Mamadou Daffé, Annaïk Quémard, and Lionel Mourey (2006). Further insight into S-adenosylmethionine-dependent methyltransferases: structural characterization of Hma, an enzyme essential for the biosynthesis of oxygenated mycolic acids in Mycobacterium tuberculosis. *J Biol Chem* 281, 4434-4444.
- Jean-Christophe Camus, Melinda J. Pryor, Claudine Médigue, and Stewart T. Cole (2002). Re-annotation of the genome sequence of Mycobacterium tuberculosis H37Rv. *Microbiology* 148, 2967-2973.
- Israël Casabon, Adam M. Crowe, Jie Liu, and Lindsay D. Eltis (2012). FadD3 is an acyl-CoA synthetase that initiates catabolism of cholesterol rings C and D in actinobacteria. *Mol Microbiol* 87, 269-283.
- Jacqueline Chevalier, Monique Mallea, and Jean-Marie Pages (2000). Comparative aspects of the diffusion of norfloxacin, cefepime and spermine through the F porin channel of Enterobacter cloacae. *Biochem J* 348 Pt 1, 223-227.
- Arush Chhabraa, Asfarul S. Haqueeb, Ravi Kant Palb, Aneesh Goyalb, Rajkishore Raic, Seema Joshid, Santosh Panjikare, Santosh Pashad, Rajan Sankaranarayananb, and Rajesh S. Gokhalea (2012). Nonprocessive [2 + 2]e⁻ off-loading reductase

- domains from mycobacterial nonribosomal peptide synthetases. *P Natl Acad Sci USA* *109*, 5681-5686.
- Sang Hyun Choa, David Goodlett^b, and Scott Franzblau^a (2006). ICAT-based comparative proteomic analysis of non-replicating persistent *Mycobacterium tuberculosis*. *Tuberculosis (Edinb)* *86*, 445-460.
- Tarun Chopra, Srijita Banerjee, Sarika Gupta, Gitanjali Yadav, Swadha Anand, Avadhesh Surolia, Rajendra P Roy, Debasisa Mohanty, and Rajesh Gokhale (2008). Novel intermolecular iterative mechanism for biosynthesis of mycoketide catalyzed by a bimodular polyketide synthase. *PLoS Biol* *6*, e163.
- Tarun Chopra, and Rajesh Gokhale (2009). Polyketide versatility in the biosynthesis of complex mycobacterial cell wall lipids. *Methods Enzymol* *459*, 259-294.
- David Clark, and John Cronan (1996). Two-carbon compounds and fatty acids as carbon sources. In *Escherichia coli and Salmonella: Cellular and Molecular Biology* (Washington, DC: ASM Press), 612-637.
- Roger Clark (2010). Treatment of Tuberculosis: guidelines for national programmes, 4th Edition. *Perspect Public Heal* *130*, 240-240.
- Stewart Cole (1999). Learning from the genome sequence of *Mycobacterium tuberculosis* H37Rv. *FEBS Lett* *452*, 7-10.
- S. T. Cole, R. Brosch, J. Parkhill, T. Garnier, C. Churcher, D. Harris, S. V. Gordon, K. Eiglmeier, S. Gas, C. E. Barry III, *et al.* (1998). Deciphering the biology of *Mycobacterium tuberculosis* from the complete genome sequence. *Nature* *393*, 537-544.
- Miles Congreve, Robin Carr, Chris Murray, and Harren Jhoti (2003). A rule of three for fragment-based lead discovery? *Drug Discov Today* *8*, 876-877.
- Elena Conti, Nick P Franks, and Peter Brick (1996). Crystal structure of firefly luciferase throws light on a superfamily of adenylate-forming enzymes. *Structure* *4*, 287-298.
- Mamadou Daffe, and Philip Draper (1998). The envelope layers of mycobacteria with reference to their pathogenicity. *Adv Microb Physiol* *39*, 131-203.
- Dee Dao, Kari Sweeney, Tsungda Hsu, Sudagar Gurcha, Ivan Nascimento, Dan Roshevsky, Gurdyal Besra, John Chan, Steven Porcelli, and William Jacobs, J. (2008). Mycolic acid modification by the *mmaA4* gene of *M. tuberculosis* modulates IL-12 production. *PLoS Pathog* *4*, e1000081.

- Andrea DeBarber, Khisimuzi Mdluli, Marlein Bosman, Linda-Gail Bekker, and Clifton Barry III (2000). Ethionamide activation and sensitivity in multidrug-resistant *Mycobacterium tuberculosis*. *P Natl Acad Sci USA* *97*, 9677-9682.
- James Douglas, Suzanne Senior, Caroline Morehouse, Benjawan Phetsukiri, Ian Campbell, Gurdyal Besra, and David Minnikin (2002). Analogues of thiolactomycin: potential drugs with enhanced anti-mycobacterial activity. *Microbiology* *148*, 3101-3109.
- Lynn Dover, Anuradha Alahari, Paul Gratraud, Jessica Gomes, Veemal Bhowruth, Robert Reynolds, Gurdyal Besra, and Laurent Kremer (2007). EthA, a common activator of thiocarbamide-containing drugs acting on different mycobacterial targets. *Antimicrob Agents Ch* *51*, 1055-1063.
- Eugenie Dubnau, John Chan, Catherine Raynaud, Vellore Mohan, Marie-Antoinette Lanéelle, Keming Yu, Annaik Quémard, Issar Smith, and Mamadou Daffé (2000). Oxygenated mycolic acids are necessary for virulence of *Mycobacterium tuberculosis* in mice. *Mol Microbiol* *36*, 630-638.
- Erwin Duitman, Leendert Hamoen, Martina Rembold, Gerard Venema, Harald Seitz, Wolfram Saenger, Frank Bernhard, Richard Reinhardt, Manuel Schmidt, Christian Ullrich, *et al.* (1999). The mycosubtilin synthetase of *Bacillus subtilis* ATCC6633: a multifunctional hybrid between a peptide synthetase, an amino transferase, and a fatty acid synthase. *P Natl Acad Sci USA* *96*, 13294-13299.
- Vinod Dubey, Tatiana Sirakova, and Pappachan Kolattukudy (2002). Disruption of *msl3* abolishes the synthesis of mycolipanoic and mycolipenic acids required for polyacyltrehalose synthesis in *Mycobacterium tuberculosis* H37Rv and causes cell aggregation. *Mol Microbiol* *45*, 1451-1459.
- Eugenie Dubnau, Marie-Antoinette Lanéelle, Sonia Soares, Anne Bénichou, Tania Vaz, Danielle Promé, Jean-Claude Promé, Mamadou Daffé, and Annaik Quémard (1997). *Mycobacterium bovis* BCG genes involved in the biosynthesis of cyclopropyl keto- and hydroxy-mycolic acids. *Mol Microbiol* *23*, 313-323.
- Dubnau, E., Marrakchi, H., Smith, I., Daffé, M., and Quemard, A. (1998). Mutations in the *cmaB* gene are responsible for the absence of methoxymycolic acid in *Mycobacterium bovis* BCG Pasteur. *Mol Microbiol* *29*, 1526-1528.
- Benjamin Duckworth, Kathryn Nelson, and Courtney Aldrich (2012). Adenylating enzymes in *Mycobacterium tuberculosis* as drug targets. *Curr Top Med Chem* *12*, 766-796.
- Kathleen Y. Dunphy, Ryan H. Senaratne, Mamiko Masuzawa, Lon V. Kendall, and Lee W. Riley (2010). Attenuation of *Mycobacterium tuberculosis* functionally

- disrupted in a fatty acyl-coenzyme A synthetase gene *fadD5*. *J Infect Dis* 201, 1232-1239.
- Christopher Dye (2006). Global epidemiology of tuberculosis. *Lancet* 367, 938-940.
- Paul Emsley, and Kevin Cowtan (2004). Coot: model-building tools for molecular graphics. *Acta Crystallogr D Biol Crystallogr* 60, 2126-2133.
- Marina Forrellad, Laura Klepp, Andrea Gioffré, Julia Sabio García, Hector Morbidoni, María de la Paz Santangelo, Angel Cataldi, and Fabiana Bigi (2013). Virulence factors of the *Mycobacterium tuberculosis* complex. *Virulence* 4, 3-66.
- Marco Fraaije, Nanne Kamerbeek, Annelies Heidekamp, Riccardo Fortin, and Dick Janssen (2004). The prodrug activator *EtaA* from *Mycobacterium tuberculosis* is a Baeyer- Villiger monooxygenase. *J Biol Chem* 279, 3354-3360.
- Hugo Fraga, G., J.C., Esteves da Silva, and Rui Fontes (2004). Identification of luciferyl adenylate and luciferyl coenzyme a synthesized by firefly luciferase. *Chembiochem* 5, 110-115.
- Rosilene Fressatti Cardoso, Robert Cooksey, Glenn Morlock, Patricia Barco, Leticia Cecon, Francisco Forestiero, Clarice Leite, Daisy Sato, Maria de Lourdes Shikama, Elsa Mamizuka, *et al.* (2004). Screening and characterization of mutations in isoniazid- resistant *Mycobacterium tuberculosis* isolates obtained in Brazil. *Antimicrob Agents Ch* 48, 3373-3381.
- Joel Freundlich, Feng Wang, Catherine Vilchèze, Gulcin Gulten, Robert Langley, Guy A. Schiehsler, David Jacobus, William Jacobs, J., and James Sacchettini (2009). Triclosan derivatives: towards potent inhibitors of drug-sensitive and drug-resistant *Mycobacterium tuberculosis*. *ChemMedChem* 4, 241-248.
- Takeshi Fukudaa, Takayuki Matsumurab, Manabu Atob, Maho Hamasakic, Yukiko Nishiuchid, Yoshiko Murakamia, Yusuke Maedaa, Tamotsu Yoshimoric, Sohkiichi Matsumotod, Kazuo Kobayashib, *et al.* (2013). Critical roles for lipomannan and lipoarabinomannan in cell wall integrity of mycobacteria and pathogenesis of tuberculosis. *MBio* 4, e00472- 00412.
- Hajime Fukunaga, Tomoyuki Murakami, Toshikazu Gondo, Kazuo Sugi, and Tokuhiro Ishihara (2002). Sensitivity of acid-fast staining for *Mycobacterium tuberculosis* in formalin- fixed tissue. *Am J Respir Crit Care Med* 166, 994-997.
- Hazbon, M.H., Brimacombe, M., Bobadilla del Valle, M., Cavatore, M., Guerrero, M.I., Varma- Basil, M., Billman-Jacobe, H., Lavender, C., Fyfe, J., Garcia-Garcia, L., *et al.* (2006). Population genetics study of isoniazid resistance mutations and evolution of multidrug- resistant *Mycobacterium tuberculosis*. *Antimicrob*

Agents Ch 50, 2640-2649.

- Eva Heinzlmann, Susanne Berger, Claudia Müller, Thomas Härtner, Karl Poralla, Wolfgang Wohlleben, and Dirk Schwartz (2005). An acyl-CoA dehydrogenase is involved in the formation of the Delta cis3 double bond in the acyl residue of the lipopeptide antibiotic friulimicin in *Actinoplanes friuliensis*. *Microbiology* 151, 1963-1974.
- Yuko Hisanaga, Hidew Ago, Noriko Nakagawa, Keisuke Hamada, Koh Ida, Masaki Yamamoto, Tesuya Hori, Yasuhiro Arii, Mitsuaki Sugahara, Seiki Kuramitsu, *et al.* (2004). Structural basis of the substrate-specific two-step catalysis of long chain fatty acyl-CoA synthetase dimer. *J Biol Chem* 279, 31717-31727.
- Neel Gandhi, Anthony Moll, Willem Sturm, Robert Pawinski, Thiloshini Govender, Umesh Laloo, Kimberly Zeller, Jason Andrews, and Gerald Friedland (2006). Extensively drug-resistant tuberculosis as a cause of death in patients co-infected with tuberculosis and HIV in a rural area of South Africa. *Lancet* 368, 1575-1580.
- Sécolène Galandrin, Valérie Guillet, Rajendra Rane, Mathieu Léger, N. Radha, Nathalie Eynard, Kaveri Das, Tanjore Balganes, Lionel Mourey, Mamadou Daffé, *et al.* (2013). Assay development for identifying inhibitors of the Mycobacterial Fadd32 activity. *J Biomol Screen* 18, 576-587.
- Sabine Gavalda, Mathieu Léger, Benoît van der Rest, Alexandre Stella, Fabienne Bardou, Henri Montrozier, Christian Chalut, Odile Burlet-Schiltz, Hedia Marrakchi, Mamadou Daffé, *et al.* (2009). The Pks13/FadD32 crosstalk for the biosynthesis of mycolic acids in *Mycobacterium tuberculosis*. *J Biol Chem* 284, 19255-19265.
- Kathleen George, Ying Yuan, David Sherman, and Clifton Barry III (1995). The biosynthesis of cyclopropanated mycolic acids in *Mycobacterium tuberculosis*. Identification and functional analysis of CMAS-2. *J Biol Chem* 270, 27292-27298.
- Jean-Francois Gibrata, Thomas Madej, and Stephen H Bryant (1996). Surprising similarities in structure comparison. *Curr Opin Struct Biol* 6, 377-385.
- Michael Glickman (2003). The *mmaA2* gene of *Mycobacterium tuberculosis* encodes the distal cyclopropane synthase of the alpha-mycolic acid. *J Biol Chem* 278, 7844-7849.
- Michael Glickman, Sean Cahill, and William Jacobs, J. (2001). The *Mycobacterium tuberculosis* *cmaA2* gene encodes a mycolic acid trans-cyclopropane synthetase. *J Biol Chem* 276, 2228-2234.

- Michael Glickman, Jeffery Cox, and William Jacobs, J. (2000). A novel mycolic acid cyclopropane synthetase is required for cording, persistence, and virulence of *Mycobacterium tuberculosis*. *Mol Cell* 5, 717-728.
- Michael Glickman, and William Jacobs Jr. (2001). Microbial pathogenesis of *Mycobacterium tuberculosis*: dawn of a discipline. *Cell* 104, 477-485.
- Stephen Gillespie (2002). Evolution of drug resistance in *Mycobacterium tuberculosis*: Clinical and molecular perspective. *Antimicrob Agents Ch* 46, 267-274.
- Sarah Gilmore, Michael Schelle, Cynthia Holsclaw, Clifton Leigh, Madhulika Jain, Jeffery Cox, Julie Leary, and Carolyn Bertozzi (2012). Sulfolipid-1 biosynthesis restricts *Mycobacterium tuberculosis* growth in human macrophages. *ACS Chem Biol* 7, 863- 870.
- Kuppan Gokulan, Seán O’Leary, William Russell, David Russell, Mallikarjun Lalgondar, Tadhg Begley, Thomas Ioerger, and James Sacchettini (2013). Crystal structure of *Mycobacterium tuberculosis* polyketide synthase 11 (pks11) reveals intermediates in the synthesis of methyl-branched alkylpyrones. *J Biol Chem*.
- Aneesh Goyal, Priyanka Verma, Madhankumar Anandhkrishnan, Rajesh S. Gokhale, and Rajan Sankaranarayanan (2011). Molecular basis of the functional divergence of fatty acyl-amp ligase biosynthetic enzymes of *mycobacterium tuberculosis*. *J Mol Biol* 416, 221-239.
- Dennis Grogan, and John Cronan, J. (1997). Cyclopropane ring formation in membrane lipids of bacteria. *Microbiol Mol Biol Rev* 61, 429-441.
- Anna Grzegorzewicz, Jana Korduláková, Victoria Jones, Sarah Born, Juan Belardinelli, Adrien Vaquié, Vijay Gundi, Jan Madacki, Nawel Slama||, Françoise Laval||, *et al.* (2012). A common mechanism of inhibition of the *Mycobacterium tuberculosis* mycolic acid biosynthetic pathway by isoxyl and thiacetazone. *J Biol Chem* 287, 38434-38441.
- Dominique Guianvarc'h, Thierry Drujon, Thearina Ear Leang, Fabienne Courtois, and Olivier Ploux (2006). Identification of new inhibitors of *E. coli* cyclopropane fatty acid synthase using a colorimetric assay. *Biochim Biophys Acta* 1764, 1381-1388.
- Andrew Gulick, Vincent Starai, Alexander Horswill, Kristen Homick, and Jorge Escalante- Semerena (2003). The 1.75 Å crystal structure of acetyl-CoA synthetase bound to adenosine-5'-prophylphosphate and Coenzyme A. *Biochemistry* 42, 2866-2673

- Andrew Gulick, Xuefeng Lu, and Debra Dunaway-Mariano (2004). Crystal structure of 4- chlorobenzoate: CoA ligase/synthetase in the unliganded and aryl substrate-bound states. *Biochemistry* 43, 8670-8680.
- Andrew Gulick (2009). Conformational dynamics in the Acyl-CoA synthetases, adenylation domains of non-ribosomal peptide synthetases, and firefly luciferase. *ACS Chem Biol* 4, 811-827.
- Hongling Guo, Qihui Seet, Steven Denkin, Linda Parsons, and Ying Zhang (2006). Molecular characterization of isoniazid-resistant clinical isolates of *Mycobacterium tuberculosis* from the USA. *J Med Microbiol* 55, 1527-1531.
- D. Gupta (1977). Acceptability of thioamides. I. Ethionamide. *J Postgrad Med* 23, 175-180.
- Darren Hansen, Stefanie Bumpus, Zachary Aron, Neil Kelleher, and Christopher Walsh (2007). The loading module of mycosubtilin: an adenylation domain with fatty acid selectivity. *J Am Chem Soc* 129, 6366-6367.
- Grant Hotter, Barry Wards, Pania Mouat, Gurdyal Besra, Jessica Gomes, Monica Singh, Shalome Bassett, Pamela Kawakami, Paul Weeler, Geoffrey de Lisle, *et al.* (2005). Transposon mutagenesis of Mb0100 at the *ppe1-nrp* locus in *mycobacterium bovis* disrupts phthiocerol dimycocerosate (PDIM) and glycosylphenol-PDIM biosynthesis, producing an avirulent strain with vaccine properties at least equal to those of *M. bovis* BCG. *J Bacteriol* 187, 2267-2278.
- Chih-chin Huang, Clare Smith, Michael Glickman, William Jacobs, J., and James Sacchettini (2002). Crystal structures of mycolic acid cyclopropane synthases from *Mycobacterium tuberculosis*. *J Biol Chem* 277, 11559-11570.
- IAkihiro Ishiwataa, Hiroko Akaoa, Yukishige Itoa, Makoto Sunagawab, Naoto Kusunoseb, and Yasuo Kashiwazakib (2006). Synthesis and TNF-alpha inducing activities of mycoloyl- arabinan motif of mycobacterial cell wall components. *Bioorg Med Chem* 14, 3049- 3061.
- Swati Joshi, Amit Pandey, Nicole Capite, Sarah Fortune, Eric Rubin, and Christopher Sasseti (2003). Genetic requirements for mycobacterial survival during infection. *P Natl Acad Sci USA* 100, 12989-12994.
- Kanishk Kapilashrami, Gopal Bommineni, Carl Machutta, Pilho Kim, Cheng-Tsung Lai, Carlos Simmerling, Francis Picart, and Peter Tonge (2013). Thiolactomycin-based beta- ketoacyl-AcpM synthase A (KasA) inhibitors: fragment-based inhibitor discovery using transient one-dimensional nuclear overhauser effect NMR spectroscopy. *J Biol Chem* 288, 6045-6052.

- Thomas Keating, Gary Marshall, Christopher Walsh, and Amy Keating (2002). The structure of VibH represents nonribosomal peptide synthetase condensation, cyclization and epimerization domains. *Nat Struct Biol* 9, 522-526.
- Baharak Khoshkholgh-Sima, Soroush Sardari, Jalal Izadi Mobarakeh, and Ramezan Ali Khavari-Nejad (2011). An in silico approach for prioritizing drug targets in metabolic pathway of *Mycobacterium tuberculosis*. *WASET* 59, 1027-1030.
- Grazyna Kochan, Ewa S. Pilka, Frank von Delft, Udo Oppermann, and Wyatt W. Yue (2009). Structural snapshots for the conformation-dependent catalysis by human medium-chain acyl-coenzyme A synthetase ACSM2A. *J Mol Biol* 388, 997-1008.
- Evgeny Krissinel, and Kim Henrick (2007). Inference of macromolecular assemblies from crystalline state. *J Mol Biol* 372, 774-797.
- Lawrence Kuo (2011). *Methods in Enzymology Volume 493 Fragment-based drug design: tools, practical approaches, and examples.* 493.
- Christophe Lambert, Nadia Leonard, Xavier De Bolle, and Eric Depiereux (2002). ESyPred3D: Prediction of proteins 3D structures. *Bioinformatics* 18, 1250-1256.
- David Lea-Smith, James Pyke, Dedreia Tull, Malcolm McConville, Ross Coppel, and Paul Crellin (2007). The reductase that catalyzes mycolic motif synthesis is required for efficient attachment of mycolic acids to arabinogalactan. *J Biol Chem* 282, 11000- 11009.
- Benfang Lei, Chih-Jen Wei, and Shiao-Chun Tu (2000). Action mechanism of antitubercular isoniazid. Activation by *Mycobacterium tuberculosis* KatG, isolation, and characterization of inhA inhibitor. *J Biol Chem* 275, 2520-2526.
- Mathieu Léger, Sabine Gavalda, Valérie Guillet, Benoît van der Rest, Nawel Slama, Henri Montrozier, Lionel Mourey, Annaïk Quémard, Mamadou Daffé, and Hedia Marrakchi (2009). The dual function of the *Mycobacterium tuberculosis* FadD32 required for mycolic acid biosynthesis. *Chem Biol* 16, 510-520.
- Uwe Linnea, Antje Schäfera, Milton T. Stubbs, and Mohamed A. Marahiel (2007). Aminoacyl-coenzyme A synthesis catalyzed by adenylation domains. *FEBS Lett* 581, 905-910.
- Jun Liu, Howard Takiff, and Hiroshi Nikaido (1996). Active efflux of fluoroquinolones in *Mycobacterium smegmatis* mediated by LfrA, a multidrug efflux pump. *J Bacteriol* 178, 3791-3795.
- Zhen Liu, Thomas Ioerger, Feng Wang, and James Sacchettini (2013). Structures of Mtb

- FadD10 reveal a new type of Adenylate-forming enzyme. *J Biol Chem*.
- Thomas Luft, Shu-Ming Li, Holger Scheible, Bernd Kammerer, and Lutz Heide (2005). Overexpression, purification and characterization of SimL, an amide synthetase involved in simocyclinone biosynthesis. *Arch Microbiol* *183*, 277-286.
- O. Lund, M. Nielsen, C. Lundegaard, and P. Worning (2002). CPHmodels 2.0: X3M a Computer Program to Extract 3D Models. CASP5 conferenceA102.
- Minkui Luo, Evgeny Fadeev, and John Groves (2005). Mycobactin-mediated iron acquisition within macrophages. *Nat Chem Biol* *1*, 149-153.
- Lozada-Ramirez, J.D., Martinez-Martinez, I., Sanchez-Ferrer, A., and Garcia-Carmona, F. (2006). A colorimetric assay for S-adenosylhomocysteine hydrolase. *J Biochem Biophys Methods* *67*, 131-140.
- Timm Maier, Marc Leibundgut, and Nenad Ban (2008). The crystal structure of a mammalian fatty acid synthase. *Science* *321*, 1315-1322.
- Hideki Makinoshima, and Michael Glickman (2005). Regulation of Mycobacterium tuberculosis cell envelope composition and virulence by intramembrane proteolysis. *Nature* *436*, 406- 409.
- Martin, A., Morcillo, N., Lemus, D., Montoro, E., Telles, M.A., Simboli, N., Pontino, M., Porras, T., Leon, C., Velasco, M., *et al.* (2005). Multicenter study of MTT and resazurin assays for testing susceptibility to first-line anti-tuberculosis drugs. *Int J Tuberc Lung Dis* *9*, 901-906.
- Samuel Martin, Cynthia Pierce, Gardner Middlebrook, and René Dubos (1950). The Effect of Tubercle Bacilli on the Polymorphonuclear Leucocytes of Normal Animals. *J Exp Med* *91*, 381-392.
- Isamu Matsunaga, and Masahiko Sugita (2012). Mycoketide: a cd1c-presented antigen with important implications in mycobacterial infection. *Clin Dev Immunol* *2012*, ID 981821.
- Mohamed Marahiel, Torsten Stachelhaus, and Henning Mootz (1997). Modular peptide synthetases involved in nonribosomal peptide synthesis. *Chem Rev* *97*, 2651-2675.
- Jurgen May, Nadine Kessler, Mohamed Marahiel, and Milton Stubbs (2002). Crystal structure of DhbE, an archetype for aryl acid activating domains of modular nonribosomal peptide synthetases. *Proc Natl Acad Sci USA* *99*, 12120-12126.
- James McGarrity, and John Armstrong (1981). Phase transition behaviour of artificial

liposomes composed of phosphatidylcholines acylated with cyclopropane fatty acids. *Biochim Biophys Acta* 640, 544-548.

- Matthew McMahon, Jason Rushc, and Michael Thomas (2012). Analyses of MbtB, MbtE, and MbtF suggest revisions to the mycobactin biosynthesis pathway in *Mycobacterium tuberculosis*. *J Bacteriol* 194, 2809-2818.
- Khisimuza Mdluli, Richard Slayden, YaQi Zhu, Srinivas Ramaswamy, Xi Pan, David Mead, Deborah Crane, James Musser, and Clifton Barry III (1998). Inhibition of a *Mycobacterium tuberculosis* beta-ketoacyl ACP synthase by isoniazid. *Science* 280, 1607-1610.
- Laxman Meena, Puneet Chopra, Ram Vishwakarma, and Yogendra Singh (2013). Biochemical characterization of an S-adenosyl-L-methionine dependent methyltransferase (Rv0469) of *Mycobacterium tuberculosis*. *Biol Chem* 394, 871-877.
- Deborah Miller, Christopher Walsh, and Lusong Luo (2001). C-methyltransferase and cyclization domain activity at the intraprotein PK/NRP switch point of yersiniabactin synthetase. *J Am Chem Soc* 123, 8434-8435.
- Carter Mitchell, Ce Shi, Courtney Aldrich, and Andrew Gulick (2012). Structure of PA1221, a nonribosomal peptide synthetase containing adenylation and peptidyl carrier protein domains. *Biochemistry* 51, 3252-3263.
- Satohide Miyakawa, Koji Suzuki, Takao Noto, Yusuke Harada, and Hiroshi Okazaki (1982). Thiolactomycin, a new antibiotic. IV. Biological properties and chemotherapeutic activity in mice. *J Antibiot (Tokyo)* 35, 411-419.
- Debasisa Mohanty, Rajan Sankaranarayanan, and Rajesh Gokhale (2011). Fatty acyl-AMP ligases and polyketide synthases are unique enzymes of lipid biosynthetic machinery in *Mycobacterium tuberculosis*. *Tuberculosis (Edinb)* 91, 448-455.
- Glenn Morlock, Beverly Metchock, David Sikes, Jack Crawford, and Robert Cooksey (2003). *ethA*, *inhA*, and *katG* loci of ethionamide-resistant clinical *Mycobacterium tuberculosis* isolates. *Antimicrob Agents Ch* 47, 3799-3805.
- Richard Morphy, and Zoran Rankovic (2005). Designed multiple ligands. An emerging drug discovery paradigm. *J Med Chem* 48, 6523-6543.
- Murshudov, G.N., Vagin, A.A., and Dodson, E.J. (1997). Refinement of macromolecular structures by the maximum-likelihood method. *Acta Crystallogr D Biol Crystallogr* 53, 240-255.
- Nagamachi, E., Shibuya, S., Hirai, Y., Matsushita, O., Tomochika, K., and Kanemasa,

- Y. (1991). Adaptational changes of fatty acid composition and the physical state of membrane lipids following the change of growth temperature in *Yersinia enterocolitica*. *Microbiol Immunol* 35, 1085-1093.
- Frank Niesen, Helena Berglund, and Masoud Vedadi (2007). The use of differential scanning fluorimetry to detect ligand interactions that promote protein stability. *Nat Protoc* 2, 2212-2221.
- Newton, G.L., Arnold, K., Price, M.S., Sherrill, C., Delcardayre, S.B., Aharonowitz, Y., Cohen, G., Davies, J., Fahey, R.C., and Davis, C. (1996). Distribution of thiols in microorganisms: Mycothiol is a major thiol in most actinomycetes. *J Bacteriol* 178, 1990-1995.
- Gerald Newton, Teresa Koledin, Batia Gorovitz, Mamta Rawat, Robert Fahey, and Yossef Av-Gay (2003). The glycosyltransferase gene encoding the enzyme catalyzing the first step of mycothiol biosynthesis (*mshA*). *J Bacteriol* 185, 3476-3479.
- Gerald Newton, Philong Ta, Krzysztof Bzymek, and Robert Fahey (2006). Biochemistry of the initial steps of mycothiol biosynthesis. *J Biol Chem* 281, 33910-33920.
- Gerald Newton, Mia Unsona, Sara Anderberga, Joseph Aguileraa, Nancy Oha, Stephen delCardayreb, Yossef Av-Gayc, and Robert Fahey (1999). Characterization of *Mycobacterium smegmatis* mutants defective in 1-D-myo-inosityl-2-amino-2-deoxy- α -D-glucopyranoside and mycothiol biosynthesis. *Biochem Bioph Res Co* 255, 239- 244.
- Solomon Nwaka, and Alan Hudson (2006). Innovative lead discovery strategies for tropical diseases. *Nat Rev Drug Discov* 5, 941-955.
- Anil Ojha, Anthony Baughn, Dhinakaran Sambandan, Tsungda Hsu, Xavier Trivelli, Yann Guerardel, Anuradha Alahari, Laurent Kremer, William Jacobs, J., and Graham Hatfull (2008). Growth of *Mycobacterium tuberculosis* biofilms containing free mycolic acids and harbouring drug-tolerant bacteria. *Mol Microbiol* 69, 164-174.
- Hugues Ouellet, Jonathan Johnston, and Paul Ortiz de Montellano (2010). The *Mycobacterium tuberculosis* cytochrome P450 system. *Arch Biochem Biophys* 493, 82-95.
- Zbyszek Otwinowski, and Wladek Minor (1997). Processing of X-ray Diffraction Data Collected in Oscillation Mode. In *Methods Enzymol*, J.R.M.S. C.W. Carter, ed. (New York, Academic Press), pp. 307-326.
- Yuriko Ozeki, Kenji Kaneda, Nagaroshi Fujiwara, Misayo Morimoto, Shiro Oka, and

- Ikuya Yano (1997). In vivo induction of apoptosis in the thymus by administration of mycobacterial cord factor (trehalose 6,6'-dimycolate). *Infect Immun* 65, 1793-1799.
- Bruce Palfey, and Claudia McDonald (2010). Control of catalysis in flavin-dependent monooxygenases. *Arch Biochem Biophys* 493, 26-36.
- Nikki Parrish, Todd Houston, Paul Jones, Craig Townsend, and James Dick (2001). In vitro activity of a novel antimycobacterial compound, N-octanesulfonylacetamide, and its effects on lipid and mycolic acid synthesis. *Antimicrob Agents Chemother* 45, 1143- 1150.
- Carey Pashley, and Tanya Parish (2003). Efficient switching of mycobacteriophage L5-based integrating plasmids in *Mycobacterium tuberculosis*. *FEMS Microbiol Lett* 229, 211- 215.
- Pascale Peyron, Julien Vaubourgeix, Yannick Poquet, Florence Levillain, Catherine Botanch, Fabienne Bardou, Mamadou Daffé, Jean-François Emile, Bruno Marchou, Pere-Joan Cardona, *et al.* (2008). Foamy macrophages from tuberculous patients' granulomas constitute a nutrient-rich reservoir for *M. tuberculosis* persistence. *PLoS Pathog* 4, e1000204.
- Amy Piatek, Amalio Telenti, Megan Murray, Hiyam El-Hajj, William Jacobs, J., Fred Russell Kramer, and David Alland (2000). Genotypic analysis of *Mycobacterium tuberculosis* in two distinct populations using molecular beacons: Implications for rapid susceptibility testing. *Antimicrob Agents Ch* 44, 103-110.
- Benjawan Phetsuksiri, Mary Jackson, Hataichanok Scherman, Michael McNeil, Gurdial Besra, Alain Baulard, Richard Slayden, Andrea DeBarber, Clifton Barry III, Mark Baird, *et al.* (2003). Unique mechanism of action of the thiourea drug isoxyl on *Mycobacterium tuberculosis*. *J Biol Chem* 278, 53123-53130.
- Florence Pojer, Shu-Ming Li, and Lutz Heide (2002). Molecular cloning and sequence analysis of the clorobiocin biosynthetic gene cluster: new insights into the biosynthesis of aminocoumarin antibiotics. *Microbiology* 148, 3901-3912.
- Damien Portevin, Célia de Sousa-D'Auria, Henri Montrozier, Christine Houssin, Alexandre Stella, Marie-Antoinette Lanéelle, Fabienne Bardou, Christophe Guilhot, and Mamadou Daffé (2005). The acyl-AMP ligase FadD32 and AccD4-containing acyl-CoA carboxylase are required for the synthesis of mycolic acids and essential for mycobacterial growth: identification of the carboxylation product and determination of the acyl-CoA carboxylase components. *J Biol Chem* 280, 8862-8895.
- Annaik Quemard, Marie-Antoinette Laneelle, Hedia Marrakchi, Danielle Prome,

- Eugenie Dubnau, and Mamadou Daffe (1997). Structure of a hydroxymycolic acid potentially involved in the synthesis of oxygenated mycolic acids of the *Mycobacterium tuberculosis* complex. *Eur J Biochem* *250*, 758-763.
- Sahadevan Raman, Xiaoling Puyang, Tan-Yun Cheng, David Young, D. Baranch Moody, and Robert Husson (2006). *Mycobacterium tuberculosis* SigM positively regulates Esx secreted protein and norribosomal peptide synthetase genes and down regulates virulence-associated surface lipid synthesis. *J Bacteriol* *188*, 8460-8469.
- Srinivas Ramaswamy, Robert Reich, Shu-Jun Dou, Linda Jasperse, Xi Pan, Audrey Wanger, Teresa Quitugua, and Edward Graviss (2003). Single nucleotide polymorphisms in genes associated with isoniazid resistance in *Mycobacterium tuberculosis*. *Antimicrob Agents Ch* *47*, 1241-1250.
- Vivek Rao, Nagatoshi Fujiwara, Steven Porcelli, and Michael Glickman (2005). *Mycobacterium tuberculosis* controls host innate immune activation through cyclopropane modification of a glycolipid effector molecule. *J Exp Med* *201*, 535-544.
- Vivek Rao, Feng Gao, Bing Chen, William Jacobs, and Michael Glickman (2006). Trans- cyclopropanation of mycolic acids on trehalose dimycolate suppresses *Mycobacterium tuberculosis* -induced inflammation and virulence. *J Clin Invest* *116*, 1660-1668.
- Mamta Rawat, Svetozar Kovacevic, Helen Billman-Jacobe, and Yossef Av-Gay (2003). Inactivation of mshB, a key gene in the mycothiol biosynthesis pathway in *Mycobacterium smegmatis*. *Microbiology* *149*, 1341-1349.
- Richa Rawat, Adrian Whitty, and Peter Tonge (2003). The isoniazid-NAD adduct is a slow, tight-binding inhibitor of InhA, the *Mycobacterium tuberculosis* enoyl reductase: adduct affinity and drug resistance. *Proc Natl Acad Sci USA* *100*, 13881-13886.
- Michael Reed, Pilar Domenech, Claudia Manca, Hua Su, Amy Barczak, Barry Kreiswirth, Gilla Kaplan, and Clifton Barry III (2004). A glycolipid of hypervirulent tuberculosis strains that inhibits the innate immune response. *Nature* *431*, 84-87.
- Jyothi Rengarajan, Barry Bloom, and Eric Rubin (2005). Genome-wide requirements for *Mycobacterium tuberculosis* adaptation and survival in macrophages. *Proc Natl Acad Sci USA* *102*, 8327-8332.
- Michelle Lopes Ribeiro-Guimarães, and Maria Cristina Vidal Pessolani (2007). Comparative genomics of mycobacterial proteases. *Microb Pathog* *43*, 173-178.

- Laura Rindi, Daniela Bonanni, Nicoletta Lari, and Carlo Garzelli (2004). Requirement of gene *fadD33* for the growth of *Mycobacterium tuberculosis* in a hepatocyte cell line. *New Microbiol* 27, 125-131.
- Kyle Rohde, Robert Abramovitch, and David Russell (2007). *Mycobacterium tuberculosis* invasion of macrophages: Linking bacterial gene expression to environmental cues. *Cell Host Microbe* 2, 352-364.
- Marc Röttig, Marnix H. Medema, Kai Blin, Tilmann Weber, Christian Rausch, and Oliver Kohlbacher (2011). NRPSpredictor2--a web server for predicting NRPS adenylation domain specificity. *Nucleic Acids Res* 39, W362-367.
- Cécile Rousseau, Nathalie Winter, Elisabeth Pivert, Yann Bordat, Olivier Neyrolles, Patrick Avé, Michel Huerre, Brigitte Gicquel, and Mary Jackson (2004). Production of phthiocerol dimycocerosates protects *Mycobacterium tuberculosis* from the cidal activity of reactive nitrogen intermediates produced by macrophages and modulates the early immune response to infection. *Cell Microbiol* 6, 277-287.
- Denise Rozwarski, Gregory Grant, Derek Barton, William Jacobs Jr., and James Sacchettini (1998). Modification of the NADH of the isoniazid target (*InhA*) from *Mycobacterium tuberculosis*. *Science* 279, 98-102.
- Christopher Sassetti, Dana Boyd, and Eric Rubin (2003). Genes required for mycobacterial growth defined by high density mutagenesis. *Mol Microbiol* 48, 77-84.
- Christopher Sassetti, and Eric Rubin (2003). Genetic requirements for mycobacterial survival during infection. *P Natl Acad Sci USA* 100, 12989-12994.
- Louise Scharf, Nan-Sheng Li, Andrew Hawk, Diana Garzón, Tejia Zhang, Lisa Fox, Allison Kazen, Sneha Shah, Esmael Haddadian, Jenny Gumperz, *et al.* (2010). The 2.5 angstrom Structure of CD1c in Complex with a Mycobacterial Lipid Reveals an Open Groove Ideally Suited for Diverse Antigen Presentation. *Immunity* 33, 853-862.
- Stefan Schmelz, and James Naismith (2009). Adenylate-forming enzymes. *Curr Opin Struct Biol* 19, 666-671.
- Elisabeth Schmutz, Marion Steffensky, Jurgen Schmidt, Andrea Porzel, Shu-Ming Li, and Lutz Heide (2003). An unusual amide synthetase (*CouL*) from the coumermycin A1 biosynthetic gene cluster from *Streptomyces rishiriensis* DSM 40489. *Eur J Biochem* 270, 4413-4420.
- Jeffrey Schorey, and Lindsay Sweet (2008). The mycobacterial glycopeptidolipids:

- structure, function, and their role in pathogenesis. *Glycobiology* 18, 832-841.
- Evelyn Schroeder, N. de Souza, Diógenes Santos, John Blanchard, and Luiz Basso (2002). Drugs that inhibit mycolic acid biosynthesis in *Mycobacterium tuberculosis*. *Curr Pharm Biotechnol* 3, 197-225.
- Angelo Scorpio, Pamela LindholmLevy, Leonid Heifets, Robert Gilman, Salman Siddiqi, Michael Cynamon, and Ying Zhang (1997). Characterization of *pncA* mutations in pyrazinamide-resistant *Mycobacterium tuberculosis*. *Antimicrob Agents Ch* 41, 540- 543.
- Jessica Seeliger, Cynthia Holsclaw, Michael Schelle, Zsofia Botyanszki, Sarah Gilmore, Sarah Tully, Michael Niederweis, Benjamin Cravatt, Julie Leary, and Carolyn Bertozzi (2012). Elucidation and chemical modulation of sulfolipid-1 biosynthesis in *Mycobacterium tuberculosis*. *J Biol Chem* 287, 7990-8000.
- Manish Shah, Cheryl Ingram-Smith, Leroy Cooper, Jun Qu, Yu Meng, Kerry Smith, and Andrew Gulick (2009). The 2.1 Å crystal structure of an acyl-CoA synthetase from *Methanosarcina acetivorans* reveals an alternate acyl-binding pocket for small branched acyl substrates. *Proteins* 77, 685-699.
- Roxane Siméone, Mathieu Léger, Patricia Constant, Wladimir Malaga, Hedia Marrakchi, Mamadou Daffé, Christophe Guilhot, and Christian Chalut (2010). Delineation of the roles of FadD22, FadD26 and FadD29 in the biosynthesis of phthiocerol dimycocerosates and related compounds in *Mycobacterium tuberculosis*. *Febs J* 277, 2715-2725.
- Tatiana Sirakova, Vinod Dubey, Hwa-Jung Kim, Michael Cynamon, and Pappachan Kolattukudy (2003). The largest open reading frame (*pks12*) in the *Mycobacterium tuberculosis* genome is involved in pathogenesis and dimycocerosyl phthiocerol synthesis. *Infect Immun* 71, 3794-3801.
- Marion Steffensky, Shu-Ming Li, and Lutz Heide (2000). Cloning, Overexpression, and purification of Novobiocin acid synthetase from *Streptomyces spheroides* NCIMB 11891. *J Biol Chem* 275, 21754-21761.
- Kuni Takayama, Cindy Wang, and Gurdyal Besra (2005). Pathway to synthesis and processing of mycolic acids in *Mycobacterium tuberculosis*. *Clin microbiol Rev* 18, 81-102.
- Amalio Telenti (1998). *Genetics and pulmonary medicine*. 5. Genetics of drug resistant tuberculosis. *Thorax* 53, 793-797.
- Telenti, A., Honore, N., Bernasconi, C., March, J., Ortega, A., Heym, B., Takiff, H.E., and Cole, S.T. (1997). Genotypic assessment of isoniazid and rifampin resistance

- in *Mycobacterium tuberculosis*: A blind study at reference laboratory level. *J Clin Microbiol* 35, 719-723.
- Graham Timmins, and Vojo Deretic (2006). Mechanisms of action of isoniazid. *Mol Microbiol* 62, 1220-1227.
- Graham Timmins, Sharon Master, Frank Rusnak, and Vojo Deretic (2004). Nitric oxide generated from isoniazid activation by KatG: source of nitric oxide and activity against *Mycobacterium tuberculosis*. *Antimicrob Agents Ch* 48, 3006-3009.
- Jordi Torrelles, and Larry Schlesinger (2010). Diversity in *Mycobacterium tuberculosis* mannosylated cell wall determinants impacts adaptation to the host. *Tuberculosis (Edinb)* 90, 84-93.
- Joaquim Trias, Vincent Jarlier, and Roland Benz (1992). Porins in the cell wall of mycobacteria. *Science* 258, 1479-1481.
- Omita Trivedi, Pooja Arora, Vijayalakshmi Sridharan, Rashmi Tickoo, Debasisa Mohanty, and Rajesh Gokhale (2004). Enzymic activation and transfer of fatty acids as acyl-adenylates in mycobacteria. *Nature* 428, 441-446.
- Alexei Vagin, and Alexei Teplyakov (1997). MOLREP: an automated program for molecular replacement. *J Appl Cryst* 30, 1022-1026.
- Tommaso Vannelli, Alina Dykman, and Paul de Montellano (2002). The antituberculosis drug ethionamide is activated by a flavoprotein monooxygenase. *J Biol Chem* 277, 12824- 12829.
- Julien Vaubourgei, Fabienne Bardou, Fanny Boissier, Sylviane Julien, Patricia Constant, Olivier Ploux, Mamadou Daffé, Annaïk Quémard, and Lionel Mourey (2009). S-adenosyl-N- decyl-aminoethyl, a potent bisubstrate inhibitor of mycobacterium tuberculosis mycolic acid methyltransferases. *J Biol Chem* 284, 19321-19330.
- Herman Verheij (2006). Leadlikeness and structural diversity of synthetic screening libraries. *Mol Divers* 10, 377-388.
- Matthew Vetting, Patrick Frantom, and John Blanchard (2008). Structural and enzymatic analysis of MshA from *Corynebacterium glutamicum*: substrate-assisted catalysis. *J Biol Chem* 283, 15834-15844.
- Aldino Viegas, João Manso, Franklin Nobrega, and Eurico Cabrita (2011). Saturation-transfer difference (std) nmr: a simple and fast method for ligand screening and characterization of protein binding. *J Chem Educ* 88, 990-994.
- Catherine Vilchèze, Feng Wang, Masayoshi Arai, Manzour Hernando Hazbón, Roberto

- Colangeli, Laurent Kremer, Torin Weisbrod, David Alland, James Sacchettini, and William R Jacobs Jr. (2006). Transfer of a point mutation in *Mycobacterium tuberculosis* *inhA* resolves the target of isoniazid. *Nat Med* *12*, 1027-1029.
- Catherine Vilchèze, Yossef Av-Gay, Rodgoun Attarian, Zhen Liu, Manzour Hazboń , Roberto Colangeli, Bing Chen, Weijun Liu, David Alland, James Sacchettini, *et al.* (2008). Mycothiol biosynthesis is essential for ethionamide susceptibility in *Mycobacterium tuberculosis*. *Mol Microbiol* *69*, 1316-1329.
- Feng Wang, Paras Jain, Gulcin Gulden, Zhen Liu, Yicheng Feng, Krishna Ganesula, Alifiya Motiwala, Thomas Ioerger, David Alland, Catherine Vilchèze, *et al.* (2010). *Mycobacterium tuberculosis* dihydrofolate reductase is not a target relevant to the antitubercular activity of isoniazid. *Antimicrob Agents Chemother* *54*, 3776-3782.
- Feng Wang, Robert Langley, Gulcin Gulden, Lei Wang, and James Sacchettini (2007a). Identification of a type III thioesterase reveals the function of an operon crucial of *Mtb* Virulence. *Chem Biol* *14*, 543-552.
- Feng Wang, Robert Langley, Gulcin Gulden, Lynn Dover, Gurdyal Besra, William Jacobs Jr., and James Sacchettini (2007b). Mechanism of thioamide drug action against tuberculosis and leprosy. *J Exp Med* *204*, 73-78.
- Martin Webb (1992). A continuous spectrophotometric assay for inorganic phosphate and for measuring phosphate release kinetics in biological systems. *Proc Natl Acad Sci U S A* *89*, 4884-4887.
- Martin Wilming, and Kai Johnsson (1999). Spontaneous formation of the bioactive form of the tuberculosis drug isoniazid. *Angew Chem Int Ed Engl* *38*, 2588-2590.
- Motoko Watanabe, Yutaka Aoyagi, Hidemichi Mitome, Tsuyoshi Fujita, Hideo Naoki, Malin Ridell, and David Minnikin (2002). Location of functional groups in mycobacterial meromycolate chains; the recognition of new structural principles in mycolic acids. *Microbiology* *148*, 1881-1902.
- Motoko Watanabe, Yutaka Aoyagi, Malin Ridell, and David Minnikin (2001). Separation and characterization of individual mycolic acids in representative mycobacteria. *Microbiology* *147*, 1825-1837.
- World Health Organization (2008). Anti-Tuberculosis Drug Resistance in the World. Fourth Global Report. WHO Press.
- Huma Yonus, Piotr Neumann, Stephan Zimmermann, Jürgen May, Mohamed Marahiel, and Milton Stubbs (2008). Crystal structure of DltA. Implications for the reaction mechanism of non-ribosomal peptide synthetase adenylation domains. *J Biol*

Chem 283, 32484-32492.

- Ying Yuan, and Clifton Barry III (1996). A common mechanism for the biosynthesis of methoxy and cyclopropyl mycolic acids in *Mycobacterium tuberculosis*. *P Natl Acad Sci USA* 93, 12828-12834.
- Ying Yuan, Deborah Crane, James Musser, Srinand Sreevatsan, and Clifton Barry III (1997). MMAS-1, the branch point between cis- and trans-cyclopropane-containing oxygenated mycolates in *Mycobacterium tuberculosis*. *J Biol Chem* 272, 10041-10050.
- Ying Yuan, YaQi Zhu, Deborah Crane, and Clifton Barry III (1998). The effect of oxygenated mycolic acid composition on cell wall function and macrophage growth in *Mycobacterium tuberculosis*. *Mol Microbiol* 29, 1449-1458.
- Ying Zhang, Beate Heym, Bryan Allen, Douglas Young, and Stewart Cole (1992). The Catalase Peroxidase Gene and Isoniazid Resistance of *Mycobacterium-Tuberculosis*. *Nature* 358, 591-593.
- Zhening Zhang, Rong Zhou, J. Michael Sauder, Peter J. Tonge, Stephen K. Burley, and Subramanyam Swaminathan (2011). Structural and functional studies of fatty acyl adenylate ligases from *E. coli* and *L. pneumophila*. *J Mol Biol* 406, 313-324.
- Xiangbo Zhao, Hong Yu, Shengwei Yu, Feng Wang, James Sacchettini, and Richard Magliozzo (2006). Hydrogen peroxide-mediated isoniazid activation catalyzed by *Mycobacterium tuberculosis* catalase-peroxidase (KatG) and its S315T mutant. *Biochemistry* 45, 4131- 4140.

APPENDIX

AUTHOR CONTRIBUTIONS FOR THE REPRINTED ARTICLES

CHAPTER II:

Daniel Barkan analysed the whole cell response (including *M. tuberculosis*, *M. smegmatis*, and BCG strains) to dioctylamine, in terms of the mycolic acid profiles and susceptibility to antibiotics.

Zhen Liu carried out *in vitro* characterizations including fluorescence titration, enzymatic assays, and crystallography; performed the fragment-based screening for CmaA2.

CHAPTER III:

Feng Wang carried out the biochemical and structural characterization for DhfR.

Catherine Vilchèze isolated the spontaneous mutants of *M. tuberculosis*, co-resistant to INH and ETH, and located the mutations to *mshA*.

Zhen Liu carried out the biochemical and structural characterization for InhA co-expressed with KatG; analyzed the model of *M. tuberculosis* MshA; and performed the enzymatic assays for EthA.